

Formation of close binaries by triple dynamics in the context of supernovae la progenitors

FELIPE LAGOS VILCHES

Instituto de Física y Astronomía
Facultad de Ciencias



Advisor: Matthias Schreiber (UV)
Co-advisor: Mónica Zorotovic (UV)
Readers: Maja Vuckovic (UV) and Claus Tappert (UV)

Universidad de Valparaíso
Magíster en Astrofísica

July 2018
Valparaíso. Chile.

This thesis is solely my own composition,
except where specifically indicated in the text.

Total or partial reproduction, for scientific or academic purposes,
is authorised including a bibliographic reference to this document.

Felipe Lagos Vilches
July 2018.
Valparaíso. Chile.

Acknowledgements

Quisiera agradecer a mi profesor guía Matthias Schreiber, no sólo por haberme dado la oportunidad de postular al magíster en astrofísica, sino que también por el constante apoyo y motivación que me entregó a lo largo de estos dos años y medio de trabajo, y que ayudaron a definir la línea de investigación que quiero continuar en mi doctorado. Sin lugar a duda su disposición a aclarar cualquier pregunta, a corregir sin descanso mi inglés y a terminar esta tesis es algo que como estudiante valoro y aprecio mucho.

También quisiera agradecer a mi co-tutora Mónica Zorotovic, quién desde el comienzo me apoyó en esta tesis, la cual está basada en gran parte en su trabajo sobre binarias y simulaciones de poblaciones de PCEBs. Su excelente disposición al momento de enseñarme y corregirme fueron parte del ingrediente que hicieron este trabajo ameno y entretenido.

Tampoco puedo dejar pasar la oportunidad de agradecer a la profesora Amelia Bayo, quien siempre está dispuesta a ayudar cuando es necesario, y en este trabajo no fue la excepción.

En general a la universidad de Valparaíso, y en particular al departamento de física y astronomía, tanto profesores como compañeros, que no sólo tienen una calidad profesional del más alto nivel, sino que también una gran calidad humana que genera un ambiente de trabajo muy grato.

A mi familia, la cual desde que supo que la astronomía era mi camino a seguir siempre me apoyo, incluso en esos momentos en que el camino se veía imposible, y a mi novia Camila, la cual a pesar de la distancia y el tiempo que se necesita en esta carrera, ha sido un pilar importante a lo largo de estos años.

Abstract

The unique capabilities of Type Ia Supernovae (SN Ia), with emission bright and uniform enough to serve as yardsticks on cosmological distance scales, has resulted in them becoming some of the most important objects in the universe, and have led to the discovery of its accelerating expansion and eventually to the award of the 2011 Nobel Prize in Physics. Although it is well established that SN Ia are related to the thermonuclear ignition of a white dwarf (WD) that surpassed the Chandrasekhar mass limit, there is not yet a general consensus on the pathways leading to the explosion. While it is clear that the progenitors of SN Ia are close binaries which contain at least one WD, how these close binaries form and the detailed nature of the second stellar component remain one of the largest unsolved problems in astronomy.

The two main progenitor channels that have been proposed are the single degenerate channel in which the WD accretes from a non-degenerate companion, and the double degenerate channel, which explains SN Ia explosions as the merger of two WDs. However, whether nature has a strong preference for one of these channels, or whether a combination of several evolutionary channels contributes to the observed SN Ia rate, remains an open question. The fact that we haven't solved yet this important issue has two main reasons. First, the evolution of initial main sequence binary stars into close WD binary stars is a very complicated process and current theories are unable to simulate it in detail. Binary population models therefore rely on rather simple empirical relations with often completely unconstrained parameters, which makes it virtually impossible to make reliable predictions on SN Ia rates produced by any of the proposed channels. On top of that, it might even be that triple star dynamics produce significant numbers of close WD binaries, which is usually entirely ignored. Second, despite some significant recent progress, we still haven't been able to provide decisive observational constraints on WD binary pathways towards SN Ia. This is largely because the direct progenitors of SN Ia explosions are either short-lived and potentially highly obscured super soft X-ray sources and/or faint and hard to detect close double WD binaries.

The difficulty of providing clear constraints from surveys of the direct progenitors of SNIa motivated us to go one step back in the evolution of the proposed progenitor systems. Before a double WD system is formed and before a WD accretes from a non-degenerate companion, these systems must have been detached binary stars consisting of a WD and an intermediate mass star (typically FGK spectral types) companion, formed in most cases after a *common envelope* (CE) phase. Characterizing a large sample of such detached WD plus main-sequence FGK star systems, that both classic SNIa progenitors originally descended from, can provide crucial constraints on close WD binary evolution in general and the SNIa progenitor problem in particular.

The compact binary star group at the University of Valparaiso runs a large scale observational project aiming at identifying a large number of detached WD+FGK binary stars. Several close binaries have already been identified and some early results have been published. Interestingly, about $33 \pm 12\%$ of the identified close binaries are in eccentric orbits, which can not be explained by the main formation channel of close WD+FGK systems, the CE phase.

Based on previous studies that involve hierarchical triple systems and the effect of a distant extra component perturbing the binary, we propose that those observed eccentric binaries are in fact triples systems, where the third star alters the orbital properties like the eccentricity in the so called Kozai-lidov Mechanisms (KLMs), and together with tidal forces can produce close binaries with eccentric orbits. As most of the observed systems only have spectroscopic measurements of the main sequence star component of the close binary, we have two possible configurations that locate the WD either orbiting this sun-like star or being a distant companion to an inner binary consisting of the sun-like star and an unseen low-mass main sequence star.

In this thesis we estimate the amount of close WD+FGK binaries that evolved through KLMs (i.e., the binary as part of the triple systems) instead of via the CE phase, and the fraction of triple systems where the WD is either part of the binary or is the distant companion itself. To do this, we use the statistical research of hierarchical multiple stars of Tokovinin [2014b] to generate the initial conditions of a population of binary and triple systems that will be evolved using the *Binary Star Evolution code* (BSE). As the BSE algorithm only includes the evolution of single and binary stars, we evolve the distant companion as an isolated stars. Four simulations (assuming different eccentricity distribution) show that on average 23% of binaries of the observed sample could be potential hierarchical triple systems that evolved via KLMs , where about 79% correspond to systems where the WD is the distant companion, in agreement

with the observations. Finally, we observationally study one of the binaries with eccentric orbit, and find the third component to be the white dwarf. We estimate that most likely the KLMs were active before the WD formed.

Contents

1	Introduction	1
1.1	Evolution of low and intermediate mass stars	2
1.2	Stellar evolution in binary systems	2
1.2.1	The Roche-Lobe model	3
1.2.2	Mass transfer in binary systems	5
1.2.3	Orbital evolution during mass transfer	7
1.2.4	Common envelope phase	7
1.3	Supernova type Ia	9
1.4	Stellar multiplicity	11
1.4.1	Definitions	13
1.4.2	Multiplicity fraction	15
1.4.3	Period distribution	16
1.4.4	Component mass ratio distribution	16
1.5	The Kozai-Lidov and eccentric Kozai-Lidov Mechanisms	17
1.5.1	Standard Kozai Mechanism (SKM)	18
1.5.2	Eccentric Kozai Mechanism	20
1.5.3	Mass loss induced eccentric Kozai mechanism	22
1.5.4	Kozai Mechanism with tidal friction	23
1.6	Motivation	26
2	Triple star population synthesis	28
2.1	The FG-67 sample: Multiplicity of F and G stars inside 67 pc	28
2.2	Statistics of hierarchical systems	29
2.2.1	Statistical formalism	29
2.2.2	Period and mass ratio distributions	30
2.2.3	Dynamical stability	31
2.2.4	Analytical distributions for q and P	33

2.3	Multiple star population synthesis	34
2.4	Simulation	37
2.4.1	Limitations	41
3	Evolution of binary and triple systems	42
3.1	Binary and triple evolution	43
3.2	Dynamical instability after mass loss	45
3.3	Measuring the influence of Kozai mechanisms	49
3.4	Classifications and Nomenclatures	49
3.4.1	Spectral type assignation	50
3.4.2	PCEBs and contaminants	50
3.5	Ejection and timescale filters	52
4	Results	53
4.1	Number of contaminants	53
4.2	WD mass-type and period distributions of contaminants	57
4.3	Number of contaminants with filters	63
4.4	Conclusion	72
5	TYC 7218-934-1	73
5.1	Target selection and HST observations	73
5.2	Radial velocities and orbital parameters	75
5.3	SPHERE observations confirm the white dwarf to be the third object	76
5.4	Kozai mechanisms at current stage	78
5.5	Kozai-Lidov mechanisms in the early stages of TYC 7218-934-1	82
5.5.1	Modelling the probability to experience Kozai-Lidov oscillations by Montecarlo simulations	83
5.6	Conclusions	85
6	Summary	86
6.1	Statement	89
A	Appendix	90
A.1	Tables	90

CHAPTER 1

Introduction

The undeniable capability of SNe Ia as standard candles on cosmological distance scales, which allows to determine cosmological parameters, has made them some of the most important events in the Universe. However, despite their importance, the nature of the progenitors of SNe Ia is still uncertain. While it is clear that SNe Ia are caused by the explosion of a white dwarf in a close binary star system, the evolutionary pathways that lead to the formation of these close binaries is poorly understood. One possibility to improve this situation, is to investigate a crucial evolutionary phase that all binaries that eventually evolve towards SN Ia must pass: close but detached white dwarf+FGK spectral type binary stars.

With the aim to significantly contribute to solving the SN Ia progenitor problem, we run a large scale observational project entirely dedicated to characterize a large sample of WD+FGK binaries. In brief, our strategy is to 1) identify candidates from correlating GALEX with optical surveys, 2) take spectra to look for radial velocity variations, and 3) to measure the orbital periods. We have measured about a dozen periods so far, and much to our surprise, about one third of these systems have eccentric orbits. The most likely explanation for this is that triple dynamics are involved. In this thesis we investigate this hypothesis using statistics of triple systems and binary population models. As this final goal involves several different areas of stellar astrophysics, we provide in this Chapter 1 the theoretical background of binary star evolution, supernovae Ia progenitors, statistics of multiple stars, and the most important effect of triple interac-

tions (the Kozai-Lidov oscillations). We need to introduce all these different topics as they all play important roles in the presented research.

1.1 Evolution of low and intermediate mass stars

The evolution of a star is driven by the conservation of hydrostatic equilibrium, where the force exerted by gravity on the gas is balanced by the force exerted by a pressure gradient. This equilibrium can be disrupted by a change in the energy production inside the star, which may lead to structural changes with the aim to conserve it.

Stars spend most of their lifetime ($\approx 90\%$) in the main sequence stage, where the energy source is hydrogen burning in the core (which contains $\approx 10\%$ of the total mass of the star). Once hydrogen in the core is significantly depleted, a hydrogen shell surrounding the remaining helium core provides almost the total luminosity of the star. During this shell burning phase the mass of the contracting core increases, while the region outside the shell expands, reaching a stellar radius from 10 to 100 R_{\odot} for stars with mass $M \lesssim 8M_{\odot}$. When the density and temperature in the core become high enough, helium burning starts causing the core to expand, while the outer parts of the star contract until the stable helium burning phase (or HBP) is reached (for intermediate mass stars) or helium ignites under degenerated conditions (for low mass stars $M \lesssim 2M_{\odot}$), which leads to a helium flash and a shorter helium burning phase. While in the core helium is converted into carbon and oxygen, the hydrogen shell burning still provides most of the total luminosity. The HBP ends with an oxygen carbon core surrounded by a helium burning shell, which is itself surrounded by the hydrogen burning shell. At this stage the star can expand even more, reaching 100 to 500 R_{\odot} . The final stage for stars with $M \lesssim 7M_{\odot}$ is a carbon oxygen white dwarf, while for stars with masses in the range $7M_{\odot} \lesssim M \lesssim 10M_{\odot}$ carbon ignites, which leads to more shell burning and an oxygen neon white dwarf as the end product.

1.2 Stellar evolution in binary systems

As a significant number of stars are members of multiple systems, and in many of these multiple systems, some close members may interact, understanding stellar evolution is inherently linked to understanding binary star interactions. This is partic-

ularly important as close interacting binary stars are supposed to be responsible for some of the most luminous and most important explosions in the Universe, e.g. SNe Ia or kilo-nova events. In what follows, we outline the basic concepts of binary star interactions and how they impact stellar evolution.

1.2.1 The Roche-Lobe model

One of the most important ingredients to understand binary star interactions is Roche geometry, which describes the effective gravitational potential exerted by the binary system on a massless test particle (the so called restricted three-body problem). This effective potential is defined in a co-rotating frame where the gravitational potential of both stars (with mass M_1 and M_2) and the centrifugal potential acting on the test particle are taken into account. Close to each star the equipotential surfaces are approximately concentric spheres, while at greater distances the equipotential surfaces are distorted to tear drop-shapes, elongated parallel to the axis joining both stars. The Roche lobe of a star in a close binary system correspond to the region in space where the test particle is gravitationally bound to one of the system's stars.

The following assumptions are commonly used to describe the Roche model:

- The binary orbit is circular.
- The rotation of stars is synchronized with the orbital rotation.
- Stellar radii are small compared to the distance between them.
- The Coriolis force is neglected.

The Roche potential has 5 Lagrangian points where its gradient is zero (i.e., the forces that contribute to the potential cancel out each other). With respect to binary interactions, specifically mass transfer, the Lagrangian point L1 (or inner Lagrangian point), which is a saddle point of the effective potential (Fig.1.1), plays an important role: if a star fills its Roche lobe, then matter can flow through L1 to the other star. This mass transfer mechanism is called Roche-lobe overflow (RLOF).

Due to the complex geometry of the Roche lobe, approximations are used to model the distance between the star and L1. The effective Roche lobe radius for the star '1' (the most massive) with mass M_1 is defined as the radius of a sphere with the same

volume of the Roche lobe, and is often approximated using a prescription provided by Eggleton [1983]:

$$R_{L,1} = \frac{0.49q^{-2/3}a}{0.6q^{-2/3} + \ln(1 + q^{-1/3})} \quad (1.1)$$

which is better than $\approx 1\%$ in all cases. Here $q = M_2/M_1$ is the mass ratio and a the semi-major axis.

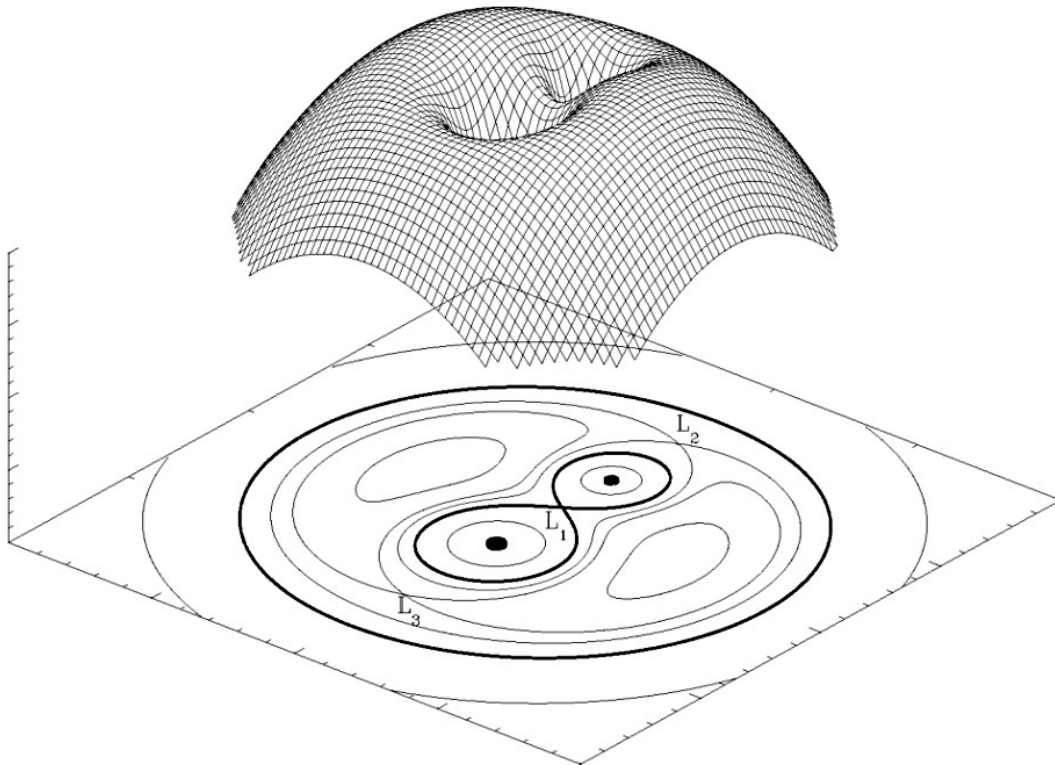


Figure 1.1: Roche lobe geometry for a binary star with a mass ratio of 2 in the co-rotating frame. The 3D surface plot (top) and a contour plot (bottom) show equipotential surfaces and the Lagrangian points L_1 , L_2 and L_3 . Figure taken from <http://hemel.waarnemen.com/Informatie/Sterren/hoofdstuk6.html#6.2>

With respect to the Roche lobe geometry, we can distinguish three types of binaries:

- **Detached binaries:** both stars fill an equipotential surface that lies within their respective Roche-lobe. Interactions between stars are only carried out by means of tides and stellar winds. The evolution of each star is usually not significantly affected by its companion; therefore, both stars evolve approximately as single stars.
- **Semi-detached binaries:** one of the stars fills its Roche-lobe. Hydrostatic equilibrium is no longer possible near L1 and matter flows over from this point to the companion. Mass transfer affects considerably the evolution of both stars.
- **Contact binaries:** If both stars fill an equipotential surface just or beyond their Roche-lobes (i.e. beyond L1 but without reaching L2), they can exchange heat as well as mass. The stars are gravitationally distorted and wrapped in a common photosphere.

1.2.2 Mass transfer in binary systems

For the formation of close binary stars with at least one white dwarf component (which could evolve into SN Ia), mass transfer from one component to the other in a semi-detached system, matters.

When one of the stars fills its Roche-lobe and mass transfer begins, the evolution of each component and the orbital properties of the system are affected. There are two possible ways to fill the Roche-lobe: the first is due to stellar evolution, where in general the more massive star evolves to a giant, and the second by orbital shrinking owing to angular momentum loss. In the latter case, angular momentum loss occurs due to tidal forces, gravitational waves or magnetic braking. Depending on the structure of the star that loses mass (the donor) and the response of both stars to mass loss/gain, mass transfer can be stable or unstable. In general, the stability in the mass transfer process depends mainly on two factors:

- The response of the donor's radius to the mass loss.
- The response of the Roche-lobe radius to the mass loss of the donor.

If the donor star fills its Roche-lobe, and the accretor gains all or most of the transferred mass without filling its Roche-lobe, the mass transfer is stable. On the other

hand, if the radius of the donor star becomes greater than the Roche radius (or the Roche radius becomes smaller than the radius of the donor star), accelerating mass transfer occurs. This case corresponds to the general scenario of unstable mass transfer. The commonly used stability criterion comes from a simplified model of the binary system, where we compare the variation of both the stellar radius (R_d) and the Roche-lobe radius (R_L) of the donor star (with mass M_d) while losing mass, assuming that the accretor star is an inert mass point (which is a very good assumption if it is a compact object). These variations in both radii are expressed by the so-called mass-radius exponents, defined as:

$$\zeta_d = \frac{d \log(R_d)}{d \log(M_d)} \quad (1.2)$$

$$\zeta_L = \frac{d \log(R_L)}{d \log(M_d)} \quad (1.3)$$

Then, if $\zeta_L \leq \zeta_s$, the system is stable against mass transfer.

Once the donor starts losing (transferring) mass, both its hydrostatic and thermal equilibrium are disturbed. Since the hydrostatic readjustment occurs on a dynamic time-scale T_{dyn} (which is much shorter than the thermal time-scale T_{th}), the first response of the star can be assumed to be almost adiabatic. Thus, in this scenario mass transfer will be stable if $\zeta_L \leq \zeta_{ad}$, where ζ_{ad} is the variation of the radius due to mass loss in the adiabatic regime. While mass transfer is stable during the adiabatic regime, the donor is able to recover hydrostatic equilibrium and thermal readjustment becomes relevant. In the thermal regime mass transfer will be stable if $\zeta_L \leq \zeta_{eq}$, where ζ_{eq} is the variation of the radius due to mass loss on the thermal time-scale.

In addition, if simultaneously $\zeta_L \leq \zeta_{eq}$ and $\zeta_L \leq \zeta_{ad}$, the mass transfer is *secularly stable* and occurs on the nuclear time-scale (i.e. mass transfer is driven by the nuclear evolution of the donor star). However, it is worth mentioning that stable mass transfer can also be achieved by orbital shrinkage due to angular momentum loss (AML) as long as $\zeta_{L,AML} \leq \zeta_{eq}$ and $\zeta_{L,AML} \leq \zeta_{ad}$, where $\zeta_{L,AML}$ is the variation of the Roche-lobe radius due to AML.

The response of the Roche-lobe radius to adiabatic mass loss depends mainly on the binary mass ratio q , while the response of the donor depends critically on the convective or radiative structure of its envelope. If the donor has a radiative envelope it shrinks in response to mass loss ($\zeta_{ad} \gg 0$), and for deeply convective envelopes the

donor tends to expand or keep a nearly constant radius ($\zeta_{ad} \leq 0$).

1.2.3 Orbital evolution during mass transfer

Mass transfer also modifies the orbital properties of a given binary system. The total orbital angular momentum and its time derivative for $e = 0$ are:

$$J = (M_1 a_1^2 + M_2 a_2^2) \frac{G^{1/2} (M_1 + M_2)^{1/2}}{a^{3/2}} \quad (1.4)$$

$$\dot{J} = J \left(\frac{\dot{a}}{2a} - \frac{\dot{M}_{tot}}{2M_{tot}} + \frac{\dot{M}_1}{M_1} + \frac{\dot{M}_2}{M_2} \right), \quad (1.5)$$

where a_1 and a_2 represent the distance of each stellar component from the center of mass, $a = a_1 + a_2$ the major axis and $M_{tot} = M_1 + M_2$ is the total mass of the system. In the simplest case mass transfer is conservative (i.e. all the mass lost by the donor is accreted by its companion) and the orbital angular momentum is conserved. In this scenario, mass transfer shifts the center of mass towards the accretor. The response of the orbital major axis to mass loss can be described as follows:

$$\frac{\dot{a}}{a} = 2 \left(\frac{M_d}{M_a} - 1 \right) \frac{\dot{M}_d}{M_d}, \quad (1.6)$$

where M_a and M_d are the masses of the accretor and the donor respectively. Since $\dot{M}_d < 0$, the orbit shrinks as long as $M_d > M_a$, reaching a minimum when $M_d = M_a$. On the other hand, if $M_d < M_a$ the orbits expand.

1.2.4 Common envelope phase

In Section 1.2.2 we have in rather general terms described under which conditions mass transfer occurs and if it is stable or not. If mass transfer is dynamically unstable, it proceeds on the very short dynamical time scale of the donor star (≈ 30 minutes for the Sun). As a consequence, the mass transfer timescale becomes much shorter than the thermal time scale of the accretor. Therefore, the transferred material accumulates in the Roche lobe of the accretor until it also fills its Roche-lobe and a gaseous envelope surrounding both stars is formed. This common envelope (CE) is not necessarily in

hydrostatic equilibrium and it is generally assumed that it does not rotate at the same rate as the binary. This has two important consequences:

- The CE is not constrained by the equipotential surface passing through the L1-L2 Lagrangian point.
- Drag forces inside the CE removes orbital energy from the stars, heating up and expanding the envelope. This energy transfer causes the binary orbit to shrink as the two stars spiral-in towards their common center of mass until the CE is expelled. This either leads to the formation of a very close binary star or the coalescence of the two stars.

The general description given above is the most accepted scenario to describe the CE phase. However, the main uncertainty is how efficient orbital energy is used to eject the envelope. In this context, the most commonly used model is the so called α -formalism (Tutukov & Yungelson [1979]) where:

$$\alpha = \frac{\Delta E_{gr}}{\Delta E_{orb}} \quad (1.7)$$

is defined as the fraction of the change in orbital energy $\Delta E_{orb} = E_{orb,i} - E_{orb,f}$ (subscripts i and f represent the initial and final stages respectively) available to expand and eject the envelope, which experiments a change of gravitational energy $\Delta E_{gr} = E_{gr,i} - E_{gr,f}$ (complete ejection corresponds to $E_{gr,f} = 0$). Different prescriptions have been used to model the final and initial values of orbital and gravitational energy. According to the PRH (Podsiadlowski-Rappaport-Han) prescription (Zorotovic et al. [2010]) the final orbital energy is calculated as the orbital energy between the core of the donor ($M_{d,c}$) and the accretor (M_{acc}) at the final separation (a_f):

$$E_{orb,f} = \frac{1}{2} \frac{GM_{d,c}M_{acc}}{a_f}, \quad (1.8)$$

while the initial orbital energy is calculated as the orbital energy between the donor and the accretor at the initial separation (a_i):

$$E_{orb,i} = \frac{1}{2} \frac{GM_d M_{acc}}{a_i}. \quad (1.9)$$

The initial gravitational energy of the envelope is calculated as being between the envelope mass ($M_{d,e}$) and the mass of the donor (M_d):

$$E_{gr,i} = \frac{1}{\lambda} \frac{GM_d M_{d,e}}{R}, \quad (1.10)$$

where R is the donor star radius and λ depends on the internal structure of the donor star.

A second prescription called ILY (Iben-Livio-Yungelson, Zorotovic et al. [2010]) takes the gravitational energy of the envelope as being between the envelope mass and the combined mass of the cores of the donor and accretor stars:

$$E_{gr,i} = \frac{G(M_{d,c} + M_{acc,c})M_{d,e}}{2a_i} \quad (1.11)$$

and the initial orbital energy as the orbital energy between the core of the donor and the accretor at the initial binary separation

$$E_{orb,i} = \frac{1}{2} \frac{GM_{d,c}M_{acc}}{a_i}. \quad (1.12)$$

The main difference between the two prescription is the presence of λ , which can lead to high values of gravitational energy for PRH compared to IYL (Zorotovic et al. [2010]). Hydrodynamic simulations of common envelope evolution that follow the entire process are currently not available because of the complexity of the process. Therefore the common envelope efficiency is usually constrained by observations and, at least for systems with low-mass secondary stars, evidence is growing that α is relatively small (Zorotovic et al. [2010]).

1.3 Supernova type Ia

Speaking in general terms, a supernova is the explosion of a star. This event is extremely energetic and its light curve can show peaks of luminosities of about 10^{43} ergs/s which declines on time-scales of weeks or months. There are two main mechanism that can cause a supernova explosion. Core collapse supernovae correspond to the rapid collapse during the final stage in the evolutionary path of massive

stars while supernovae type Ia (hereafter SNe Ia) are caused by the thermonuclear explosion of a white dwarf approaching the Chandrasekhar limit due to mass accretion. SNe Ia have been very useful as standard distance candles to map out the extragalactic distance scale, providing evidence for the accelerating expansion of the Universe. The use of SNe Ia as standard candles relies on the facts that: (1) its light curves seem to result from the same physical process and (2) there is an empirical relation between the peak luminosity and the shape of the supernova light curve.

Despite their importance, the mechanisms and progenitors that trigger SNe Ia are still controversial. The general consensus is that SNe Ia are thermonuclear explosions of carbon-oxygen white dwarfs with masses near the Chandrasekhar mass limit. This causes the ignition of carbon in the degenerated core, which completely destroys the white dwarf.

The two classical channels involving a white dwarf near the Chandrasekhar mass limit are the so called single degenerated-channel (SD) and double degenerated channel (DD). In the SD channel, the white dwarf accretes mass from a non-degenerate companion star until it reaches a mass of $1.44M_{\odot}$ and explodes (the exact mass at which the white dwarf explodes depends on its rotational speed). The DD channel involves two carbon white dwarfs that merge due to loss of angular momentum by emission of gravitational waves. In order to reach the mass limit, the combined mass of both white dwarfs must be equal or greater to $1.44M_{\odot}$.

In the following we will summarize the most relevant *pros* and *cons* for both the SD and DD channels.

- SD *pros*
 - There are observed systems where the mass transfer rate is high enough to allow that the overflowing material causes stable hydrogen burning on the surface of the WD. These systems are called *Supersoft X-ray Sources* (SSSs) and represent a direct path to produce SN Ia if matter can be retained until the Chandrasekhar mass limit is achieved.
 - It can explain the presence of calcium, sodium, and other absorption lines possibly associated with a non-degenerate donor star (Patat et al. [2007]; Simon et al. [2009]; Sternberg et al. [2011]; Dilday et al. [2012]).
- SD *cons*

- The accretion rate on the WD must be in a narrow range with the aim to avoid nova events (low accretion rate) and red-giant-like expansions (high accretion rate), which produce mass loss.
 - The predicted *delay time distribution* (SN Ia rate versus the time that would follow a brief burst of star formation; Maoz & Mannucci [2012]), or DTD, drops drastically after a few Gyr. This can be understood as follow: as we move towards low mass WD progenitors, the mass transfer required to reach the Chandrasekhar mass must be greater. Low-mass donors do not meet the required quantities of mass and transfer rates, so only relatively massive short-lived stars can provide the necessary conditions.
- *DD pros*
 - The absence of hydrogen and helium in observed SN Ia spectra emerges as a natural consequence in a C-O WD merger.
 - It explains the presence of systems with short and long time delays, which come from the timescales required to form WDs and mergers (taking into account only gravitational radiation effects), respectively.
 - *DD cons*
 - It is uncertain whether the WD merge can lead to a SN Ia or rather an accretion-induced collapse that ends with a neutron star (Nomoto & Kondo [1991]).
 - Despite the large amount of confirmed WD binaries (e.g., Saffer et al. [1998]), the discovery of a system with a total mass $M > 1.4M_{\odot}$ has remained elusive.

1.4 Stellar multiplicity

For any population study of potential SNe Ia progenitor systems, it is required to observationally constrain the properties and frequency of multiple star systems. As the most popular channels towards SN Ia are related to binary star interactions, traditionally only binary stars have been considered. In this work however, we will test how important triple interactions might be in the context of SNe Ia, so we need to take a detailed look at stellar multiplicity beyond the binary star fraction. Several large efforts

have been made in the last 40 years to measure stellar multiplicity (Abt & Levy [1976]; Duquennoy & Mayor [1991]; Tokovinin [1997]; Raghavan et al. [2010]; Tokovinin [2014a]), improving considerably our knowledge for the case of main sequence stars of spectral type F and G. However, for main sequence stars with intermediate-high mass, the multiplicity fraction is less well known, mainly for two reasons:

- Massive stars are less numerous than low mass stars.
- The very high luminosity of massive stars produces extreme brightness contrasts to potential low mass companions.

However, through the information obtained in previous surveys, taking into account the observational biases and comparing the data with simulations of multiple systems populations, a general picture of the statistical properties of multiple systems emerged. In what follows we summarize the main properties of multiple systems based on the review given by [Duchêne & Kraus, 2013] (hereafter DK13) for three different mass bins: (1) Solar-type stars ($0.7M_{\odot} \lesssim M \lesssim 1.3M_{\odot}$), (2) intermediate-mass stars ($1.5M_{\odot} \lesssim M \lesssim 5M_{\odot}$) and (3) high mass stars ($8M_{\odot} \lesssim M$). Table 1.1 compiles the main results found in DK13.

Mass Range	Mult./Comp. Frequency	Mass Ratio Distribution	Orbital Period Distribution
$0.7 M_{\odot} \lesssim M_{\star} \lesssim 1.3 M_{\odot}$	$MF = 44 \pm 2\%$ $CF = 62 \pm 3\%$	$\beta = 0.3 \pm 0.1$	Unimodal (log-normal) $\bar{a} \approx 45 \text{ AU}, \sigma_{\log P} \approx 2.3$
$1.5 M_{\odot} \lesssim M_{\star} \lesssim 5 M_{\odot}$	$MF \geq 50\%$ $CF = 100 \pm 10\%$	$\beta = -0.5 \pm 0.2$	Bimodal $\bar{P} \approx 10\text{d} \ \& \ \bar{a} \approx 350 \text{ AU}$
$8 M_{\odot} \lesssim M_{\star} \lesssim 16 M_{\odot}$	$MF \geq 60\%$ $CF = 100 \pm 20\%$

Table 1.1: Multiplicity properties for Population I MS stars, taking into account three different mass ranges (first column). MF and CF correspond to the multiplicity fraction and companion fraction respectively (second column), while β is the exponent of the power law used to model the mass ratio distribution (third column). The fourth column shows the best fit models for the observed orbital period distribution. Dots indicate that none of the analytical models fits well the data. Table adopted from DK13.

1.4.1 Definitions

With the aim of providing an unambiguous nomenclature of multiple stellar systems we summarize some important concepts:

- **Hierarchical system** : stellar systems with three or more components are hierarchical if the motion of the close inner binary is not strongly perturbed by the outer companion(s). Components of the hierarchical system are nearly on Keplerian orbits.
- **Primary star** : Corresponds to the assignment that is given to the most massive star in a (inner) binary system. Following this logic, the primary star's companion is called secondary star.
- **Multiplicity fraction (f_M)** : corresponds to the fraction of non-single stellar systems
- **Hierarchical level** : Hierarchical systems with three or more components can be present a *configuration degeneracy* for the same number of components. Hereafter we will use the Hierarchical nomenclature used in the Multiple Star Catalogue (MSC, Tokovinin [1997]). Figure 1.2 represents a scheme or *binary tree* for two

different configurations of a hierarchical system with five components. The position of each pair in the tree is called level, where the widest pair (level L1) is the root of the tree. Level L11 corresponds to an inner binary associated with the primary star, while Levels 12, 13, etc. are inner binaries associated with the secondary stars.

- **Companion fraction (f_C)** : is the number of systems at all levels divided by the total sample size.
- **Component mass ratio (q)** : corresponds to the mass ratio of primary stars of two consecutive levels and ranges from 0 to 1. As an example, in a triple system with level 12 (i.e. a close binary B,C with the primary star A as a distant tertiary companion), the component mass ratio at level L1 is $q = M_B/M_A$, where M_A and M_B are the masses of the primary stars at levels L1 and L12 respectively. For the level L12, $q = M_C/M_B$, where this time M_B is the mass of the primary star, while M_C is the mass of the secondary star. In some cases we will use the system mass ratio for triple stars, which corresponds to $q_{sys} = (M_B + M_C)/M_A$ for the previous example; for triple systems with level L11 (close binary A,B with tertiary companion C) $q_{sys} = M_C/(M_A + M_B)$. Because the definition of q_{sys} is ambiguous and may result in $q_{sys} > 1$, in the followings chapters we will only refer to the component mass ratio, unless otherwise stated.

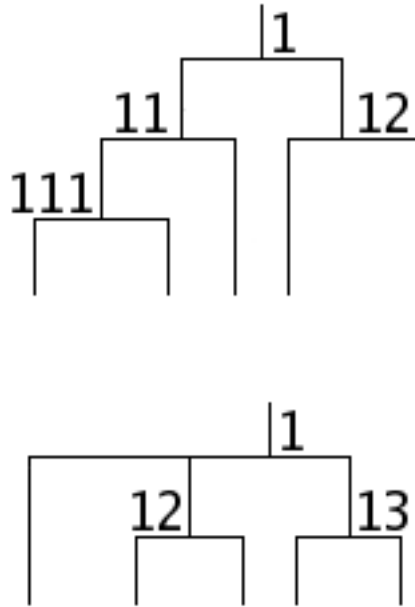


Figure 1.2: Tree diagram for two quintuple systems with different configurations. The upper diagram shows an inner triple system orbiting an inner binary, while the bottom diagram shows two binary systems orbiting the primary star.

1.4.2 Multiplicity fraction

Among solar-type stars, the survey performed by Duquennoy & Mayor [1991] (hereafter DM91), studied 164 primary main sequence stars out to 22 pc. They derived a companion fraction of $f_C = 62 \pm 3\%$ which agrees with the value obtained by Raghavan et al. [2010] (hereafter R10). In addition R10, using a larger sample (454 primary stars out of 25 pc) found that the multiplicity and companion fractions for stars with $1M_\odot \leq M \leq 1.3M_\odot$ are $f_M = 50 \pm 4\%$ and $f_C = 75 \pm 5\%$ respectively, while for stars with $0.7M_\odot \leq M \leq 1M_\odot$ they find $f_M = 41 \pm 3\%$ and $f_C = 56 \pm 4\%$. Additionally T14b, using the largest modern solar-type stars survey (4847 primary stars out of 67 pc with $0.9M_\odot \leq M \leq 1.5M_\odot$) found values for multiplicity and companion fractions of $f_M = 46 \pm 1\%$ and $f_C = 57 \pm 1\%$ respectively.

The observed ratios of single:double:triple:quadruple systems for DM91, R10 and T14b are 57:38:4:1, 56:33:8:3 and 54:32:7:5 respectively. For R10 and T14b the quadruple systems also take into account systems with more than four components.

For intermediate mass stars, the frequency of spectroscopy binaries (SBs) according to Abt [1983] can range from 30 – 45%, and is at least 30% for the Sco-Cen OB as-

sociation. In this association Kouwenhoven et al. [2005] found a frequency of visual binaries (VBs) of 37%, while Kouwenhoven et al. [2007] (K07) found in the Sco-OB2 association an intrinsic binary fraction larger than 70%. Finally, DK13 estimate that the multiplicity fraction for intermediate mass stars on the main sequence is $f_M \geq 50\%$. For massive mass stars the frequency of SBs is estimated at $70 \pm 9\%$ for periods out to 3000 days and down to $q \approx 0.1$ (Sana et al. [2012]) while for VBs the fraction is $\approx 45 \pm 5$ (Peter et al. [2012], Turner et al. [2008]). The companion and multiplicity fractions for stars with $8M_\odot < M < 16M_\odot$ are estimated as $100 \pm 20\%$ and 60% respectively. It is important to point out that due to the small sample size of massive stars, selection biases, and incompleteness, the values previously given are only relatively rough estimates and may undergo changes in the future.

1.4.3 Period distribution

Solar-type binaries span a wide range of periods, which can go from some hours to thousands of years. One of the most frequently used models to describe the observed period distribution is the log-normal description, which shows a peak for all pairs (that is, regardless of its hierarchical level) at $\log P \approx 5$ and a dispersion $\sigma_{\log P} \approx 2.3$ for DM91 and R10 (P in days), while T14b shows a median at $\log P \approx 4.54$ and dispersion $\sigma_{\log P} \approx 2.4$.

The period distribution of intermediate mass stars is less well constrained. Carquillat & Prieur [2007] found a bimodal distribution for A type stars, peaking around 5 days and 1000 days for SBs and VBs respectively. K07 tried to fit the observed distribution for the Sco-OB2 association with both power-law and log-normal models but none of them can reproduced well the data.

For massive stars the observed period distribution shows a peak for $4d < P < 8d$, which might be the effect of a strong selection biases (Abt et al. [1990]; Garmany et al. [1980]; Sana et al. [2012]). DK13 suggest that by combining two independent distributions it is possible to match the complete sample: for binaries with $\log P \leq 1d$ a power law $p(P) \propto P^\alpha$ ($\alpha \simeq 0.5$), and an Opik law ($\alpha = -1$) for $1 \leq \log P \leq 4$.

1.4.4 Component mass ratio distribution

The model commonly used to fit the observed mass ratio distribution in the three stellar groups is a power law $f(q) \propto q^\beta$. For solar type stars DM91 found a peak around $q \approx 0.3$ that decreases for higher values of q , while R10 establishes a constant distri-

bution above $q \approx 0.1$ with a strong peak at $q \approx 1$. Meanwhile, DK13 fitted the power law to the overall sample of R10, finding for solar-type stars with $0.7M_{\odot} \leq M \leq 1M_{\odot}$ a value of $\beta = 0.28 \pm 0.05$, while splitting the same sample in short ($\log P \leq 5$) and long ($\log P > 5$) periods values of $\beta = 1.16 \pm 0.16$ and $\beta = -0.01 \pm 0.03$ respectively are obtained. Finally, T14b plotted a mass ratio histogram for 766 wide binaries with $5 \leq \log P \leq 8$, showing a nearly flat distribution.

The q distribution for SBs with intermediate mass stars is relatively flat according to Carquillat & Prieur [2007] ($\beta = -0.3 \pm 0.2$), while for visual companions the VAST survey shows a distribution with $\beta \approx -0.6$. For the Sco-Cen OB association K07 derived the value $\beta = -0.45 \pm 0.15$, including both SBs and VBs.

For high-mass SBs Kiminki & Kobulnicky [2012] and Sana et al. [2012] found a flat distribution for q , with a peak around $q \simeq 0.8$, while for VBs Peter et al. [2012] concluded that a flat distribution and a broad Gaussian distribution centred on $q \approx 0.45$ fits well the observations of high mass stars in the Carina region.

As we will see in Chapter two, the work presented in this thesis is based on a multiple star population synthesis algorithm developed for solar-type stars, extrapolating their properties, like multiplicity fraction and period and mass ratio distribution to more massive stars. One direct consequence of this, as we saw in section 1.4.2 is that we are likely under estimating the true value of multiple systems on intermediate and high mass stars, while according to section 1.4.3 we are under estimating the number of binaries with orbital periods less than 10 days, where such increment of close binaries could be, however, the effect of observational biases. For the mass ratio distribution, each one of the three mass range used show a nearly flat distribution. Although this approximation might under estimate the number of multiple systems that we are trying to identified (mainly due to the extrapolation in the multiplicity fraction), our final results confirms in a fist instance the presence of a non negligible fraction of triple systems in our sample..

1.5 The Kozai-Lidov and eccentric Kozai-Lidov Mechanisms

Detached binaries with wide (say $P \approx 100$ days) orbits can evolve into close binaries ($P \lesssim 16$ days) mainly by means of tidal interactions. However, such a close configura-

tion can also be achieved with a third companion perturbing the orbital properties of the binary (see e.g. Eggleton & Kisseleva-Eggleton [2006]). In what follows we present the effect of such perturbations, the so called Kozai-Lidov oscillations, introducing its physical formalism and variants.

1.5.1 Standard Kozai Mechanism (SKM)

The secular stability of triple-star systems is generally achieved if the system is hierarchical, that is, the semi major axis of the inner binary a_{in} is much smaller than the semi mayor axis a_{out} of the distant companion that orbits the center of mass of the inner pair, with a low or moderate eccentricity. The effect of a third companion on the inner binary can produce some important long-term effects on this, like precession of the orbital plane. In 1962 Kozai [1962] and Lidov [1962] independently discovered from the secular perturbation theory unexpected behaviours in the orbital evolution of asteroids and artificial satellites perturbed by Jupiter and the Moon respectively. In their model, called Test Particle Quadrupole or "TPQ" (Lithwick & Naoz [2011]), where the outer orbit (Jupiter/Moon orbit) is assumed to be circular and the asteroid/satellite a massless test particle, the Hamiltonian for the system can be written as the sum of two Keplerian Hamiltonians plus a term representing the interaction between the two orbits (H_p):

$$H = \frac{G^2 M_1 M_2}{2a_{in}} + \frac{G^2 M_3 (M_1 + M_2)}{2a_{out}} + H_p, \quad (1.13)$$

where G is the gravitational constant, M_1, M_2 the masses of the inner binary and M_3 the mass of the outer companion. Since the triple system is hierarchical ($\alpha \equiv a_{in}/a_{out} \ll 0$) the perturbative term can be expanded in orders of α using Legendre polynomials as follows:

$$H_p = \sum_{n=2}^{\infty} \left(\frac{a_{in}}{a_{out}} \right)^n \left(\frac{r_{in}}{a_{out}} \right)^n \left(\frac{a_{out}}{r_{out}} \right)^{n+1} M_n P_n(\cos\Phi). \quad (1.14)$$

In this expression P_n are the Legendre polynomials, r_{in} the relative position vector from M_1 to M_2 , r_{out} the relative position vector of M_3 from the centre of mass of the inner binary, Φ the angle between r_{in} and r_{out} (Fig.1.3), and

$$M_n = M_1 M_2 M_3 \frac{M_1^{n-1} - (-M_2)^{n-1}}{(M_1 + M_2)^n}. \quad (1.15)$$

Since the outer orbit is circular ($e_{out} = 0$), high order terms ($n > 2$) in the perturbative expansion become zero. This approximation is called *quadrupolar* expansion. Besides, the z-component of the particle angular momentum J_z ($J_z \propto \cos(i) \sqrt{(1 - e_{in}^2)}$), is conserved. This implies the possibility of an exchange between inclination and eccentricity, allowing highly eccentric orbits for low values of i , and vice versa.

The evolution of such an angular momentum exchange depends strongly on the initial values of i and e . For the case of very small initial eccentricities and an initial inclination between 39.2° and 140.77° (the so called Kozai angles) the maximum eccentricity occurs simultaneously with the minimum inclination (39.2°) following the relation:

$$e_{max} = \sqrt{1 - 5/3 \cos^2(i_0)}, \quad (1.16)$$

allowing the extreme case of collision for $i_0 = 90^\circ$. The timescale of the eccentricity (inclination) oscillations according to (Li et al. [2015]) is given by:

$$t_{SKM} = \frac{2\pi a_{out}^3 (1 - e_{out}^2)^{3/2} \sqrt{(M_1 + M_2)(1 - e_{in}^2)}}{G^{1/2} a_{in}^{3/2} M_3}. \quad (1.17)$$

For very small initial eccentricities and initial inclinations below 39.2° (or above 140.77°), the solutions of equations of motion are quasi-periodic with small fluctuations on eccentricity and inclination.

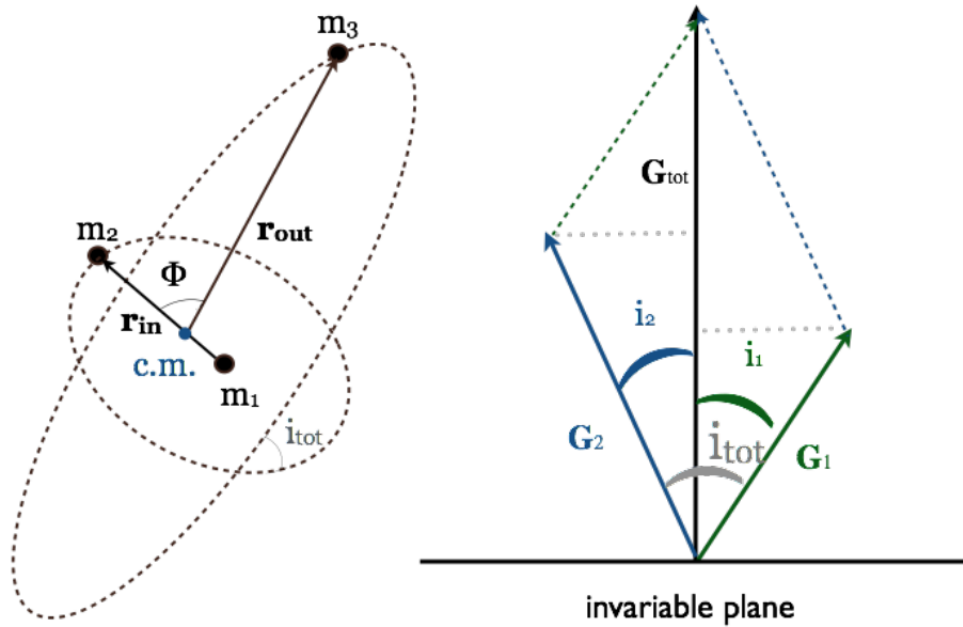


Figure 1.3: Left: Schematic description of the used coordinate system. The term “c.m” correspond to the center of mass between M_1 and M_2 . Right: Schematic description of the invariable plane. Here G_{tot} corresponds to the total angular momentum vector, which is the sum of the angular momentum vector of the inner and outer orbits, G_1 (with angle i_1 respect to G_{tot}) and G_2 (with angle i_2 respect to G_{tot}) respectively. Figure adopted from Naoz [2016].

1.5.2 Eccentric Kozai Mechanism

Although the TPQ describes new behaviours for the hierarchical three body problem, the assumption of circular outer orbits and massless inner binary components does not necessarily represent a good description of the whole population of triple systems and may overlook some interesting effects. For instance, if the test particle mass is not negligible or the outer orbit is eccentric, orbital flips (i passing through 90°) and large values of the eccentricity can be achieved for initial inclinations that are outside the classic Kozai-Lidov range 39.2° - 140.77° . In such case, the next level of approximation, called test particle octupole (TPO), expands the term H_p in the Hamiltonian until $n=3$, leaving the Hamiltonian of the system as:

$$F = F_q + \epsilon_{oct} F_{oct}, \quad (1.18)$$

where F_q represents the Hamiltonian in the quadrupole approximation, F_{oc} the new contribution to the Hamiltonian due to the octupole approximation and

$$\epsilon_{oct} = \left(\frac{M_1 - M_2}{M_1 + M_2} \right) \left(\frac{a_1}{a_2} \right) \frac{e_{out}}{1 - e_{out}^2} \quad (1.19)$$

measures the importance of the octupole term relative to the quadrupole term. Since $e_{out} > 0$, the z component of the angular momentum of the inner binary is no longer conserved, allowing quasi-periodic cycles in i through 90° while e_{in} can be excited to values very close to unity ($1 - e_{in} \sim 10^{-5}$, Shappee & Thompson [2013]).

The general case for eccentric outer orbits is called eccentric Kozai mechanism (EKM) and can have an important effect when $|\epsilon_{oct}| \gtrsim 0.01$ (Naoz et al. [2011]; Shappee & Thompson [2013]). Figure 1.4 shows two configurations for a triple system with $\epsilon_{oct,1} = 0.0299$ (left panels) and $\epsilon_{oct,2} = 0.06$ (right panels) illustrating that the TPQ approximation is not capable of capturing the flip and the extremely high values of eccentricity that even occur for an initial inclination of 1° . Another interesting effect in the octuple approximation is that beyond the Kozai angles the flips occur on a much shorter timescale.

According to (Li et al. [2015]), the timescale for extremely high inclinations and orbital flips is

$$t_{EKM} = \frac{t_{SKM}}{\epsilon_{oct}} \quad (1.20)$$

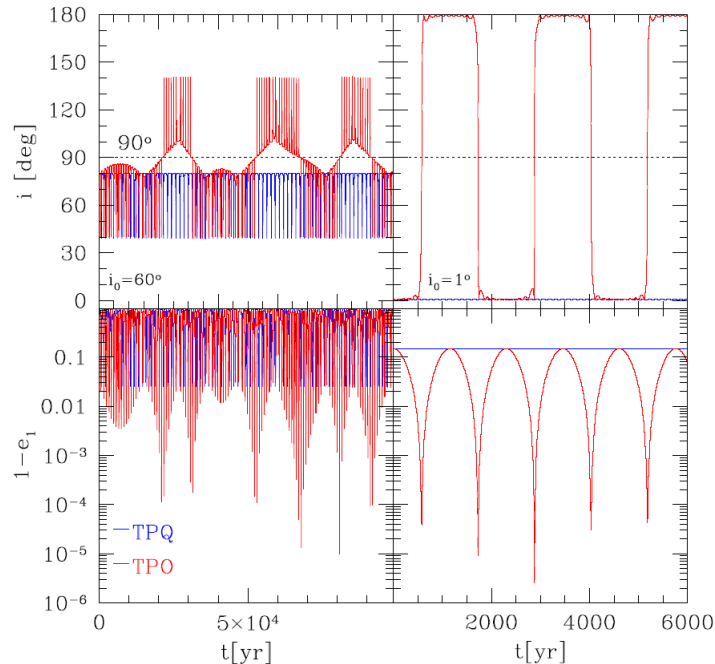


Figure 1.4: Comparison of the time evolution of inclination (top panels) and eccentricity (bottom panels) for the TPQ (blue line) and TPO (red line) approximations. The example considers a test particle at 135 AU around a $10^4 M_\odot$ black hole located 0.03 pc from a $10^6 M_\odot$ massive black hole. The initial configuration for the left panels is $e_{in} = 0.01$, $e_{out} = 0.7$, $i = 60^\circ$, $\Omega_{in} = 60^\circ$ and $\omega_{in} = 0^\circ$. In the right panels the system is initially set with $e_{in} = 0.85$, $e_{out} = 0.85$, $i = 1^\circ$, $\Omega_{in} = 180^\circ$ and $\omega_{in} = 0^\circ$. Figure adopted from Naoz [2016]

1.5.3 Mass loss induced eccentric Kozai mechanism

According to equation (1.19), the dominant Kozai mechanism during the evolution of a given system depends on the mass ratio of the inner binary. For $M_1 \simeq M_2$, $\epsilon \approx 0$ and F_{oct} can be neglected, i.e. the standard Kozai mechanism drives the dynamical behaviour of the system. Conversely, if $M_1 \gg M_2$ the octupole term may take relevance and the EKM is the dominant mechanism. This fact implies that mass transfer and mass loss due to stellar evolution can indeed affect the long-term evolution of the system, changing the predominant Kozai mechanism from SKM to EKM and vice versa. The former is of particular interest when one of the stars in the inner binary becomes a white dwarf, in such a case the switch between SKM to EKM can drive mass transfer close to the periastron that combined with tidal forces can produce a close inner binary with mass transfer towards the white dwarf, i.e., a possible supernova type Ia

progenitor.

1.5.4 Kozai Mechanism with tidal friction

An interesting effect triggered by SKM and EKM is observed in binary systems with an outer companion. When the separation of the binary components at periastron becomes comparable to the stellar radii due Kozai mechanisms, tidal friction absorbs the orbital energy and its period can be shortened by 1 or 2 orders of magnitude after formation. Harrington [1968] first suggested that Kozai cycles with tidal friction (KCTF) play an important role in the secular evolution of triple stars. Eggleton & Kisseleva-Eggleton [2006] explicitly suggested that KCTF might produce many close or contact binaries. They also show that the effect of the apsidal motion due to either general relativity (GR) or the quadrupolar distortion of the components due to rotation may reduce the initial inclination and the maximum eccentricity predicted by equation 1.16. For instance, for a hierarchical triple with equal (solar) masses, $P_{in} = 10$ days, $P_{out} = 10$ yr, initial $e_{in} = e_{out} = 0$ and $i = 80^\circ$ the effect of GR, spin ($P_{rot} = 1$ d) and mutual distortion reduce the peak eccentricity from 0.975 to 0.78 while the inclination reduced to 74° (Fig.1.5). However, despite this reduction, the Kozai cycle allows tidal forces to operate on a relatively short timescale.

Fabrycky & Tremaine [2007] simulated a population of triple systems and by integrating the equation of motion under the effect of Kozai oscillations and tidal friction they found that binary stars with orbital periods of 0.1-10 days are produced from binaries with initial periods of 10 to 10^5 days (top of Fig.1.6). Similarly, Naoz & Fabrycky [2014] simulated a population of triple systems but considering the EKM case, for which they got the same final bimodal period distribution as in Fabrycky & Tremaine [2007], which is also reproducing the period distribution of inner binaries in triples observed by Tokovinin [2008] (bottom of Fig.1.6). According to these results, the final population of close binaries and mergers seems to come from two distinct populations. The main contribution of the close binary population comes from systems with inner binaries with periods of 4-16 days (blue line in bottom panel of Fig.1.6), and $\sim 41\%$ comes from periods larger than 16 days. This shows that 8.6% of all triples simulated with initial periods $\gtrsim 16$ days have become close binaries, representing an efficiency of 2.4 times larger than predicted by the SKM. The merger population is, however, more likely to originate from initially wider inner binaries (solid red line in bottom panel of Fig.1.6).

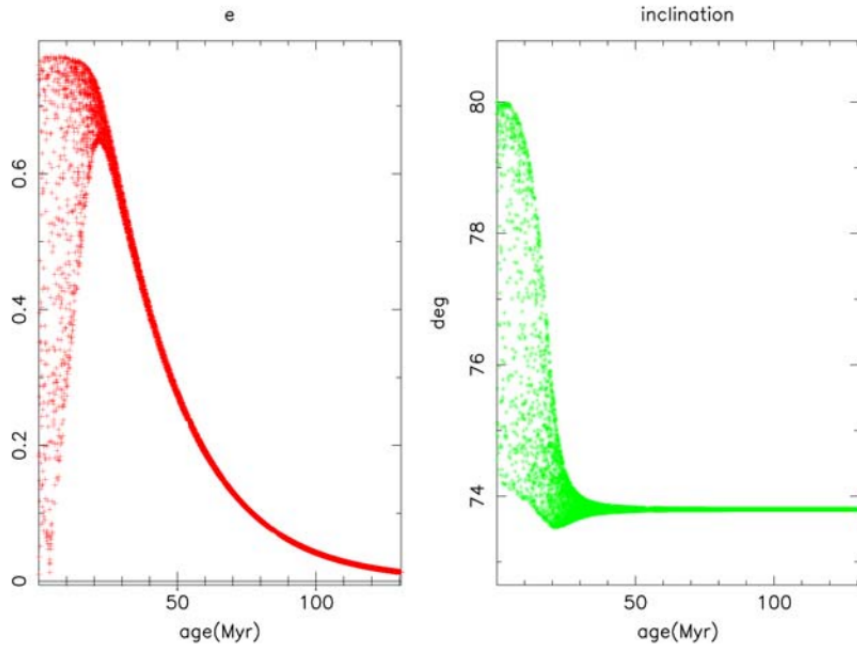


Figure 1.5: Effect of KCTF on time evolution of eccentricity (left) and inclination (right) for a triple system composed of sun-mass stars, inner and outer periods of 10 days and 10 years respectively, $i_{tot} = 80^\circ$, and initially circular orbits. According to equation 1.16 the eccentricity peak is at 0.975. However, when they include GR effects and the quadrupolar distortion the value of e_{max} is reduced to 0.74. The final long-term result (after about 50 Myr) is a circularized inner orbit at a period of 2.5 days. Figure adopted from Eggleton & Kisseleva-Eggleton [2006].

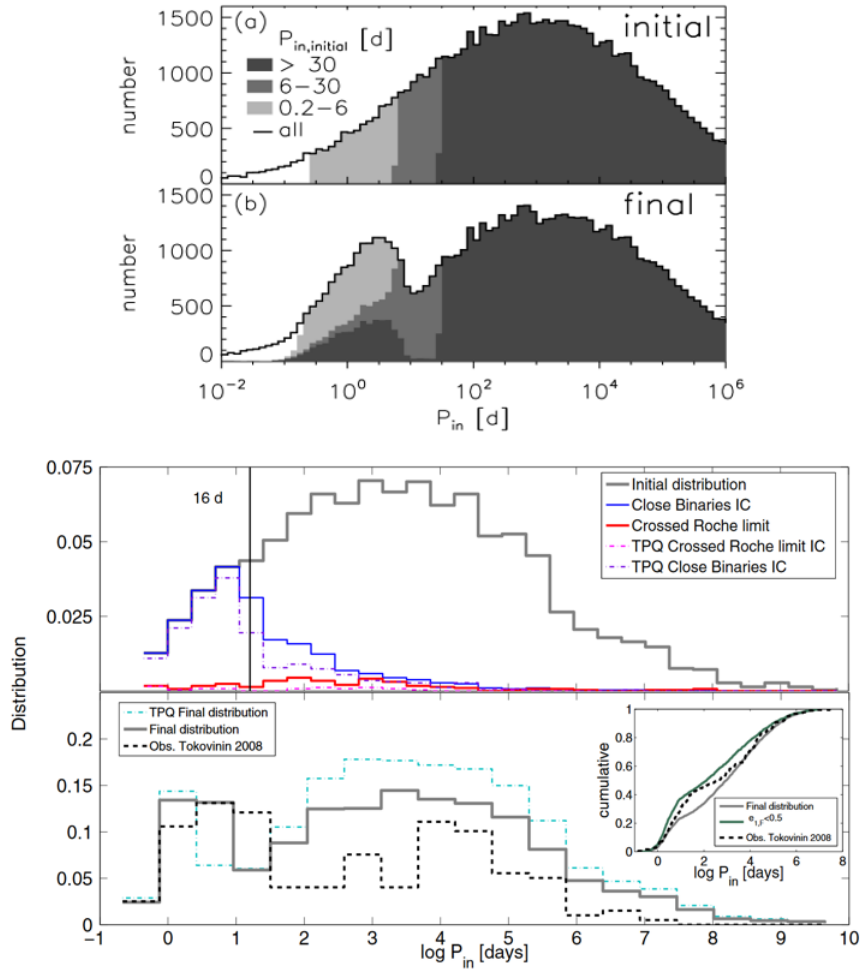


Figure 1.6: Top: initial and final period distribution of the inner binaries in the triples simulated by Fabrycky & Tremaine [2007]. Gray scale colors in the final stage represent the initial period of the system. A log normal period distribution is assumed as initial. Bottom: initial and final period distribution of the inner binaries in the triples simulated by Naoz & Fabrycky [2014]. To be able to compare the period distribution observed by Tokovinin (2008) (black dashed line), gray lines in the bottom panel represent the total inner binaries simulated with final eccentricity $e_{in,f} < 0.5$. Figures adopted from Fabrycky & Tremaine [2007] and Naoz & Fabrycky [2014]

1.6 Motivation

SNe Ia are one of the most energetic events produced by stars, and due to their almost uniform luminosities, they have been used as distance indicators, providing a tool for obtaining cosmological parameters. However, the exact nature of their progenitors is still unknown.

The *White Dwarf Binary Pathways Survey I* (Parsons et al. [2016], hereafter P16), initiated by researchers from the University of Valparaiso has the aim to progress with our understanding about the evolution of binary stars towards SN Ia. As all potential SN Ia progenitor systems must pass through a stage of detached WD+FGK binary stars, these systems are ideal to constrain binary evolution towards SN Ia. Therefore, if a large sample of WD+FGK binary stars can be observationally characterized, crucial constraints can be derived for binary evolution theories. The targets selected in the survey include FGK stars from the Radial Velocity Experiment (RAVE, Kordopatis et al. [2013]) and the Large Sky Area Multi-Object Fiber Spectroscopic Telescope (LAMOST, Cui et al. [2012]; Luo et al. [2012]; Yuan et al. [2015]) survey, which present measurements from GALEX in both far and near ultraviolet (UV) wavelengths. Then, if the FGK stars show an excess flux at UV wavelengths, we interpret this as a potential WD companion. The effectiveness of the survey was confirmed by taking the UV spectra of nine targets with the Hubble Space Telescope, which showed that for eight cases the UV excess was indeed caused by a WD, while the remaining one was a hot subdwarf or pre-helium white dwarf. Until now, we have 15 systems with orbital properties measured and, interestingly, 5 binaries have eccentric orbits that can not be explained by CE evolution. Since the orbital solutions of such systems are based on radial velocities measured from the absorption lines of the FGK-type component, there are two possible general configurations. Either, these objects are indeed close FGK+WD binaries formed through the SKL/EKM/MIEK mechanism and may therefore provide the first observational evidence for a new channel towards SN Ia or the WD is the third distant object that triggered the eccentric Kozai-Lidov mechanism, which led to the formation of the inner binary star consisting of the FGK-type star plus an unseen late M dwarf.

The main aim of this thesis is to provide a rough estimate whether triple statistics and KL can explain the large number of eccentric orbits and whether nature favors the first (close binary with WD component plus third object) or the second (close main sequence binary plus distant white dwarf companion) scenario. Combining statistical

analysis of stellar multiplicity with analytical expressions for the importance of KL effects, we will estimate the fraction of both configurations.

CHAPTER 2

Triple star population synthesis

The first key ingredient to evaluate how frequent triple dynamics may lead to close binaries with one white dwarf component are observational constraints on the multiplicity fractions, mass ratios, periods and eccentricities of triple systems. Despite the difficulties to observe close or wide faint companions (Section 1.4), the latest instrumental improvements have allowed a more robust analysis, and algorithms that reproduce the observed population of multiple star systems have been developed.

In this Chapter we describe the perhaps most complete of these algorithms, presented by Tokovinin [2014b] (T14b). This algorithm is based on observations of 4847 F and G type stars within 67 pc of the Sun and takes into account selection effects and observational biases. As we base our initial population of multiple systems on this prescription, we provide a detailed description of the algorithm in what follows.

2.1 The FG-67 sample: Multiplicity of F and G stars inside 67 pc

Tokovinin [2014a] (hereafter T14a) presented the currently most complete sample of multiple stellar systems with Sun-like primary stars. Those stars correspond to spectral types from F5V to G6V and masses that range from 0.85 to $1.5M_{\odot}$. The total number of stellar pairs is 2196 and of those 361 belong to hierarchical systems from triples

to quintuples, giving a observed value of $f_M = 0.36$. Since only systems with non-evolved components are considered in the analysis of T14b, systems with white dwarf components were removed from the sample, leaving 2162 systems and subsystems to consider, of which 355 have missing information (unknown periods and separations).

2.2 Statistics of hierarchical systems

In this section we summarize the statistical analysis made in T14b, emphasizing the final results and the analytical distributions used to mimic the observed periods, mass ratios and multiplicity fractions at all hierarchical levels.

2.2.1 Statistical formalism

The goal of T14b is to model the intrinsic distribution of periods and mass ratios through the joint probability density function $f(x, q|\theta)$ (with θ the parameter array), by using the available data and taking into account that some binaries have missing data (unknown periods and mass ratios). The detection probability of a binary with logarithmic period x and mass ratio q is given by the Poisson distribution

$$p = \frac{\mu^m}{m!} e^{-\mu}, \quad (2.1)$$

where $\mu = \int f(x, q|\theta) d(x, q)$ is the probability of a detectable companion given the detection probability $d(x, q)$. For single stars $m = 0$, while for binaries $m = 1$. If the binary has unknown mass ratio, then μ is averaged over the range where the detection techniques are unable to measure the mass ratio. For binaries with both unknown period and mass ratio, μ is averaged over the parameter space where detection techniques are unable to measure x and q . In this way systems with missing data are included in the statistical analysis, which is important since although they have unknown periods and mass ratios, they are actually discovered.

The best fit parameters are achieved by minimizing $S = -2 \ln L$, where L is the likelihood function. As the targets are observed independently of each other, L is the product of p_i , where i is referred to the i th target.

2.2.2 Period and mass ratio distributions

Figure 2.1 shows the observed and corrected distribution of periods for all pairs and level L11 in the sample. The corrected distribution takes into account the incompleteness by detection limits that depends on the values of P and q . The detection probability $d(x, q)$ (where $x = \log(P/1\text{day})$) is averaged over an uniform q distribution (see below) and applied in each period bin. The periods of L11 are shorter than the periods of all binaries, which can be explained by dynamical stability restrictions and show a depletion at $x \sim 2$ and excess at $x < 1$ probably due to missing data or migration of inner subsystems towards short periods owing to tidal interactions combined with Kozai mechanisms.

Regarding the distribution of q , assuming that it is distributed as a power law like q^β , T14b studied the possible dependence with period, finding that at both short and long periods the mass ratio between the main target and its companion (regardless the hierarchical level) distribute uniformly ($\beta \sim 0$). Figure 2.2 shows this dependence, where the high value of β observed close to $x = 4$ is because of the binaries with missing data, while for $x > 5$ (where there is no missing data) there is a weak dependence of β on period.

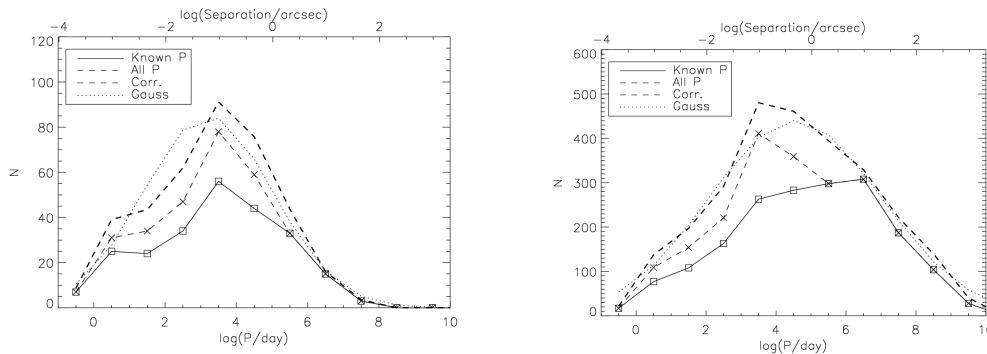


Figure 2.1: Histogram of periods with $\Delta x = 1$ bins. The solid line represent the systems with known period, the dashed line adds fictitious periods chosen (only used to generate this histograms), the thick dashed line adds the correction effects and the dotted line is the log-normal distribution with the parameters found in the ML method. Left: only level L11. Right: all pairs. Figure adopted from T14b.

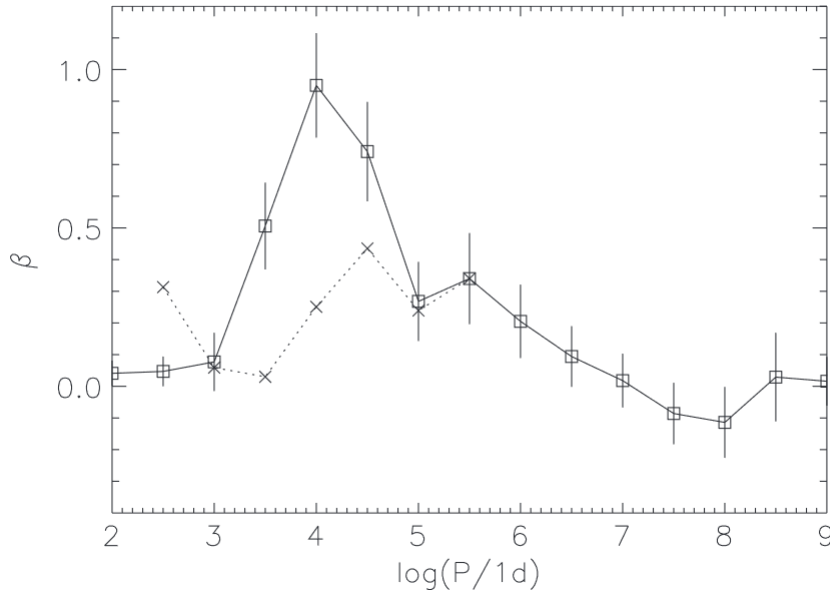


Figure 2.2: Dependence of β on period. The bin size is $\Delta x = 1$. The crosses and dotted lines are generated by adding fictitious values to unknown mass ratios and periods. It is important to emphasize that the fictitious values only have the aim of quantifying how much the dependence of β on period changes if we assume that they come from arbitrary but reasonable period and mass ratio distributions. Figure adopted from T14b.

2.2.3 Dynamical stability

Since the condition of hierarchy for a multiple system implies that it must be secularly stable, the next question to solve is how to define a general criterion that separates those systems where the inner pair is strongly perturbed by an outer companion from those with a stable hierarchical configuration. Mardling & Aarseth [2001] derived a long term stability criterion that describes the capability of triple systems to suffer exchange of a component between the inner and outer binary. In terms of the ratio between the inner and outer orbital periods P_S and P_L this can be written as:

$$\frac{P_L}{P_S} > 4.7(1 - e_L)^{-1.8}(1 + e_L)^{0.6}(1 + q_{out})^{0.1}f, \quad (2.2)$$

where e_L is the eccentricity of the outer orbit, q_{out} the mass ratio of the distant companion to the combined mass of the inner binary and

$$f = 1 - \frac{0.3i}{180} \quad (2.3)$$

is a factor obtained from numerical experiments that accounts for the increased stability of inclined and retrograde motion (with i in degrees).

Figure 2.3 compares the values of P_S at inner hierarchical levels L11 and L12 with the outer period P_L of the T14b sample. Two remarkable features are observed here: all the points are above the constant period ratio $P_L/P_S = 4.7$ with no typical or preferred values, and the absence of outer periods shorter than $x < 3$ which is not caused by observational selection but is an intrinsic property of the population.

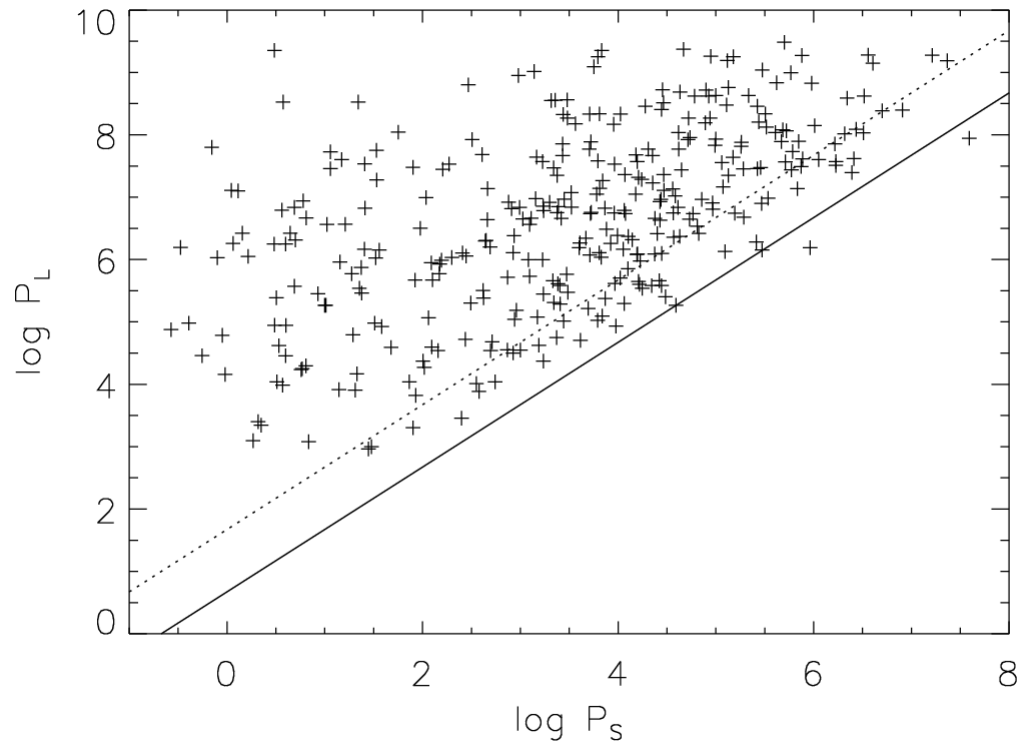


Figure 2.3: Outer orbital period at level L1 compared with inner periods at levels L11 and L12. The solid and dotted line represent the ratio $P_L/P_S = 4.7$ and 47 respectively. Figure adopted from T14b

2.2.4 Analytical distributions for q and P

Based on the work done by DM91, the distribution chosen by T14b to fit the observed periods is a log-normal law. The disadvantage of this choice are its wings that produce either extremely short and long periods compared to the observed one, therefore the distribution must be truncated at $x < -0.3$ and $x > 10$ according to observation of the tightest and widest binaries with main sequence stars. For the mass ratio distribution a power law with $\beta > -1$ and truncated at $q < 0.05$ to avoid brown dwarf companions is used (Section 1.4.4). Making use of the non-dependence of the mass ratio on period, the analytical model used to fit the sample is:

$$f(x, q) = C\epsilon q^\beta \exp\left(\frac{-(x - x_0)^2}{2\sigma^2}\right), \quad (2.4)$$

where ϵ is the multiplicity fraction, x_0 the median period, σ the period dispersion and C is a constant of normalization.

The model (2.4) was fitted to various sub samples using the maximum likelihood method (ML) taking into account the detections limits and missing data. Table 2.1 summarizes the results obtained with this method for all pairs, regardless of their hierarchies, and the sub samples at levels L1, L11 and L12. The given errors correspond to 68% confidence intervals but they should only be considered as a lower limit of the true errors. The multiplicity fraction ϵ obtained for level L1, that equals the intrinsic f_M of the T14b sample (all multiples systems start with L1) is 0.46 ± 0.01 , in agreement with R10. At levels L11 and L12 the values of ϵ refer to the frequency of subsystems in the sample of L1 systems only, therefore the intrinsic fraction of hierarchies L11 and L12 are $0.1 (\approx 0.46 \times 0.214)$ and $0.073 (\approx 0.46 \times 0.157)$ respectively. The results for β show a nearly flat distribution for almost all sub samples. Subsystems at L12 seem to show a tendency towards equal mass components ($\beta = 1.32$) that maybe reflects an observational bias towards large q . If we suppose the latter is true, and that T14b observed a lower unbiased value for β , a higher number of L12 subsystems will be non-detected, which means that actually the number of subsystems L12 is equaling or even exceeding the number of secondary subsystems with respect to L11.

Case	N	ϵ	x_0	σ	β
All pairs	2162	0.571	4.54	2.40	0.094
		± 0.012	± 0.06	± 0.06	± 0.020
L1	1747	0.464	4.93	2.34	0.051
		± 0.011	± 0.06	± 0.06	± 0.011
L11	296	0.214	3.25	1.80	0.121
		± 0.012	± 0.12	± 0.09	± 0.026
L12	95	0.157	2.67	1.68	1.32
		± 0.016	± 0.17	± 0.10	± 0.28

Table 2.1: Fitted distribution parameters (taken from T14b).

2.3 Multiple star population synthesis

Once the free parameters of equation (2.4) have been fitted, the next step is to generate a population of multiple systems using these prescriptions. The algorithm developed by T14b starts generating a population of single and binary stars by random selection of a value l uniformly distributed over the range $[0, 1]$, followed by x_{L1} and q_{L1} drawn from the distribution (2.4) with parameters $(x_0, \sigma, \beta) = (5.0, 2.3, 0)$. If $l < \epsilon$ (criterion *i*) and $-0.3 < x_{L1} < 10$ (criterion *ii*), then the system is a binary star, otherwise a single star is created. When a binary system is created, the algorithm now must decide if it stays as such or each star is converted into a new (inner) binary, and the whole systems becomes a triple, quadruple, etc.. For instance, for each star in the binary the algorithm draws again values for l x_j and q_j , where $j = L11, L12$. If the main criteria *i* and *ii* plus certain conditions related to the dynamical stability are met, the star is transformed into a new inner binary with mass ratio q_j and period x_j . This procedure is repeated recursively for each star created, but for our purpose we only produce systems until quadruple configurations.

T14b used the absence of inner periods at $x_{L1} < 3$ (Fig.2.3) as first criterion for a potential bifurcation towards levels L11 and L12: if the binary has $x_{L1} > 3$ (criterion *iii*), each component is a candidate to transform into an inner binary, otherwise the system remains as binary. A fourth criterion is related to dynamical stability conditions described in Section 2.2.3 and makes use of the period ratio cutoff observed in systems with levels L11 and L12.

Tokovinin [2004] studied the dependence of the period ratio on e_L and suggests an

empirical stability limit similar to 2.2:

$$\frac{P_L}{P_S} > 5(1 - e_L)^{-3}. \quad (2.5)$$

Figure 2.4 shows the cumulative distribution of (2.2) and (2.5) for a cosine distribution of e_L between 0 and 0.8, that is, assuming moderate values of e_L for multiple stars (Shatsky [2001]). From this figure T14b proposes a crude model:

$$T(\Delta x) = \begin{cases} 0 & \Delta x \leq 0.7 \\ \Delta x + 0.7 & 0.7 \leq \Delta x \leq 1.7 \\ 1 & 1.7 \leq \Delta x \end{cases} \quad (2.6)$$

which allows to separate dynamically stable systems from those that are unstable. Here Δx is the difference between the logarithm of the outer and inner binary periods, where the latter is drawn from the same distribution defined for the outer binary. If $T(\Delta x) > T(\Delta x_{rand})$ (criterion iv), where Δx_{rand} is uniformly distributed in $[0, 1]$, the whole system is stable and retained.

To decide whether the generated inner binary is at level L11, L12 or both components of the outer binary are bifurcated (i.e, quadruple systems called 2+2), T14b used a correlation between levels L11 and L12, which was noted from an excess of 2+2 systems in the observed sample that can not be explained assuming a mutually independent occurrence. To account for this excess, the value of ϵ is increased by a factor of $\epsilon_+ = 1.2$ for the secondary subsystem at L12, if the primary subsystem at L11 is already present without subsystems. Otherwise, the frequency of L12 is multiplied by $\epsilon_- = 0.5$. This implies that it is mandatory to first evaluate the presence of L11 (and its possible subsystems) before producing a possible level L12 with high-order hierarchies. In addition, T14b adopted $\beta = 1.0$ for L12.

If a triple system with level L11 fulfilled the four aforementioned criteria for the primary component of the inner binary, the system becomes a quadruple star with level L111. For the purpose of this thesis we only need to generate a star population with at most three components, so bifurcations until level L111 allow us to discard those systems that continue bifurcating after reaching the triple configuration. Once the generation of subsystems at L11 has finished, we decide whether the components at level L12 become inner binaries or not. The occurrence of levels L121 (inner binary in the primary component at L12) and L122 (inner binary in the secondary component

at L12) is calculated in the same way as the subsystems at L11.

This procedure is repeated for each system and the final result only depends on five parameters: ϵ , ϵ_+ , ϵ_- , x_0 and β . However, the simulation with a fixed ϵ overproduces binaries and under-produces triples, while the multiplicity fraction is correct. To solve this issue, the final population consists of three equally large groups, each one with a specific value for ϵ . When ϵ is high, many hierarchical multiples are produced, and when it is low, we get mostly single stars and simple binaries. This reflects the idea that the observed sample is a mixture of "multiple-rich" and "multiple-poor" populations. The values adopted by T14b for the three groups are $\epsilon_i=[0.05,0.6,0.75]$ and its mean matches the multiplicity fraction of 0.466. The fraction of binaries, triples, quadruples, etc. is proportional to $\epsilon_i, \epsilon_i^2, \epsilon_i^3$ and so on. Compared to the case with constant ϵ , the multiplicity fraction of triples is increased by $\langle \epsilon^2 \rangle / \langle \epsilon \rangle^2 = 1.41$.

The final result of the simulation a is population composed by:

1. single star
2. binary system
3. triple system with level L11 (triple L11)
4. triple system with level L12 (triple L12)
5. quadruple system with level L111 (quadruple L111)
6. quadruple system with level L121 (quadruple L121)
7. quadruple system with levels L11 and L12 (2+2 systems)

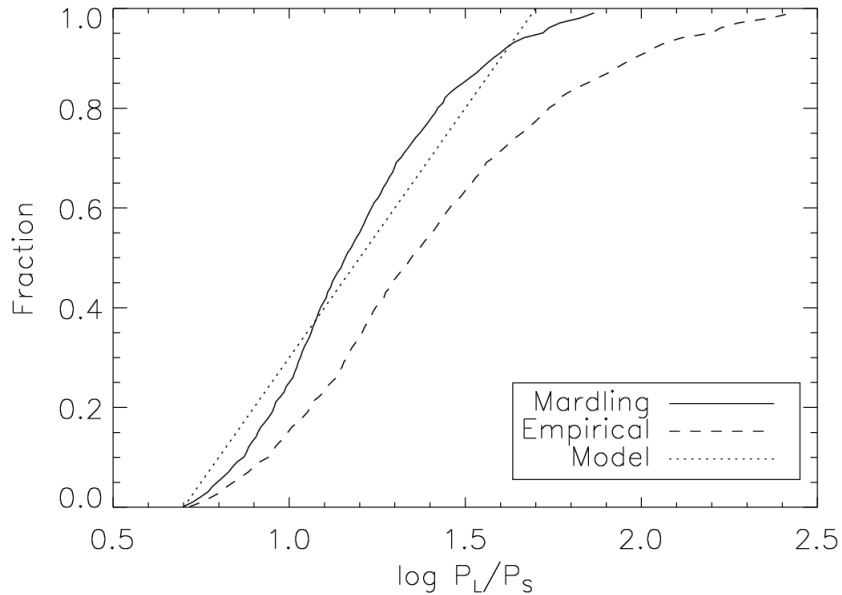


Figure 2.4: Comparison between the cumulative distributions of (2.2) (solid line) and (2.5) (dashed line) with the model (2.6). Figure adopted from T14b.

2.4 Simulation

Following the methodology presented in Section 2.3, a population of $N=3 \times 10^7$ systems composed by single, binary, triple and quadruple stars was simulated. Because this simulator only returns the periods and mass ratios of the systems, it is necessary to add the inclination between orbits, eccentricities, masses and ages to estimate potential effects of the Kozai mechanisms on triple system.

DM91 found an eccentricity distribution that depends on the period and is divided into three segments: $e = 0$ for $P < 11.6$ days, a “bell shaped” distribution for $11.6d < P < 1000d$ and $f(e) = 2e$ (Hadjidemetriou [1963]) for $P < 1000d$. Tokovinin [1997] and Tokovinin & Kiyaeva [2016] support the idea of a linear distribution for wide binaries from observations, while Sterzik et al. [2003] get a bell-shaped distribution for the outer binary in triple stars after removing systems with high eccentricities that do not meet Eq.(2.2). Based on these previous works, the eccentricity distribution used here is:

$$f(e) = \begin{cases} f_1(e) = 0 & x \leq 1 \\ f_2(e) = K \exp(-e^2/2\sigma^2) & 1 < x \leq 3 \\ f_3(e) = 2e \text{ or } f_3(e) = 1 & 3 < x \end{cases} \quad (2.7)$$

where a Rayleigh distribution was chosen for $f_2(e)$ (Fabrycky & Tremaine [2007]). Here we used two values for σ : 0.239 and 0.398, each one with $\langle e \rangle = 0.3$ and $\langle e \rangle = 0.5$ respectively. $f_3(e)$ follows the aforementioned linear distribution, but we also experiment with a more conservative uniform distribution. Figure 2.5 shows the eccentricity distribution for inner and outer orbits for triple systems, where according to criterion *iii* the two first segments ($f_1(e)$ and $f_2(e)$) correspond only to the distribution for inner orbits, while the third is a combination of eccentricities of inner and outer orbits. The mass of the primary component at level L1 is distributed according to the initial mass function (IMF) of Kroupa [2001]

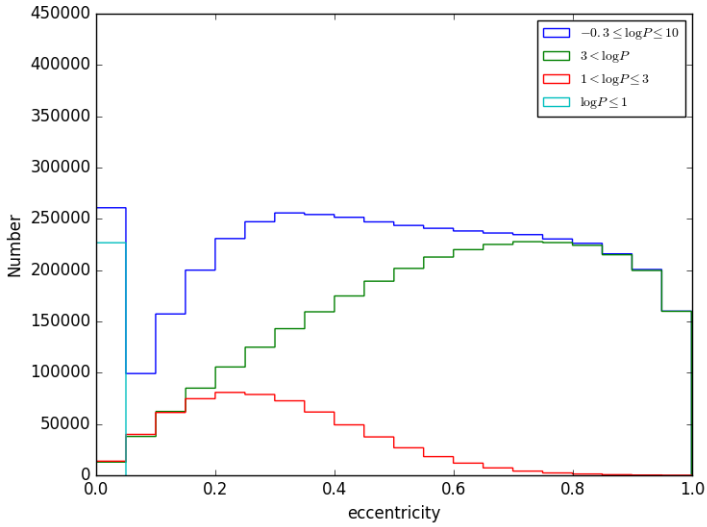
$$f(M_p) = \begin{cases} 0 & M/M_\odot < 0.01 \\ 1.987M^{-0.3} & 0.01 \leq M/M_\odot \leq 0.08 \\ 0.159M^{-1.3} & 0.08 < M/M_\odot \leq 0.5 \\ 0.079M^{-2.3} & 0.5 < M/M_\odot \leq 100 \end{cases} \quad (2.8)$$

where masses of inner binary components are calculated by using the mass ratio. Finally, a uniform birth rate is used in the range 0-10 Gyr (where 10 Gyr is today), while the inclination is drawn from an isotropic distribution i.e., uniform in $\cos(i)$. We synthesized in total four different populations (combination of different configurations for σ and the last segment of equation (2.7)), which follow the nomenclature given below:

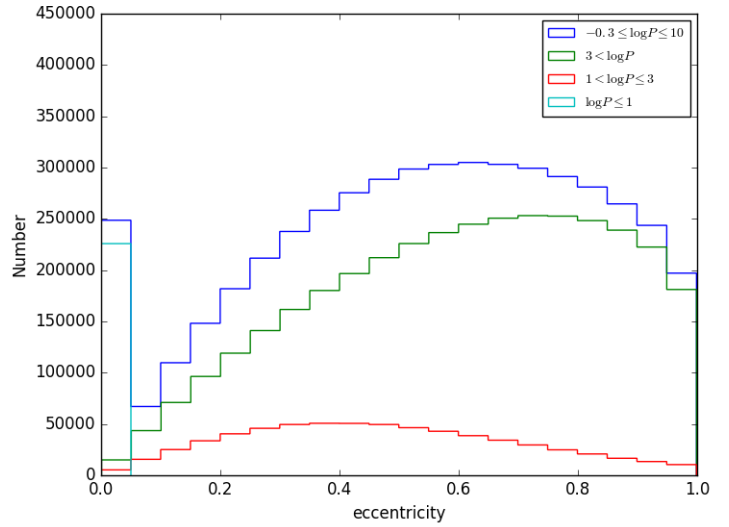
- SL03: **Simulation with Linear** $f_3(e)$ and $\langle e \rangle = \mathbf{0.3}$ for $f_2(e)$. Here $\sigma = 0.239$.
- SL05: **Simulation with Linear** $f_3(e)$ and $\langle e \rangle = \mathbf{0.5}$ for $f_2(e)$. Here $\sigma = 0.398$.
- SU03: **Simulation with Uniform** $f_3(e)$ and $\langle e \rangle = \mathbf{0.3}$ for $f_2(e)$. Here $\sigma = 0.239$.
- SU05: **Simulation with Uniform** $f_3(e)$ and $\langle e \rangle = \mathbf{0.5}$ for $f_2(e)$. Here $\sigma = 0.398$.

In all populations about 24% failed to fulfill the condition (2.2) after including

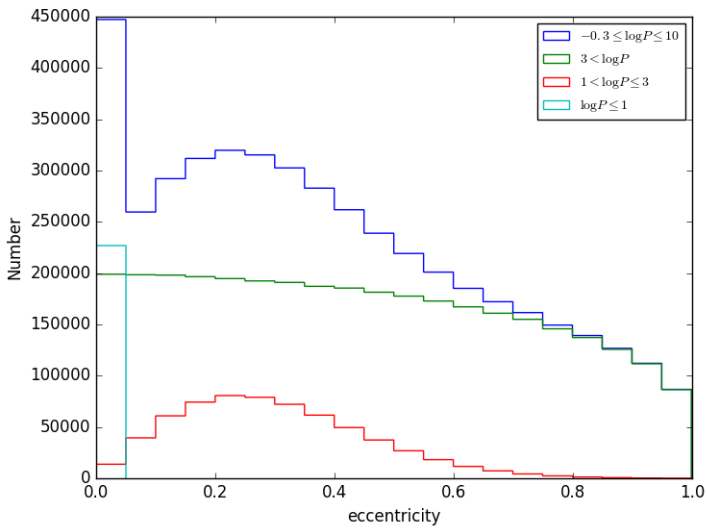
eccentricities and inclinations. Since the periods had already been chosen, we choose randomly the eccentricities, mass ratios and inclinations until the stability criterion was fulfilled. This readjustment only partially affects the distribution of eccentricity, shifting $f(e)$ to moderated values for $x > 3$ (Figure 2.5).



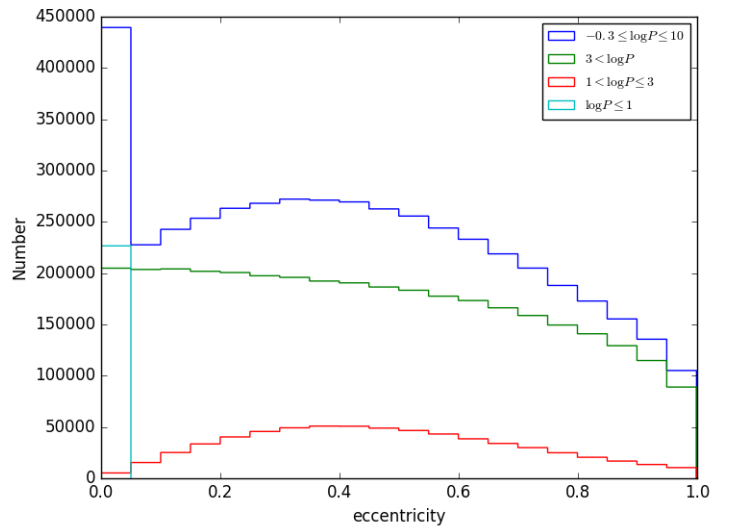
(a) $\sigma = 0.239$, linear



(b) $\sigma = 0.398$, linear



(c) $\sigma = 0.239$, uniform



(d) $\sigma = 0.398$, uniform

Figure 2.5: initial eccentricity distributions of inner and outer orbits of triple systems for the four simulations. The light blue, red and green histograms represent the three segments of $f(e)$ while the blue histogram is the combination of all of them.

2.4.1 Limitations

The multiplicity generator of T14b is certainly the best currently available tool to reproduce the observed multiplicity distributions. However, there are still serious limitations we have to be aware of:

- The method described above is subject to errors not only because of the missing information in observed samples, but also by the limited knowledge of the detection probabilities, uncertain data, subjective decisions, biases against multiple stars, uncertain number of white dwarf components, and approximations made in the data analysis. However T14b estimate that the fraction of hierarchical systems should be correct within 2%.
- The probability distributions and multiplicity fractions used here represent the final properties of multiple star populations, and not necessarily correspond to the primordial stage.
- Although we have used the simulator for a wide range of stellar masses, the original model of T14b only applies for sun-like stars. Despite this fact, according to table 2.1 the parameter β and the period distribution $f(P)$ for intermediate and high mass stars do not differ significantly from those used by T14b, while the multiplicity fraction f_M (or ϵ) estimated for more massive stars can be significantly higher than for Sun-like stars (at least 50%), increasing the fraction of triple systems to $\sim 50\%$ for B type stars (Toonen et al. [2016]).

CHAPTER 3

Evolution of binary and triple systems

Our observational survey is based on spectra of FGK stars plus UV excess that clearly indicates the presence of a WD. We also took radial velocity measurements in order to evaluate whether the FGK star is member of a close binary. If the latter is true, we then measured the periods and eccentricities of the close binaries. We expect the identified eccentric systems to be triples with the WD component either being part of the inner binary or the distant companion. To test this hypothesis we simulate both the evolution of binary and triple systems into systems with at least one WD, one close ($P \lesssim 100$ days) binary, and an FGK star. Each system is evolved using the BSE code, which in addition to simulating single star evolution, includes models of binary processes such as mass transfer, mass accretion, tidal interactions, common envelope evolution, and angular momentum loss mechanisms. In this chapter we introduce the main assumptions used in the Binary Stellar Evolution (BSE) code for the evolution of triple systems, the effect of mass loss on the final stability of triple systems, and how to measure the potential effects of the Kozai mechanisms.

3.1 Binary and triple evolution

The systems found in P16 (i.e. WD+FGK and the latter in a close binary setting) can have mainly two origins:

- Common envelope evolution.
- Triple interactions.

In this section we show the main assumptions in BSE to follow the common envelope evolution and how to combine the BSE algorithm with the *adiabatic mass loss* model in order to model the orbital evolution in triple systems.

Once the initial conditions for each system have been generated using the multiplicity statistics described in the previous chapter, the evolution of each binary (being part of a triple or just a simple binary) before the RLOF is described by a detached binary model considering stellar winds, tides and angular momentum loss mechanisms like gravitational radiation and magnetic braking. Both stars begin on the ZAMS with metallicity $Z = 0.02$. If one of the binary components fills its Roche Lobe and mass transfer begins, the stability of the process is determined by the mass radius exponent ζ discussed in Section 1.2.2. The common envelope stage is described by a mixture between the PRH and IYL prescriptions, where the gravitational energy of the envelope is taken in the same way as in the PRH formulation (Eq. 1.9) and the initial orbital energy as in the ILY formulation (Eq. 1.10). The orbital energy efficiency is $\alpha = 0.25$ (Zorotovic et al. [2010]) for all runs and the structural parameter λ is calculated at each time step. Since the BSE code only allows us to evolve single and binary stars, as a first approximation we will use the definition of hierarchical system to treat triples as binaries, composed by the inner binary (star 1, with mass $M_{bin} = M_1 + M_2$) and the farthest companion (star 2, with mass $M_{2,out} = M_3$), where the latter will be evolved as single star. Thus, the evolution of the outer orbit is not determined by BSE and must be approximated in an alternative way. Here we will use the *adiabatic mass loss model*, i.e. the expelled mass moves away from the inner binary isotropically without interacting with the distant companion and the outer orbit directly, while the outer eccentricity (e_{out}) remains constant. This approximation ($e_{out} = \text{constant}$) is valid only if the mass loss timescale is longer than the orbital period. In this case, the amount of angular momentum taken away by the lost

mass can be written as

$$\dot{J} = \dot{M}_{bin} a_{bin}^2 \omega, \quad (3.1)$$

where a_{bin} is the distance of the binary to the center of mass of the triple and

$$\omega = \frac{G(M_{bin} + M_{2,out})}{a^3} \quad (3.2)$$

the angular velocity. Replacing Eq. (3.1) in (1.5) (recalling that $\dot{M}_{2,out} = 0$ and $M_{tot} = M_{bin}$) and solving the equation, the relation between initial and final semi-major axes can be written as:

$$\frac{a_{2,f}}{a_{1,i}} = \frac{(M_{1,i} + M_{2,i}) + M_{3,i}}{(M_{1,i} + M_{2,i}) + M_{3,i} - \Delta m}, \quad (3.3)$$

where the subscript i and f represent the initial and final stages, M_3 is the mass of the furthest companion and

$$\Delta m = (M_{1,f} + M_{2,f}) - (M_{1,i} + M_{2,i}) \quad (3.4)$$

is the total amount of mass lost by the inner binary during the evolution. If the inner binary does not evolve through stages of mass loss but the third object does (this happens if the third object is the initially most massive one), Eq. (3.4) must be rewritten as $\Delta m = M_{3,f} - M_{3,i}$.

In the *adiabatic mass loss* model all the mass lost by the binary has left the triple system. This assumes that it has enough kinetic energy to escape not only from the inner binary but also from the entire triple system including the distant companion, which might not necessarily be true. To test this assumption in our simulations we express the escape velocity v_{esc} required to leave the inner and outer binaries as follows:

$$v_{esc,in} = \left(\frac{2G(M_1 + M_2)}{a_{in}(1 + e_{in})} \right)^{1/2}, \quad (3.5)$$

$$v_{esc,out} = \left(\frac{2G(M_1 + M_2 + M_3)}{a_{out}(1 + e_{out})} \right)^{1/2}. \quad (3.6)$$

If $v_{esc,in} > v_{esc,out}$ the mass lost by the donor is able to escape from the triple system. The criterion can be written as a function of inner (P_{in}) and outer (P_{out}) orbital period:

$$\frac{v_{in}}{v_{out}} = \left(\frac{1 + e_{out}}{1 + e_{in}} \right)^{1/2} \left(\frac{M_1 + M_2}{M_1 + M_2 + M_3} \right)^{2/3} \left(\frac{P_{out}}{P_{in}} \right)^{1/3} > 1. \quad (3.7)$$

The ratio between the velocities depends mainly on the ratio between the mass of the inner binary and the total mass of the triple as well as the eccentricity. In our simulations we find that 99,9% of triple systems that end with a inner binary composed of non-degenerate stars plus a distant WD companion fulfill the criterion given by Eq. (3.7), while for triples that end with an inner binary composed by a WD plus a non-degenerate companion and another non-degenerate star the fraction is $\sim 95\%$. The small fractions of systems in which the third companion might accrete a small fraction of the expelled mass is clearly negligible.

In addition to the above outlined change in separation of the outer binary, the adiabatic mass loss model assumes that the eccentricity of the outer orbit, e_{out} remains constant. This approximation is only valid if the mass loss timescale is larger than the orbital period. For systems where mass loss is only due to single star evolution (mainly mass loss on the asymptotic giant branch), the mass loss time scale ranges from 10^5 yr for a $10M_{\odot}$ star to $\approx 10^7$ yr for a solar type star ($M \approx 1M_{\odot}$). These long time scales justify the use of the adiabatic mass loss model. However, this approximation must be revised if mass loss is generated during a CE phase which is believed (from numerical simulations) to be very short ($\lesssim 10^3$ yr, Zorotovic et al. [2010]). What might happen in this case is described in the next section.

3.2 Dynamical instability after mass loss

One of the possible consequences of mass loss in a binary system is the ejection of one of its components. Hadjidemetriou [1963] showed that the sum of the

isotropic mass variation of both bodies is equivalent to a perturbative force with acceleration

$$a_{ML} = -\frac{1}{2} \frac{d}{dt} (\log m) v_{ML} \quad (3.8)$$

where v_{ML} is the magnitude of the velocity at the time t_{ML} when the mass variation begins. Here we use a crude approximation to evaluate the occurrence of ejection in the outer binary and the subsequent dissolution of the triple system, by assuming that the mass loss is instantaneous. To decide whether a body is ejected or not, we suppose that at t_{ML} a fraction $(1 - \beta)$ ($0 \leq \beta \leq 1$ is the remaining mass) of the total initial mass $M_{tot,0} = (M_{1,0} + M_{2,0}) + M_{3,0}$ is removed from the system. With the subscripts '0' and 'f' representing the stages before and after mass loss, the kinetic energy per unit mass at t_{ML} is

$$E_k(t = t_{ML}) = \frac{1}{2} v_{ML}^2 = \frac{1}{2} G M_{tot,0} \left(\frac{2}{r_{ML}} - \frac{1}{a_{out}} \right), \quad (3.9)$$

where r_{ML} is the distance between the inner binary and the furthest companion. This energy must be greater than the gravitational energy per unit mass just after mass loss

$$E_G(t = t_{ML}) = G \frac{M_{tot,f}}{r_{ML}}. \quad (3.10)$$

With $E_k(t = t_{ML}) > E_G(t = t_{ML})$ and using the polar equation of the ellipse for the outer orbit

$$r_{ML} = \frac{a_{out}(1 - e_{out}^2)}{1 + e_{out} \cos f} \quad (3.11)$$

where f is the eccentric anomaly, the ejection occurs if

$$\frac{1 - e_{out}^2}{2(1 + e_{out} \cos f)} > 1 - \beta \quad (3.12)$$

This is the *Impulse regime evolution* (Veras et al. [2011]), and for the case of circular

orbits the minimum amount of mass loss required for ejection is $(1 - \beta) = 1/2$ (Fig. 3.2). For eccentric orbits this mass depends on the eccentric anomaly with ejection being more likely near the periastron ($f \approx 0^\circ$).

In order to estimate the occurrences of ejection in eccentric systems we model the probability to find the outer object at certain f according to the time spent to pass a distance df . From second Kepler's law the distant companion sweeps an area dA in a time

$$dt = \frac{2(dA)\mu}{L}, \quad (3.13)$$

where $L = \mu[Ga_{out}(M_1 + M_2 + M_3)(1 - e_{out}^2)]^{1/2}$ is the total angular momentum of the outer binary and

$$\mu = \frac{(M_1 + M_2)M_3}{M_1 + M_2 + M_3} \quad (3.14)$$

is the reduced mass of the triple system. Using $dA = r_{out}^2 df/2$ and normalizing Eq.(3.13) with the orbital period

$$P_{out} = \left(\frac{4a_{out}^3 \pi^2}{G(M_1 + M_2 + M_3)} \right)^{1/2} \quad (3.15)$$

the probability density function of f can be write as:

$$p(f) = \frac{(1 - e_{out}^2)^{3/2}}{2\pi(1 + e_{out} \cos f)^2}. \quad (3.16)$$

Figure 3.1 shows $p(f)$ for five eccentricities. As expected, there is a large probability to find the outer companion near the apastron.

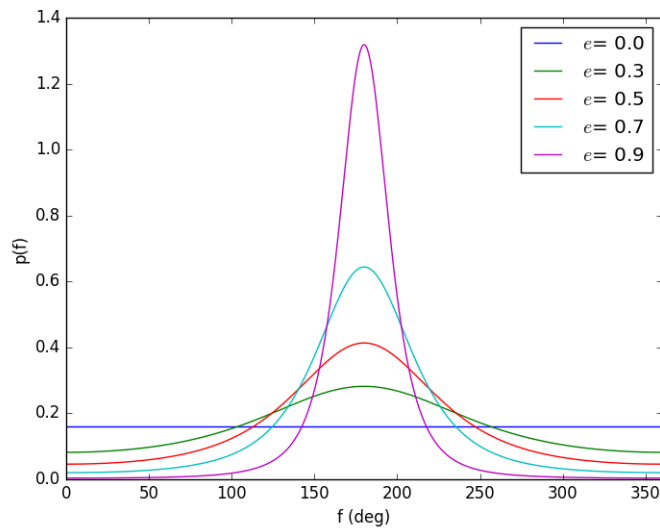


Figure 3.1: Probability density function of f (Eq. 3.16) for 5 eccentricity values. For $e = 0$ f is uniformly distributed, while for higher eccentricities it is more likely to find the object near $f \approx 180^\circ$.

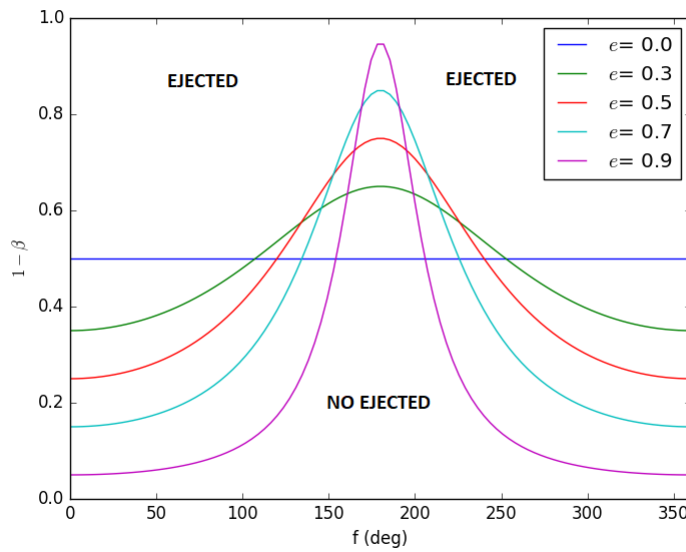


Figure 3.2: Ejection criteria (Eq. 3.12) for 5 eccentricity values. The star remains bound in the region below each curve, while it is ejected if it is located above them.

3.3 Measuring the influence of Kozai mechanisms

Due to the complex behavior of Kozai cycles during the evolution of triple systems, its strong dependence on initial conditions, and because performing detailed N-body simulations for each system is beyond the scope of this thesis, we only will be able to determine whether a system is potentially be affected by SKM, EKM or MIEK. To that end, we use the following criteria:

1. Initial inclination between inner and outer orbits in the range of Kozai angles (39.2° - 140.77°) implies SKM.
2. Initial $\epsilon_{oct,0} \geq 0.01$ implies EKM.
3. Initial $\epsilon_{oct,0} \leq 0.01$ and final $\epsilon_{oct,f} \geq 0.01$ implies MIEK.

For the test particle approximation we have that if $\epsilon_{oct} \geq 0.001$ the EKM is important (Shappee & Thompson [2013]). This implies that if we use this condition in criterion 2 and 3 we will have more systems with EKM and less systems with MIEK. This is because the first condition in criterion 3 is that the system initially does not experience EKM. However, as the simulated systems have non negligible mass components we make use of the condition $\epsilon_{oct} = 0.01$ based on previous simulations (see section 1.5.2).

The SKM, unlike the EKM, does not have a parameter that allows us to measure its influence on the triple evolution. For this reason we use the Kozai angles as a way to estimate the amount of systems that might be affected by the standard Kozai mechanism. Although this criterion is less restrictive than the other two and can overestimate the real fraction of systems where the SKM has some significant effect, this effect is to some degree compensated by the large eccentricity excitations that can take place for inclinations beyond the Kozai angles if we relax the test particle condition ($M_2 \neq 0$, Naoz [2016]).

3.4 Classifications and Nomenclatures

The presence of WD+FGK systems with the latter in a close eccentric binary in the survey of P16 can be explained if the whole system is triple. In what follows

we will explain the criteria to classify triples that may be confused as binaries, based on the properties of the unseen companion and the impact of different Kozai-Livov mechanisms on the formation of the inner close binary.

3.4.1 Spectral type assignation

As discussed in Section 1.6, we are interested in two particular configurations of triple systems, which can be confused with PCEBs in the spectroscopy data obtained in our observational project. Each of these configurations involve main sequence stars of spectral type F,G,K, and M. Here we will use the relation between mass and spectral type to extract from the BSE output the desired systems:

- stars with final mass in the range $0.45M_{\odot} \leq M \leq 1.4M_{\odot}$ are classified as stars with spectral type F,G, or K (hereafter FGK).
- stars with final mass in the range $0.08M_{\odot} \leq M < 0.45M_{\odot}$ are classified as stars with spectral type M.

3.4.2 PCEBs and contaminants

Aiming to organize all the final configurations and secular effects in binary and triple systems in each simulation, we identify two main groups and its respective sub-groups, which are described as follow:

- PCEBs: systems where the (inner) binary passed through a common envelope phase. They are the main target in the study of P16 and can be present in two configurations:
 - * WD/FGK: intrinsic close binary systems composed of a WD plus a FGK main sequence companion. This configuration corresponds to the population of interest in the survey of P16.
 - * WD/FGK + M: triple systems composed of a WD/FGK (PCEB) inner binary plus a faint companion of spectral type M. These systems may be affected by the Kozai mechanism, which together with the tight nature of the inner binary can lead to mergers.

– Contaminants: Triple systems where one of the components is a WD and the effect of Kozai mechanisms promotes the formation of close inner binaries. Here again we have two possible configurations:

- * $\overline{\text{WD/FGK}} + \text{M}$: Triple systems where one of the components of the inner binary is a WD formed by stellar evolution or stable mass transfer (and is therefore not a PCEBs). If the system experienced SKM or EKM since its primordial configuration, it is classified as SKM_0 or EKM_0 respectively, being a potential candidate to end as a triple system with a tight inner binary. The EKM_0 classification includes systems that experiences EKM during all the evolution and those where the EKM acts until the WD forms ($\epsilon_{\text{oct},0} > 0.01$, $\epsilon_{\text{oct},f} < 0.01$). Finally, if the Kozai mechanism is triggered by the mass loss, the system is classified as MIEK. Systems with general classification $\overline{\text{WD/FGK}} + \text{M}$ are named contaminants of class 1 or C1

- * $\text{FGK/M} + \text{WD}$: Triple systems where the inner binary is composed by an FGK main sequence star and a faint (unseen) M type star, while the WD is the distant companion. The classification for systems that experiences SKM or EKL since its primordial configuration is the same used for systems $\overline{\text{WD/FGK}} + \text{M}$. In this case the systems do not suffer MIEK since the FGK and M stars do not change significantly their mass during the evolution, which together with the increase of P_{out} (or a_{out} , Eq. 3.3) makes it impossible for the system to have EKM after the WD formation if it did not experience it before. In this configuration we also have systems that are not affected by Kozai mechanisms, but the primordial configuration of the system is a close FGK/M binary with inner period $P_{\text{in},0} < 100$ days that remains unchanged (or slightly decreases) during the evolution. These systems are labeled as $P_{\text{in},0} < 100d$.

We define systems with general classification $\text{FGK/M} + \text{WD}$ as contaminants of class 2 or C2.

3.5 Ejection and timescale filters

To measure the effect of mass loss on the short-term stability of triple systems we use Eq. (3.12), extracting f from the distribution (3.16). This *ejection filter* was applied 300 times to each simulation, to take into account the statistical effect of f in the final results. At the same time, if the system has SKM or EKM we compare the corresponding timescales T_{SKM} and T_{EKM} with the evolutionary time assigned to the system T_{evol} . If $T_{SKM} \leq T_{evol}$ or $T_{EKM} \leq T_{evol}$ then the Kozai mechanisms have enough time to alter the inner orbit eccentricity, otherwise the system is discarded as SKM or EKM. As the general relativity (GR) precession may suppress the Kozai mechanisms, a second *timescale filter* is applied by comparing its timescale

$$t_{GRP} = 2\pi \frac{a_{in}^{5/2} c^2 (1 - e_1^2)}{3G^{3/2} (M_1 + M_2)^{3/2}} \quad (3.17)$$

with the Kozai timescales, where c is the speed of light. If $T_{SKM} \leq T_{GRP}$ or $T_{EKM} \leq T_{GRP}$ then the GR precession is insufficient to prevent the Kozai mechanisms from acting. For systems $\overline{\text{WD/FGK}} + \text{M}$ with MIEK, we must consider that this process only acts after the mass loss (or WD birth), so that we must replace T_{evol} by T_{cool} and T_{GRP} by $T_{GRP,f}$, the WD cooling time and the GR precession timescale after the WD birth respectively.

Panel (b) in tables A.1 to A.4 shows the final results of each simulation after the filters are applied. Subgroups marked with (*) were not affected by the Kozai mechanism and we thus only applied the ejection filter.

CHAPTER 4

Results

In what follows we will describe and explain the main characteristics of contaminants for the four simulation and the effect of the filters on its total fraction.

4.1 Number of contaminants

We will describe the most relevant results concerning the fraction and nature of contaminants obtained in our simulations.

1. **The average fraction of contaminant is 23 %:** From Panel (a) in tables A.1 to A.4 the fraction of contaminants defined as

$$f_c = \frac{\text{Contaminants}}{\text{Contaminants} + \text{PCEBs}} \quad (4.1)$$

is 19.5%, 24.3%, 22.7% and 25.8% for simulations SL03, SL05, SU03 and SU05, respectively. Our estimated average fraction of contaminants is concordant with the observed fraction of WD/FGK binaries with eccentric fraction (≈ 33), taking into account that we do not consider observational biases.

2. **PCEB production is the responsible of variations in f_c** : the differences among the fractions of contaminants for each simulation are mainly due to variations in the total amount of intrinsic binaries that end up as PCEBs instead of the number of contaminants itself, since the number of PCEBs is higher than the latter by a factor of ≈ 3 for all simulations (Fig. 4.1).

It is to be expected that differences among the values of f_c obtained for each simulation depend only on the chosen eccentricity distribution. The increase of 3.1% and 4.8% observed between simulations with equal $f_3(e)$ (SU03 with SU05 and SL03 with SL05 respectively) arises mainly from the fact that when $\sigma = 0.398$ (SU05, SL05) the fraction of inner binaries with $x_{in,0} \leq 3$ and higher eccentricity values ($e > 0.4$) increases, promoting the formation of contact binaries (CBs) or mergers instead of PCEBs. For simulations with same σ in $f_2(e)$ the increase between 1.5 – 3.2% (SL05 with SU05 and SL03 with SU03) is due to the absence of wide binaries ($3.5 \leq x_{in,0}$) with very high eccentricity values. In this context values of $0.8 \leq e \leq 0.95$ allow tidal interactions that can not be possible for lower values of e . Figures 4.2 (a) and (b) show the wide binary population aforementioned with high eccentricities that evolve into PCEBs while figures 4.2 (a) and (c) show the fraction of binaries with $x_{in,0} \leq 3$ that become PCEBs instead CBs or mergers. Furthermore, note that only binaries with $e \lesssim 0.95$ (upper limit of figure 4.2) are present, since all binaries beyond this value end up in mergers or collisions.

3. **The main contribution to f_c comes from contaminants type 2:** This occurs for all simulations and can be understood as an effect of the following assumptions:

- Due to the mass range used to define the spectral types FGK and M ($\Delta m_{FGK} = 0.95$ and $\Delta m_M = 0.37$ respectively) and the uniform distribution ($\beta = 0$) used to randomly select the mass ratio at level L1, it is more likely to find the WD progenitor with an FGK type than an M type companion. This means that, previous to deciding whether the system becomes a triple with level L11 or L12, the algorithm favors the presence of contaminants C2.
- The ratio of systems WD/FGK + M that end up with an inner PCEB and those that end up as contaminants C1 ranges from $\approx 1 : 1$ (SL03)

to $\approx 2 : 3$ (SU05). This decrease of systems with PCEB in SU05 is a consequence of the second result given above.

4. **A small fraction of systems FGK/M + WD (about 1.3% of the total of contaminants C2 for all simulations) are $P_{in,0} \lesssim 100d$.**

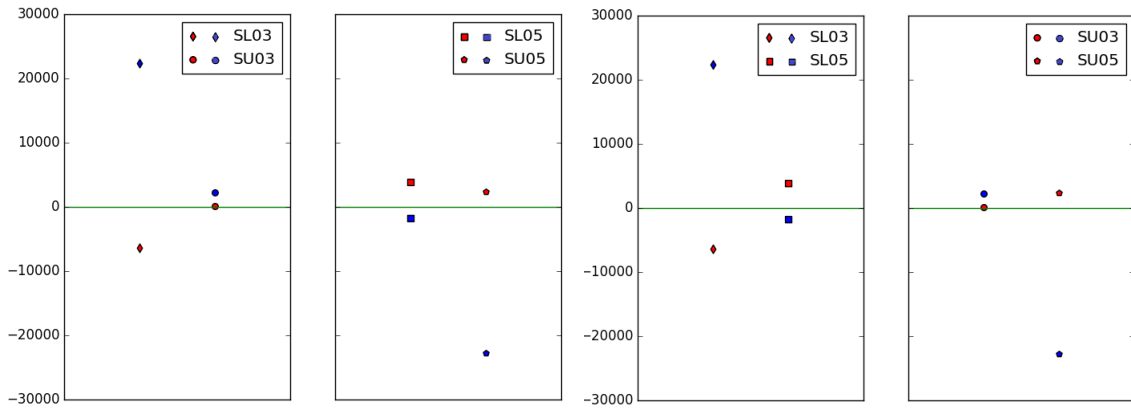


Figure 4.1: Difference between the number of PCEBs (blue) and contaminants (red) with respect its mean values (green lines), taking into account the four simulations. The number of PCEBs in each simulation varies more drastically with respect to the number of contaminants. Left: simulations with same σ (L03/U03 or L05/U05). Right: simulations with same distribution in $f_3(e)$.

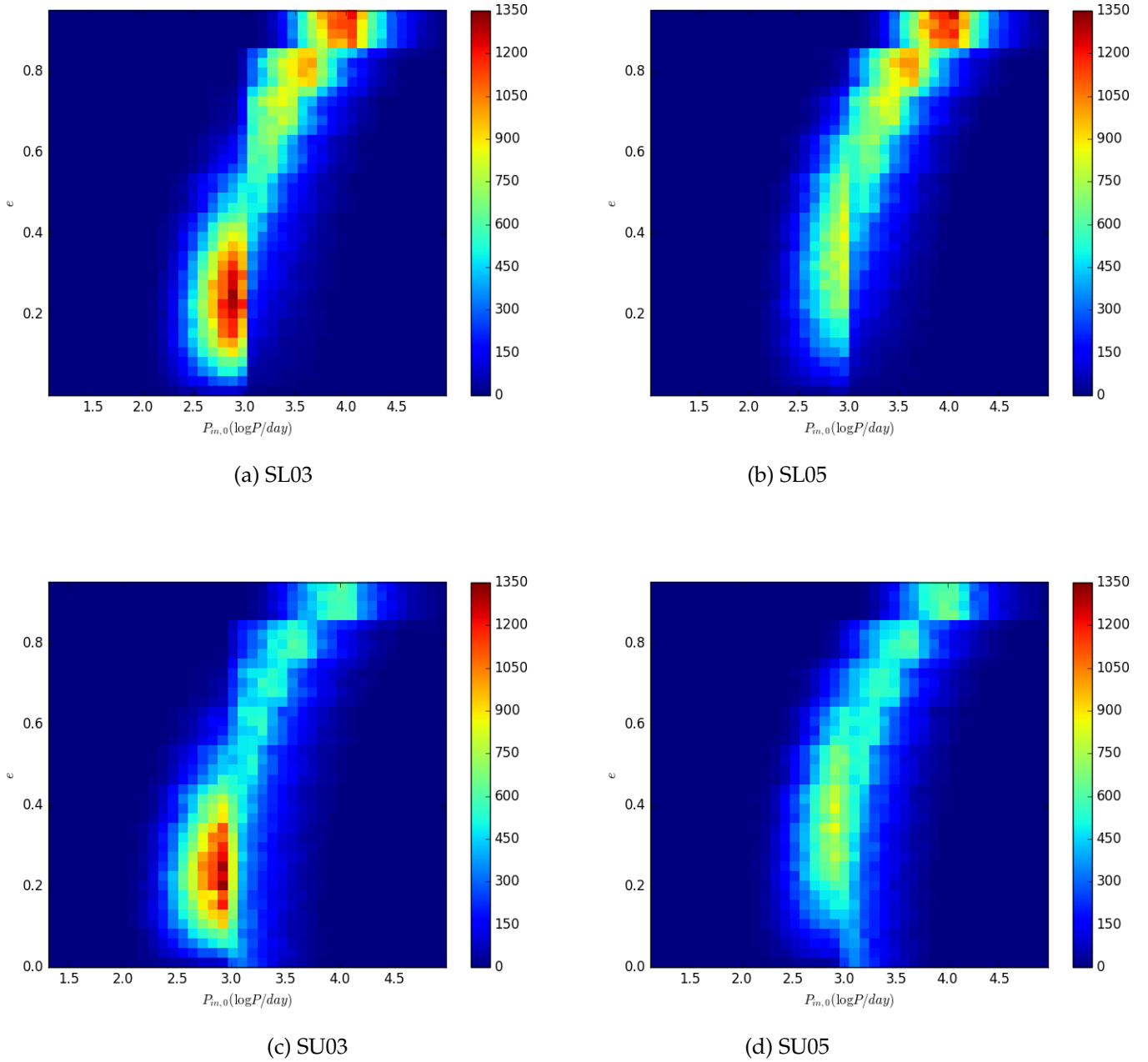


Figure 4.2: Initial distribution of periods and eccentricities for intrinsic binaries that become PCEBs.

4.2 WD mass-type and period distributions of contaminants

Table 4.1 resumes the number of WD types (He, CO and ONe) found in all simulations for each contaminant type, while Fig. 4.3 shows its mass distribution. The most relevant results are described below:

1. **$\approx 99\%$ of WDs in contaminants are CO WD:** This is because of the definition that we have used for contaminants, where almost all of the WD progenitors that have masses in the range $1M_{\odot} \lesssim M_{prog} \lesssim 6M_{\odot}$ evolve within a binary configuration but without significant interactions with its nearest companion (i.e, the WD progenitor evolves as a single star).
2. **Only contaminants C1 present He WDs:** A small fraction of inner binaries in contaminants C1 experiences stable mass transfer, allowing the formation of He WDs.
3. **The fraction of ONe WDs among C2 contaminants is $\approx 1\%$:** As WDs progenitors in contaminants C2 evolve as single stars, the more massive progenitors ($6 \lesssim M_{prog} \lesssim 8$) end up as ONe WDs. Although ONe WDs are present in just 1% of contaminants C2, this type of WDs is the second most frequent. .

Figures 4.4 and 4.5 show the initial inner and outer periods of contaminants C1 and C2 with classification EKM_0 . The main feature is the absence of contaminants C1 with $\log(P_{in,0}) \lesssim 3$, which is due to the fact that inner binaries with periods below this value end up as PCEBs, as seen in Fig. 4.6.

4.2. WD MASS-TYPE AND PERIOD DISTRIBUTIONS OF CONTAMINANTS

	He	CO	O/Ne
C1	29	12389	11
C2	0	43505	567

(a) SL03

	He	CO	O/Ne
C1	24	12697	6
C2	0	53277	624

(b) SL05

	He	CO	O/Ne
C1	22	14158	8
C2	0	47711	566

(c) SU03

	He	CO	O/Ne
C1	28	14053	7
C2	0	50066	614

(d) SU05

Table 4.1: WD type distribution for contaminants C1 and C2 for each simulation.

4.2. WD MASS-TYPE AND PERIOD DISTRIBUTIONS OF CONTAMINANTS

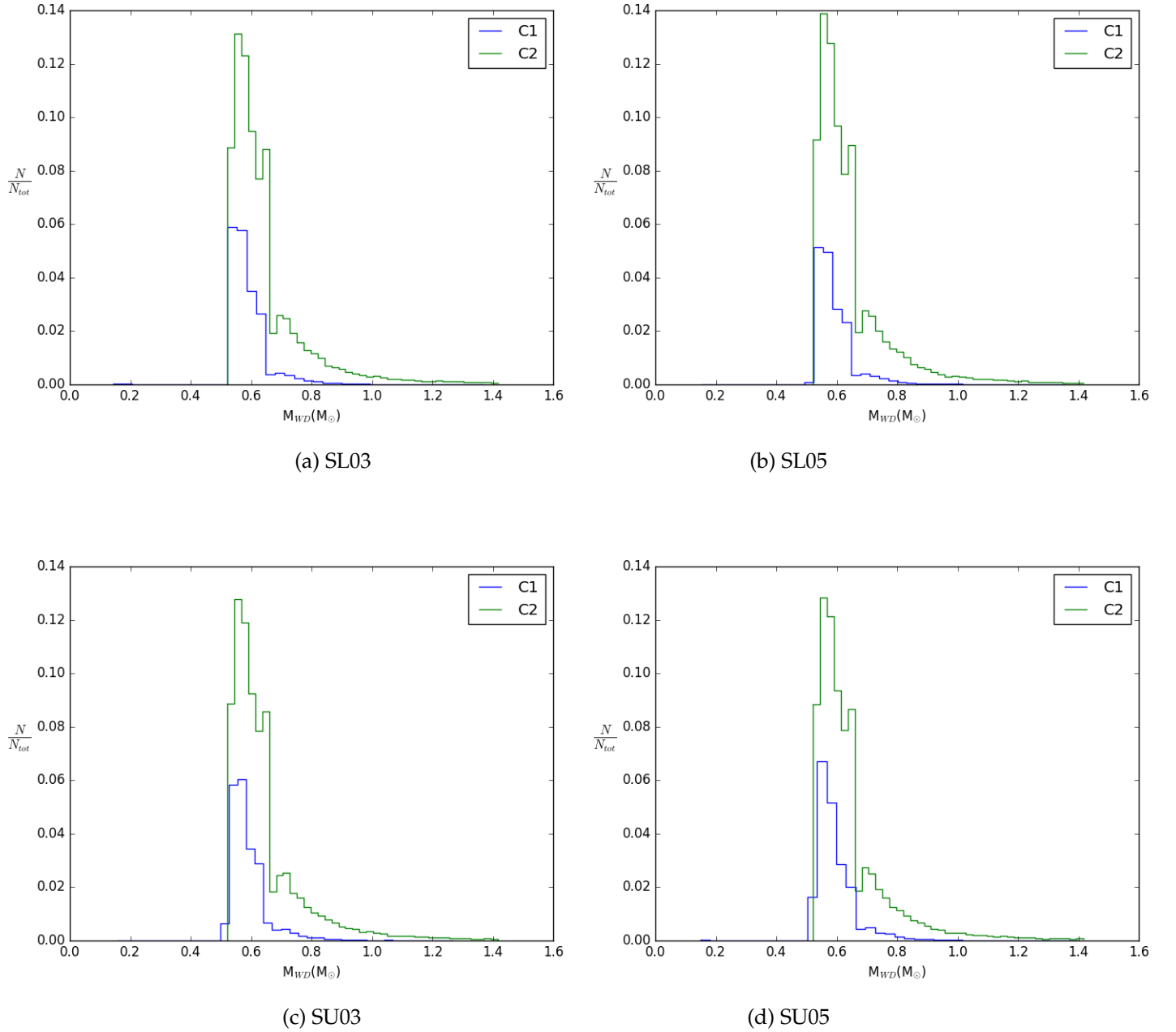
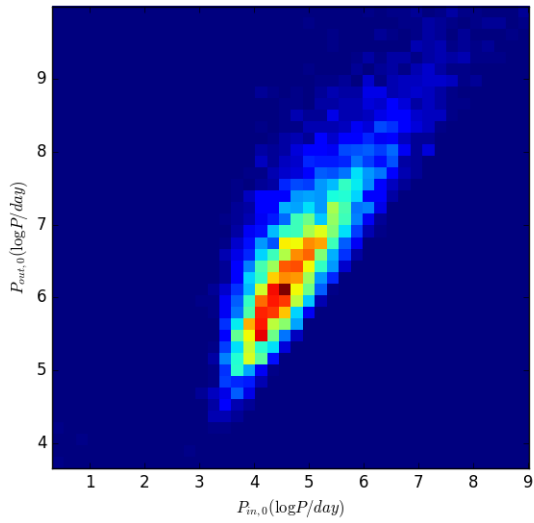
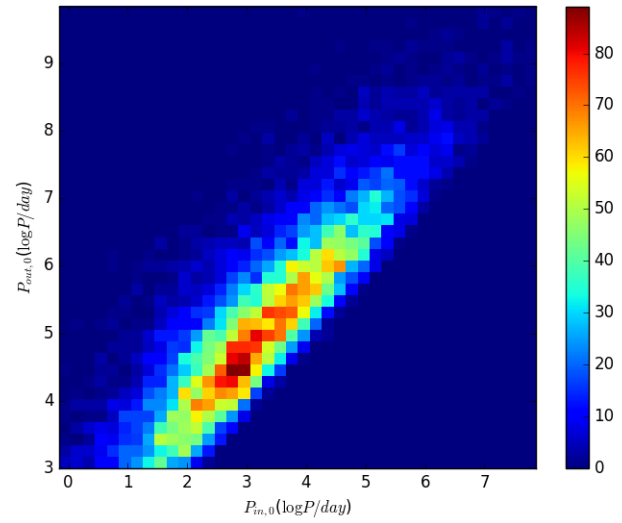


Figure 4.3: WD mass distribution for the different simulations. Blue and red histograms represent the WDs that belong to contaminants C1 and C2 respectively.

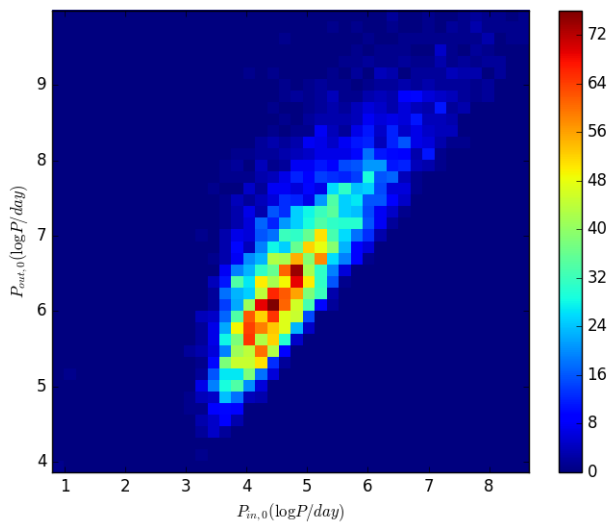
4.2. WD MASS-TYPE AND PERIOD DISTRIBUTIONS OF CONTAMINANTS



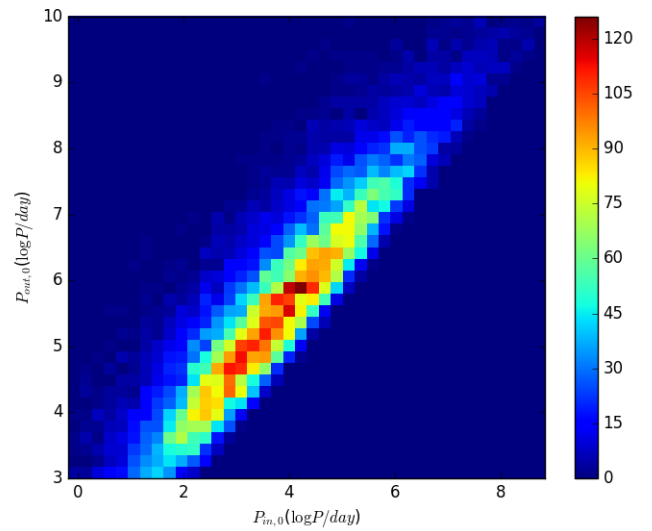
(a) C1 EKM₀ contaminants of SL03



(b) C2 EKM₀ contaminants of SL03



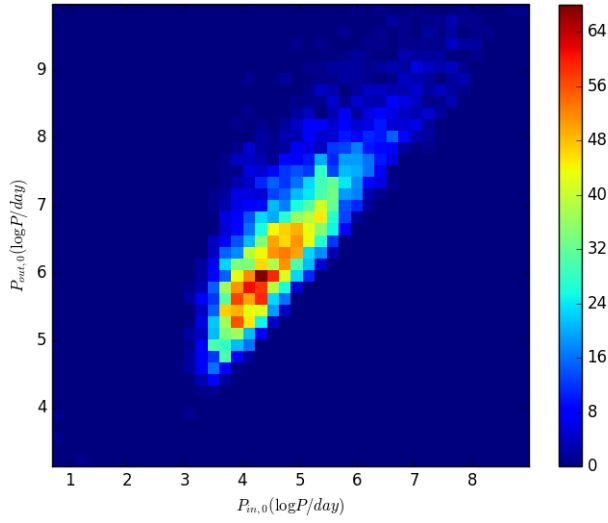
(c) C1 EKM₀ contaminants of SL05



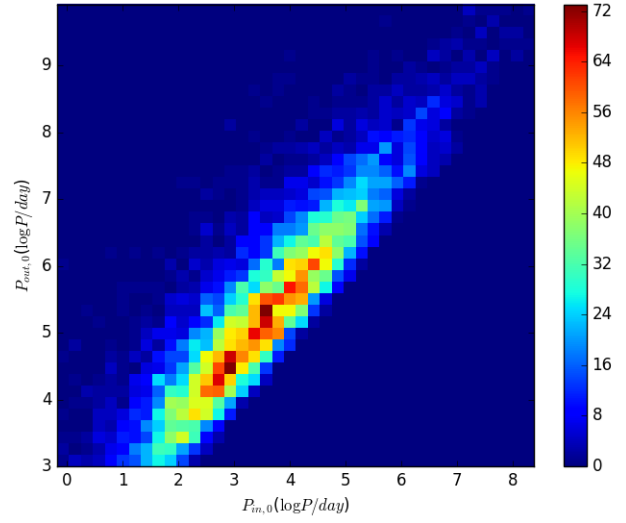
(d) C2 EKM₀ contaminants of SL05

Figure 4.4: Inner and outer initial period distribution of contaminants C1 (left panels) and C2 (right panels) with classification EKM₀. Top panels: simulation SL03. Bottom panels: simulation SL05.

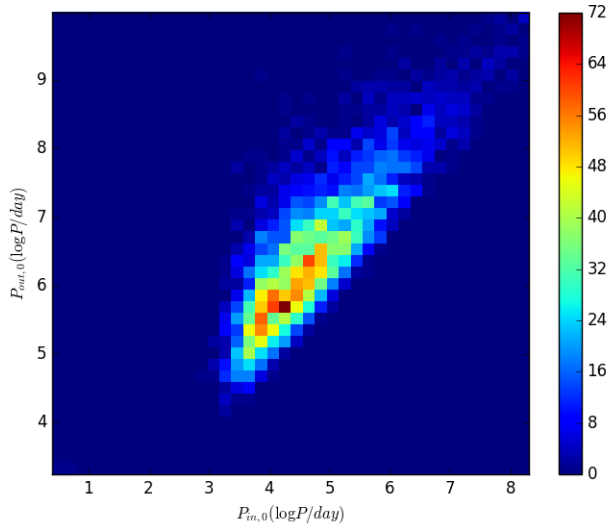
4.2. WD MASS-TYPE AND PERIOD DISTRIBUTIONS OF CONTAMINANTS



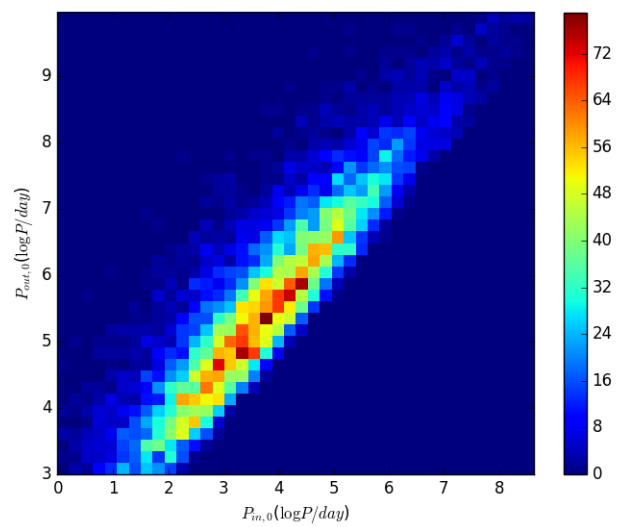
(a) C1 EKM₀ contaminants of SU03



(b) C2 EKM₀ contaminants of SU03



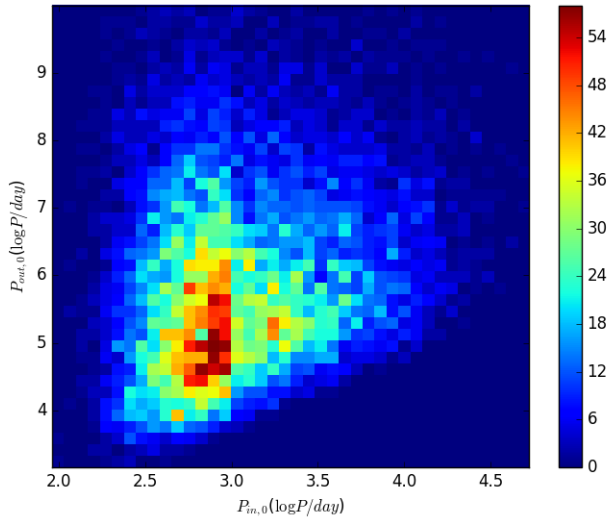
(c) C1 EKM₀ contaminants of SU05



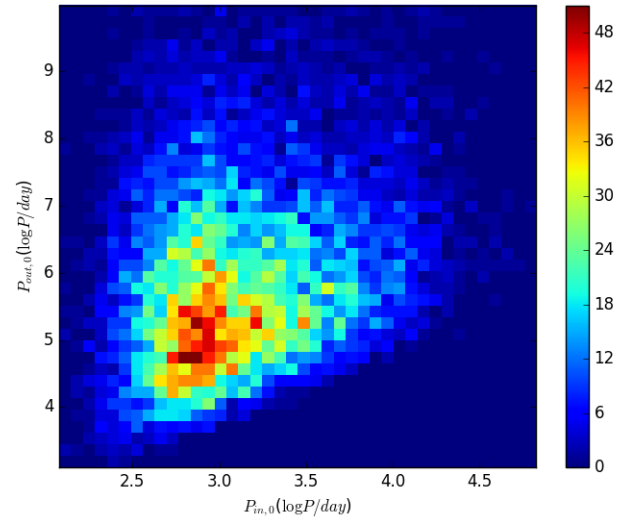
(d) C2 EKM₀ contaminants of SU05

Figure 4.5: Inner and outer initial period distribution of contaminants C1 (left panels) and C2 (right panels) with classification EKM₀. Top panels: simulation SU03. Bottom panels: simulation SU05.

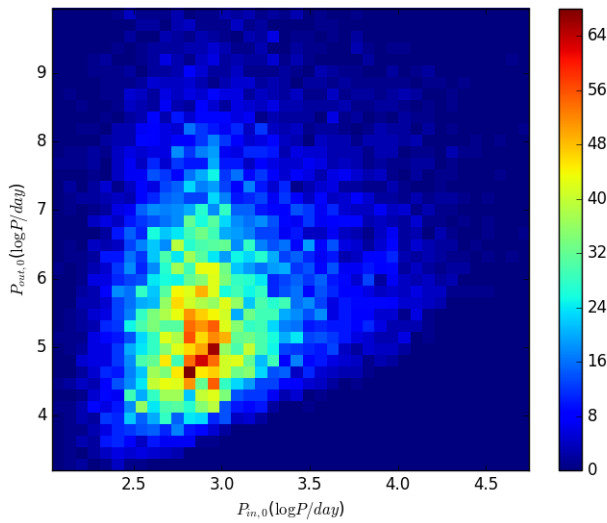
4.2. WD MASS-TYPE AND PERIOD DISTRIBUTIONS OF CONTAMINANTS



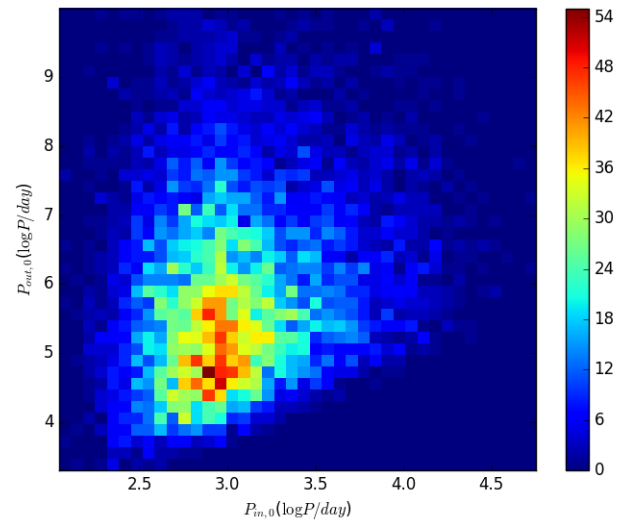
(a) WD/FGK + M triples of SU03



(b) WD/FGK + M triples of SU03



(c) WD/FGK + M triples of SU05



(d) WD/FGK + M triples of SU03

Figure 4.6: Inner and outer initial period distribution of triples with PCEBs (WD/FGK + M classification) for each simulation.

4.3 Number of contaminants with filters

As we discussed in section 3.1, the ejection filter used here is valid only if the mass loss time-scale is greater than the outer orbital period (P_{out}). This is true for WD/FGK + M triples (i.e., triples with an inner PCEB), where we assume that the mass loss by CE evolution occurs on time-scales of $\lesssim 10^3$ yr ($\approx 10^{5.5}$ days). In our simulations, about 57 per cent of the WD/FGK + M triples match that 10^3 yr $< P_{out,0}$. Taking into account this consideration and applying the ejection filter only to WD/FGK + M triples (time-scale filters remains over all contaminants) the fraction of contaminants for SL03, SL05, SU03 and SU05 is 15%, 19.5%, 17.8% and 20.6% respectively, giving a mean contaminant fraction of 18.2%, which is still concordant with the observed fraction of WD/FGK binaries with eccentric orbits (recalling that we do not take into account observational biases).

In what follows we describe how the filters act on each type of contaminant.

The effect of the filter by evolutionary time on contaminants C1 and C2 is shown in the upper and bottom panels of figure 4.7 respectively. The main observed feature is that the combined population of contaminants C1 with SKM₀ and EKM₀ shows longer Kozai-Lidov(KL) time-scales (with peak at $\approx 10^{7.7}$ yr) compared to contaminants C2 (peak at $\approx 10^{5.7}$ yr). This tendency towards shorter KL time-scales for the latter can be explained by three factors:

1. According to equations 1.17 and 1.20 $t_{SKM} < t_{EKM}$ for a given triple, since $\epsilon_{oct} < 1$ (Eq. 1.19)
2. Since $t_{SKM} \propto M_3^{-1}$, where M_3 is the mass of the distant companion, contaminants C2 tend to have shorter SKM time-scales than contaminants C1.
3. The ratio between systems with standard (SKM₀) and eccentric (EKM₀) Kozai-Lidov mechanisms before applying any filter for contaminants C2 ranges from 2.8 to 4.4, while for contaminants C1 it is between 0.9 and 1.9. This tendency of contaminants C2 to have more systems with SKM₀ than with EKM₀ remains after applying the evolutionary time filter.

Then, since we have more SKM₀ than EKM₀ systems, and these have shorter time-scales, the upper histogram in figure 4.7 (bottom panel) also moves to shorter time-scales.

On the other hand, the distribution of evolutionary time (right histogram) is constrained by the time required to form the WD. As most of the WD progenitors

had masses close to $1M_{\odot}$, their lifetimes are $\approx 10^{10}$ yr, which is reflected in the peak observed at $\approx 10^{10}$ yr.

Following the same analysis, the effect of the time-scale filter by general relativity (GR) precession on contaminants C1 and C2 is shown in the upper and bottom panels of figure 4.8 respectively. Here we can observe the same feature related with shorter KL time-scales for contaminants C2, which in turn shift the distribution of the GR precession time-scale (t_{GRP}) to lower values. Another interesting feature in Fig. 4.8 is the cut at $\approx 10^8$ yr on t_{GRP} , which is due by its strong dependence with the inner semi-major axis ($t_{GRP} \propto a_{in}^{5/2} \propto P_{in}^{5/3}$, Eq. 3.17) and the fact that for contaminants C1 $P_{in} \gtrsim 10^3$ days (see panels (a) and (c) of figures 4.4 and 4.5), setting the observed lower limit for t_{GRP} . However, three systems are clearly beyond this lower limit. Unlike the rest of contaminants C1, the formation of its WDs at shorter periods (avoiding the CE evolution) was possible by stable mass transfer.

Contaminants C1 with MIEK follow approximately the same behaviour than contaminants with SKM and EKM, taking into account that for this type of systems, we must replace the evolutionary time by the cooling time of the WD, since the oscillations begin after the formation of the WD.

Regarding the filter by ejection, figures 4.10, 4.11 (contaminants C1) and figures 4.12, 4.13 (contaminants C2) show that as expected, systems with high eccentricities can avoid ejection events even for high amount of mass lost, since it is more likely to find the distant companion (or the inner binary) near the apastron, which in turn increase the tolerance to ejection (see Eq. 3.12). We also observe that contaminants C2 experience more mass loss than contaminants C1, since for the former we assume that all the mass lost by the WD progenitor is completely removed from the triple, while for the later some of the mass lost by the WD progenitor can be transferred (e.g. by stellar wind) to its companion.

4.3. NUMBER OF CONTAMINANTS WITH FILTERS

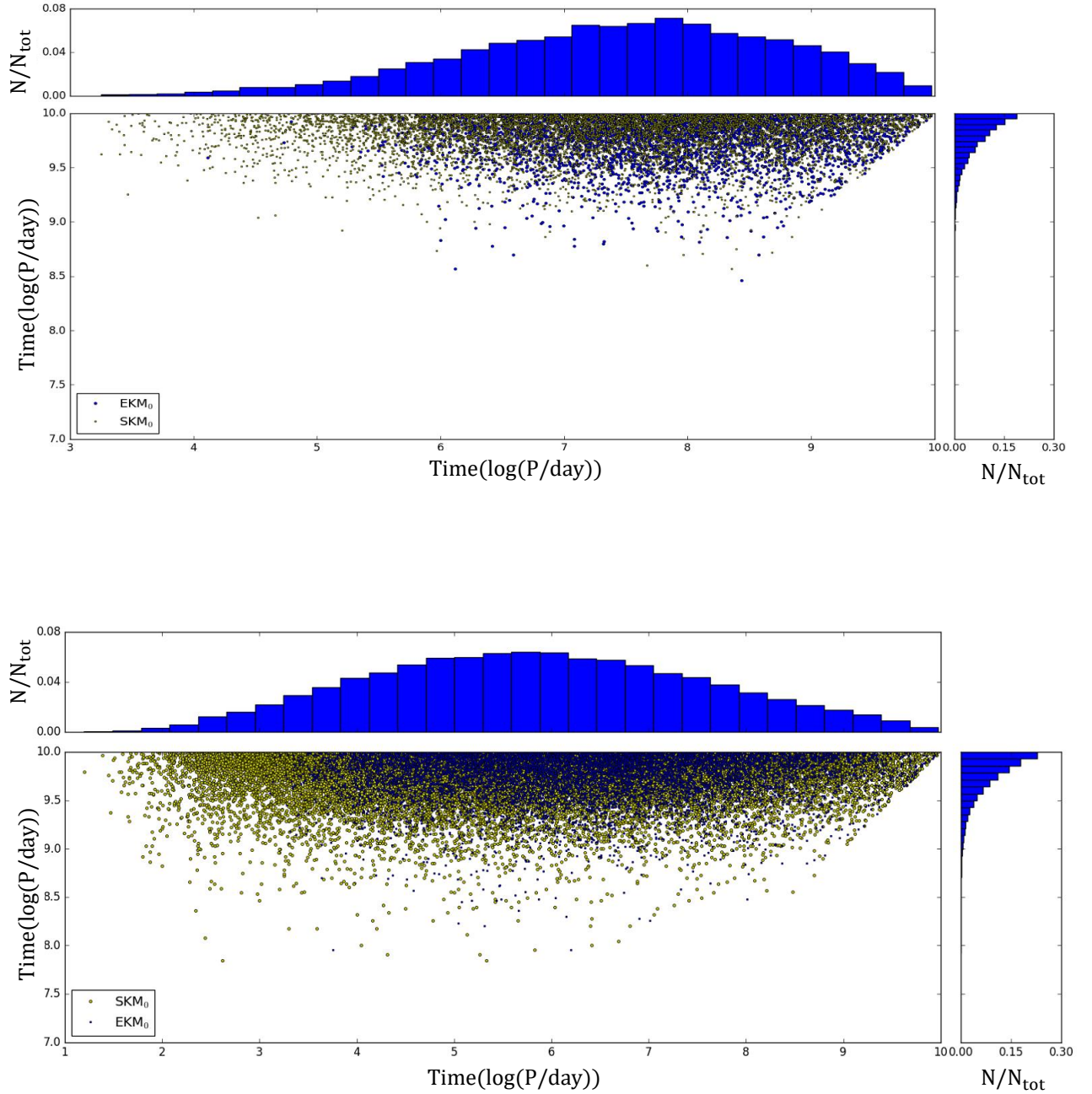


Figure 4.7: Comparison between the Kozai-Lidov mechanisms time-scales (X axis) vs the evolutionary time (Y axis) for contaminants C1 (upper panel) and C2 (bottom panel) that have passed the filter by evolutionary time. For the case of MIEK system the Y axis corresponds to the WD cooling time. Here we only show the results for the simulation SU05, since it reflects in a good way the general behaviour for the rest of simulations.

4.3. NUMBER OF CONTAMINANTS WITH FILTERS

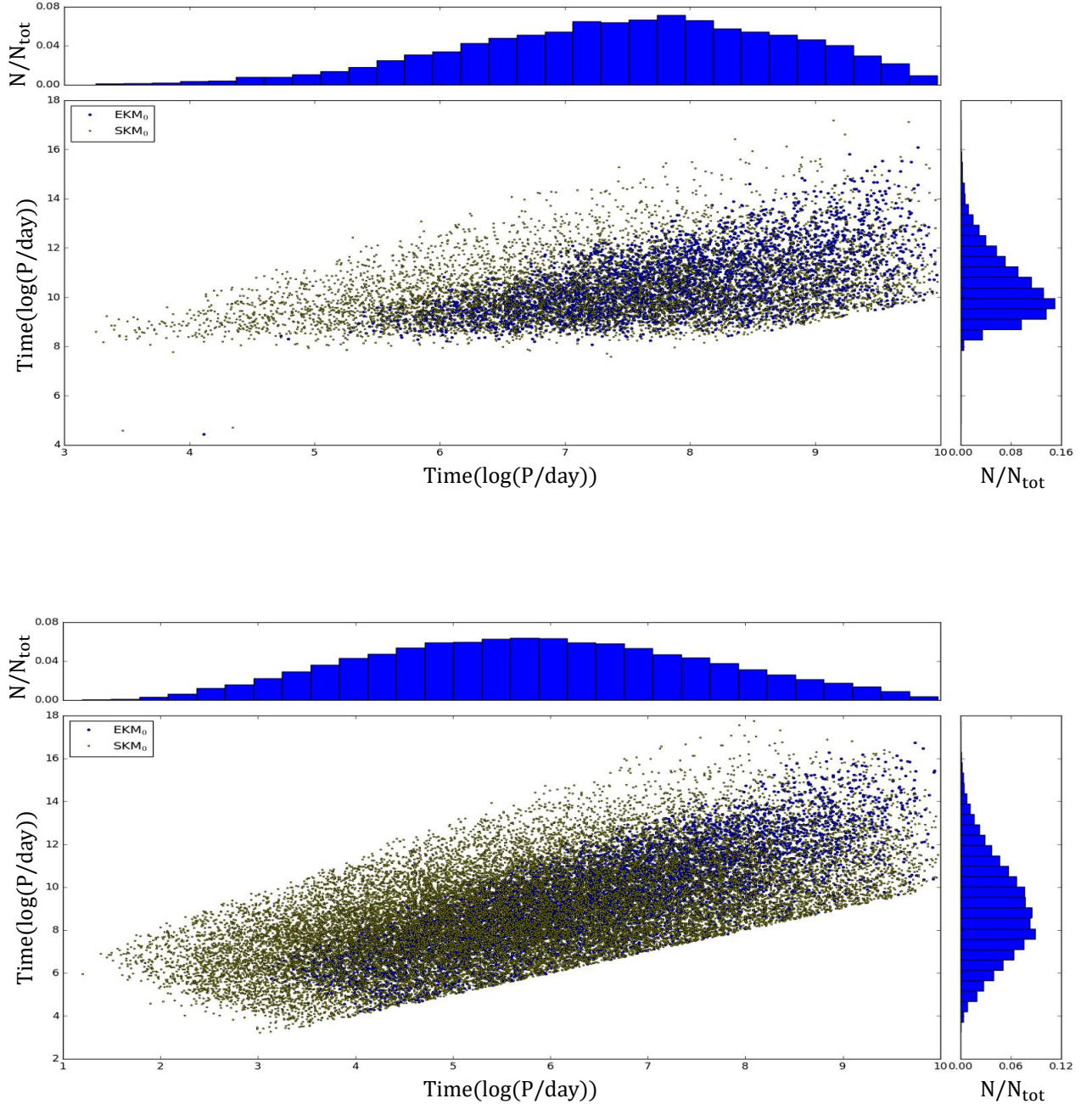


Figure 4.8: Comparison between the Kozai-Lidov mechanisms time-scales (X axis) vs the GR precession time-scale (Y axis) for contaminants C1 (upper panel) and C2 (bottom panel) that have passed the filter by GR precession. Here we only show the results for the simulation SU05, since it reflects in a good way the general behaviour for the rest of simulations.

4.3. NUMBER OF CONTAMINANTS WITH FILTERS

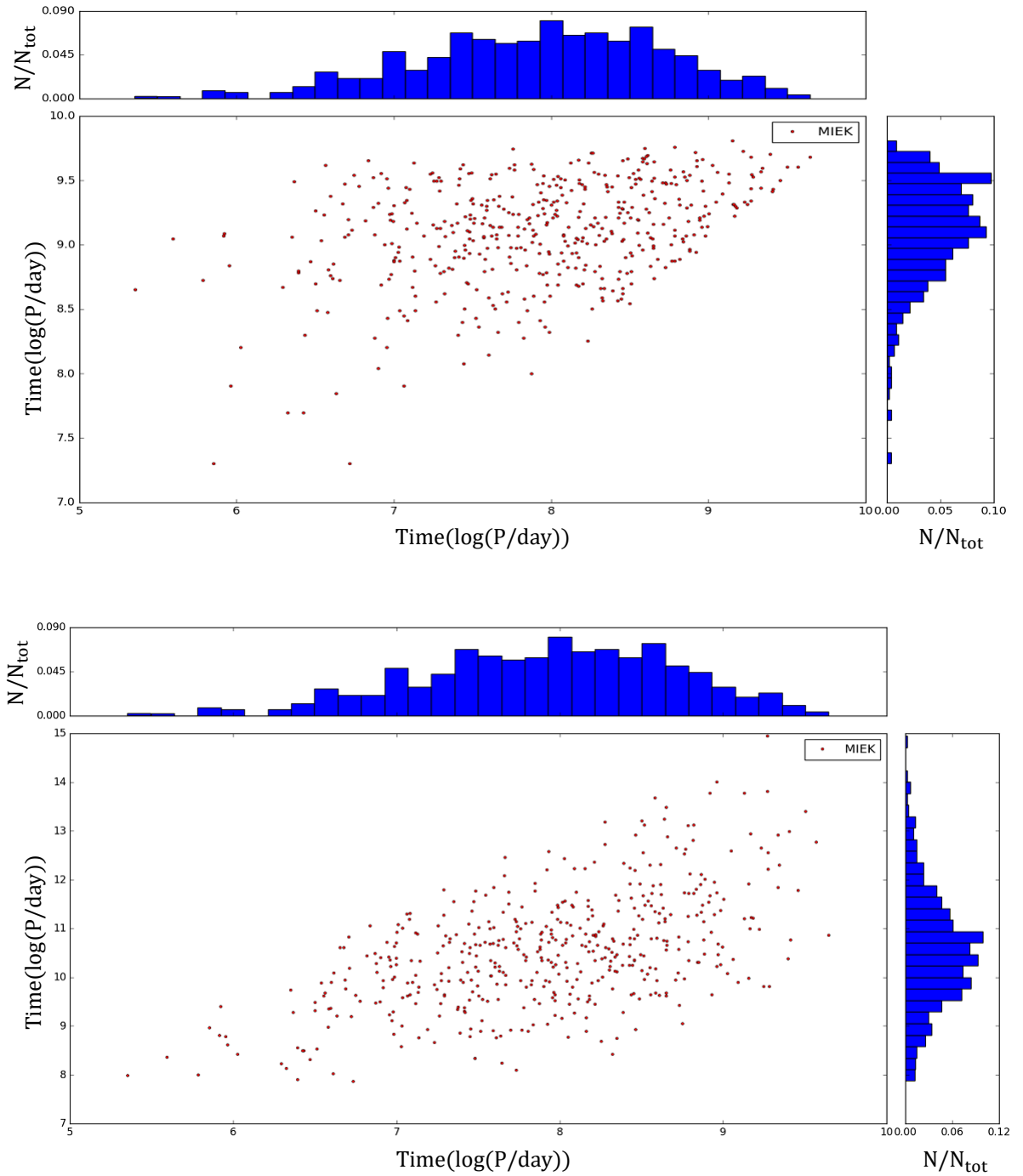


Figure 4.9: MIEK systems that have passed the time-scale filters. **Upper panel:** Comparison between the Kozai-Lidov mechanisms time-scales (X axis) vs the cooling time (Y axis) for contaminants that have passed the filter by cooling time. **Bottom panel:** Comparison between the Kozai-Lidov mechanisms time-scales (X axis) vs the GR precession time-scale (Y axis) that have passed the filter by GR precession. Here we only show the results for the simulation SU05, since it reflects in a good way the general behaviour for the rest of simulations.

4.3. NUMBER OF CONTAMINANTS WITH FILTERS

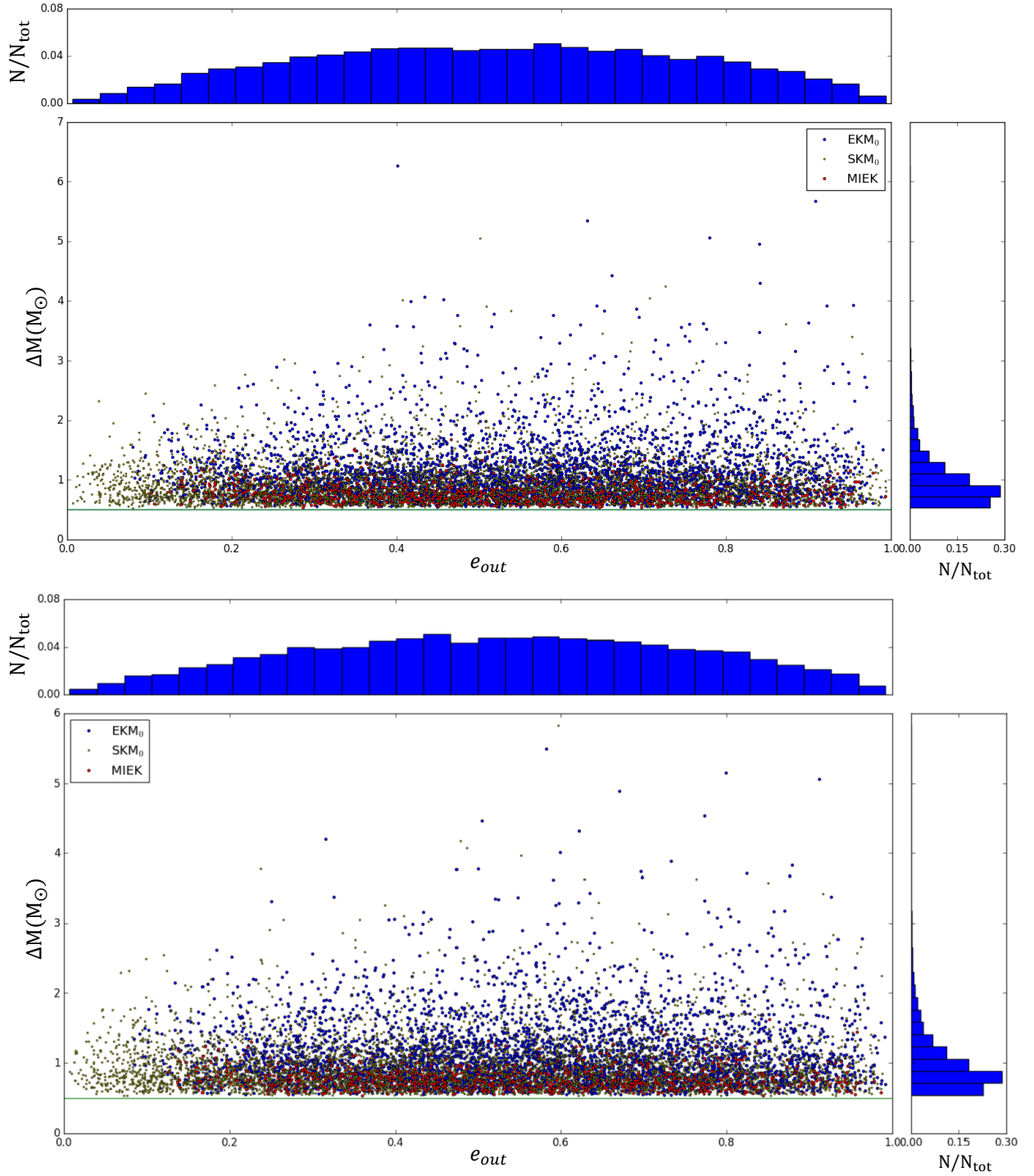


Figure 4.10: Distribution of outer eccentricities (X axis, upper histograms) and the amount of mass lost (Y axis, right histograms) of contaminants C1 that have passed the ejection filter. The bottom and upper panel correspond to the simulations SL05 and SL03 respectively.

4.3. NUMBER OF CONTAMINANTS WITH FILTERS

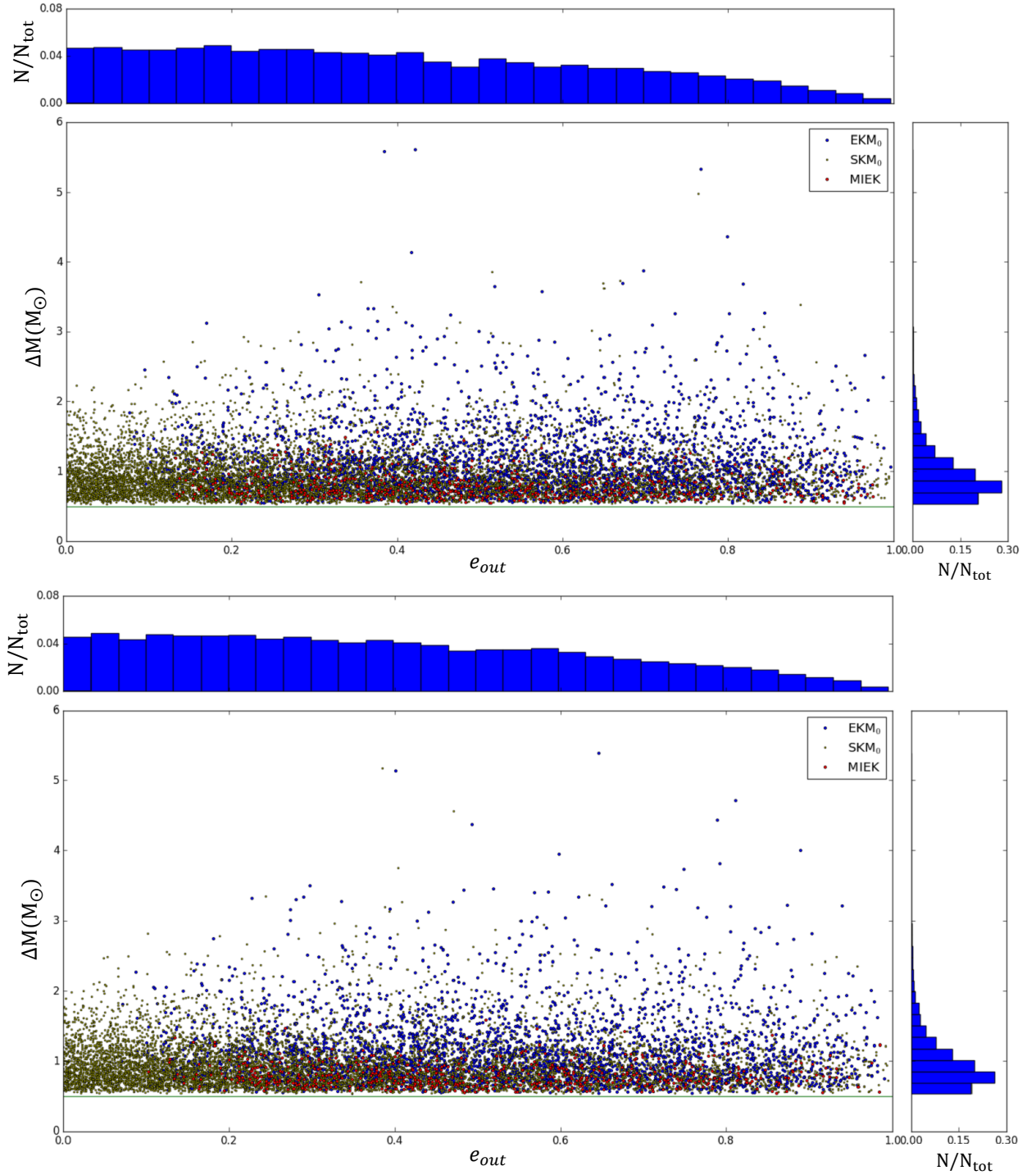


Figure 4.11: Distribution of outer eccentricities (X axis, upper histograms) and the amount of mass lost (Y axis, right histograms) of contaminants C1 that have passed the ejection filter. The bottom and upper panel correspond to the simulations SU05 and SU03 respectively.

4.3. NUMBER OF CONTAMINANTS WITH FILTERS

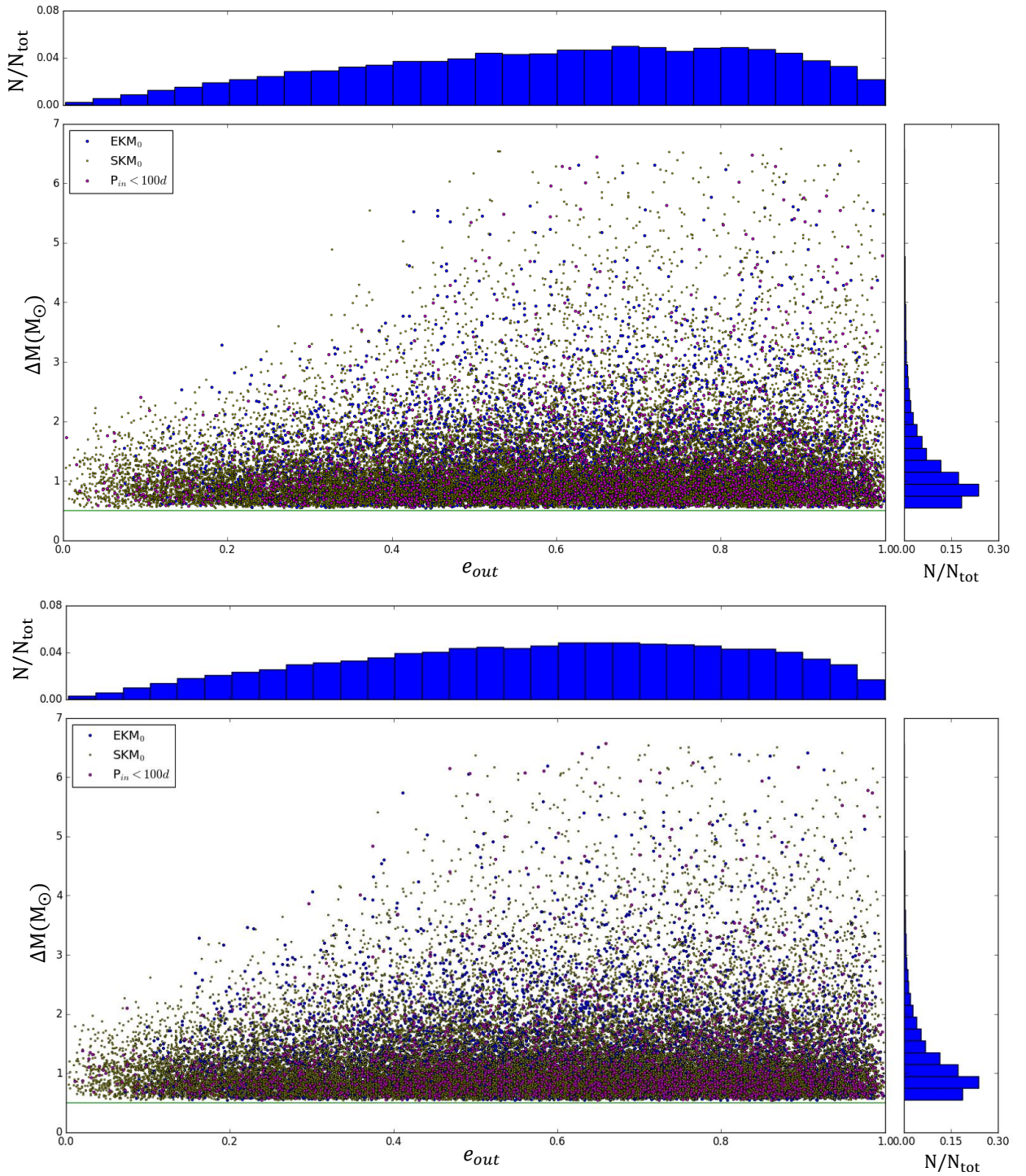


Figure 4.12: Distribution of outer eccentricities (X axis, upper histograms) and the amount of mass lost (Y axis, right histograms) of contaminants C2 that have passed the ejection filter. The bottom and upper panel correspond to the simulations SL05 and SL03 respectively.

4.3. NUMBER OF CONTAMINANTS WITH FILTERS

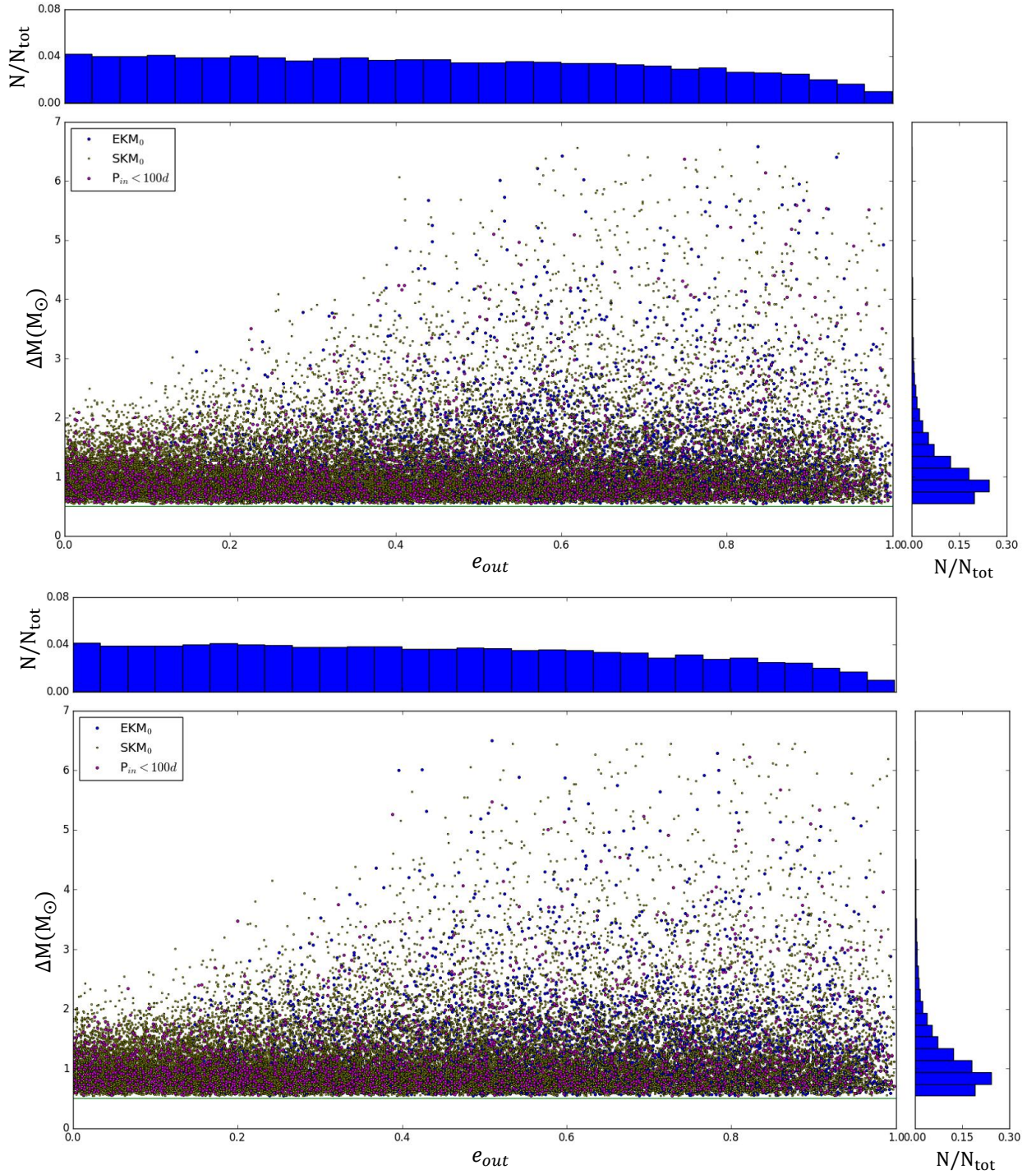


Figure 4.13: Distribution of outer eccentricities (X axis, upper histograms) and the amount of mass lost (Y axis, right histograms) of contaminants C1 that have passed the ejection filter. The bottom and upper panel correspond to the simulations SU05 and SU03 respectively.

4.4 Conclusion

We found that, on average, 23% of PCEBs composed by a main sequence star of type F,G or K plus a white dwarf could be indeed triple systems. About 79% of these triples have the WD outside the inner binary, which is composed by a main sequence FGK star plus a M type star hidden due the high contrast with its closest companion, while the remaining 21% correspond to triples where the WD belongs to the inner binary and the distant companion is a M type star. When we apply the ejection and time-scale filters, the fraction of contaminants is reduced to ≈ 18 percent, keeping almost the same ratio between contaminants C1 and C2 without filters.

It is worth recalling that all these fractions are subject to errors associated to the different assumption that we made along this work, and need to be improved implementing a binary and triple population synthesis that covers both low and intermediate-high mass stars, and a more accurate algorithm to describe the secular orbital dynamics of hierarchical triples. Nevertheless, our estimated fractions of contaminants (obtained without considering observational biases) are in the same order of magnitude as the observed number of eccentric systems, which in turn, could therefore be triple systems.

CHAPTER 5

TYC 7218-934-1

One of the first targets in our survey of WD/FGK binaries showing radial velocities variations and where we measured the orbital period was TYC 7218-934-1. Interestingly, this object clearly has an eccentric orbit with a period 13.6 days. The estimated mass of the G-type star is $m_0 = 1.04M_{\odot}$, while the calculated minimum mass for its companion is $m_1 = 0.2M_{\odot}$. The eccentric orbit implies that this close binary system cannot be a post common envelope binary as friction inside the common envelope would quickly circularize the orbit. Thus, the close binary nature of TYC 7218-934-1 has been most likely generated by triple star interactions, where either an unseen distant companion perturbs the FGK/WD orbit or the WD itself is the outer component. We observed the system with SPHERE looking for the third object.

In what follows we describe the observations of TYC 7218-934-1 and then explore the possible influence of Kozai-Lidov mechanisms during its evolution.

5.1 Target selection and HST observations

The targets selected in our survey come from the Radial Velocity Experiment (RAVE) survey data release 4 (Kordopatis et al. [2013]) in the Southern Hemisphere, and the Large Sky Area Multi-Object Fiber Spectroscopic Telescope

(LAMOST) survey in the Northern Hemisphere (Cui et al. [2012]; Luo et al. [2012]; Yuan et al. [2015]). In order to identify stars with UV data, stars classified as F, G or K from the RAVE/LAMOST surveys were cross correlated with the UV database of the GALEX survey (Martin et al. [2005]), selecting all the sources with both far-UV (FUV) and near-UV(NUV) measurements. The final sample was obtained by comparing the observed UV colours with those calculated for main sequence stars from the PHOENIX stellar synthetic spectra (Husser, T.-O. et al. [2013]). Targets with FUV-NUV colour at least 1.5 magnitudes bluer than the bluest main-sequence star models are flagged with UV excess, denoting the likely presence of a white dwarf companion. In this way we obtained 430 stars from RAVE and 504 stars from LAMOST with UV-excess.

From our final 934 surveyed UV-excess objects, nine of them (among which is TYC 7218-934-1) were spectroscopically observed with *HST* in order to confirm that the excess is due to a white dwarf companion. For the observations of our system of interest we used the Cosmic Origins Spectrograph (COS), with the G130M grating centred on 1291Å, during one spacecraft orbit. The data were processed using CALSTIS V3.4 and CALCOS V3.1.

We fitted TLUSTY/SYNSPEC (Hubeny & Lanz [1995]) white dwarf model spectra to the *HST* observation. Since it is not possible to obtain simultaneously the surface gravity, temperature and distance of the white dwarf from the UV data only, we fix the mass of the white dwarf at $0.6M_{\odot}$ and fitted the spectrum to get an estimate of the temperature and distance for the white dwarf. We also estimated the distance to the corresponding main-sequence stars in these systems by fitting their spectral energy distributions (SEDs) using the virtual observatory SED analyzer (Bayo, A. et al. [2008]). We used archival optical data from the TYCHO and NOMAD catalogues and infrared data from the 2MASS and WISE databases. We fitted the SED with BTSettl models (Allard et al. [2012]) and kept the physical parameters of the stars (effective temperature, surface gravity and metallicity) fixed at the values from the RAVE and LAMOST databases and scaled the models to best fit the SED, then used the resulting scale factor to determine the distance to the star.

Figure 5.1 shows the UV to infrared SED of TYC 7218-934-1 observed with *HST* and the best fit of the white dwarf and main-sequence star models.

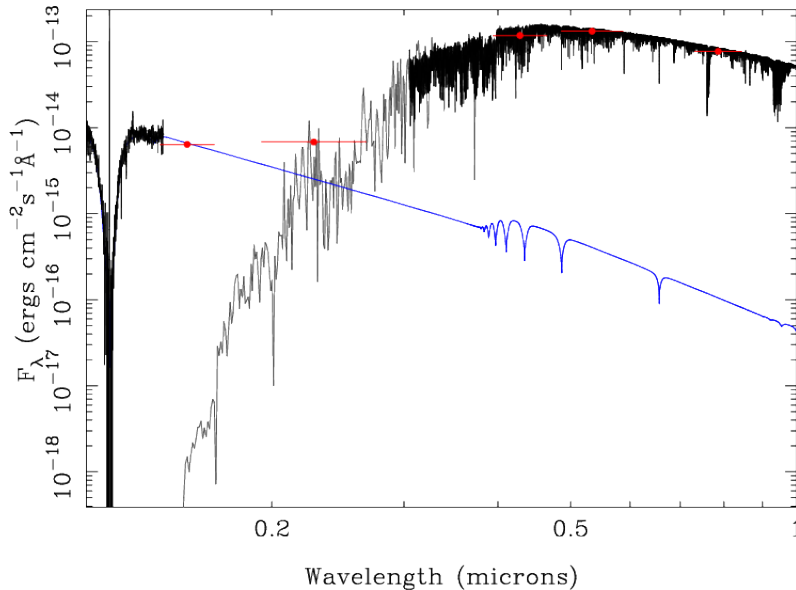


Figure 5.1: Spectral energy distribution (SED) of TYC 7218-934-1. The red points show archival photometry of the system and the black line represent the HST spectrum. The grey and blue line show the best fit of the main sequence star and white dwarf models. The HST data clearly shows that the UV excess is caused by the presence of a white dwarf.

5.2 Radial velocities and orbital parameters

High resolution spectroscopy of TYC 7218-934-1 was obtained with the echelle spectrograph ($R \sim 40,000$) on the 2.5-m Du Pont telescope located at Las Campanas Observatory, Chile, and with FEROS ($R \sim 48,000$) on the 2.2-m Telescope at La Silla, Chile. FEROS covers the wavelength range from $\sim 3500\text{\AA}$ to $\sim 9200\text{\AA}$, while the Du Pont echelle covers $\sim 3700\text{\AA}$ to $\sim 7000\text{\AA}$. In addition, a medium resolution spectrum ($R \sim 5,000$) of TYC 7218-934-1 was obtained with X-shooter D’Odorico et al. [2006] mounted at the Cassegrain focus of VLT-UT2 at Paranal on the 11th of May 2015. X-shooter is comprised of three detectors that enable one to obtain simultaneous data from the UV cutoff at $0.3\mu\text{m}$ to the K -band at $2.4\mu\text{m}$.

The stellar parameters for the main-sequence star in TYC 7218-934-1 were estimated by comparing the observed spectra against a synthetic grid of stellar spectra (Coelho et al. [2005]). The synthetic spectra were degraded to the resolution of the Du Pont echelle and FEROS by convolving them with a Gaussian. The optimal fit for each spectrum was found by chi-square minimization, we then com-

binned the results from each spectral fit and used the average values, yielding: $T_{\text{eff}} = 5790 \pm 50$ K, $\log g = 4.51 \pm 0.05$ (in cgs units), $[\text{Fe}/\text{H}] = 0.00 \pm 0.05$. Using the Torres relation Torres et al. [2010] implies a mass and radius of $1.04 \pm 0.02 M_{\odot}$ and $1.06 \pm 0.06 R_{\odot}$ for the G2V star in TYC 7218-934-1.

The orbital parameters of TYC 7218-934-1 were measured using EXOFAST Eastman et al. [2013]. The best fit orbit is shown in Figure 5.2 and has a period of 13.6 days with an eccentricity of $e = 0.46$. The minimum mass of the unseen companion to the G star is $0.2 M_{\odot}$.

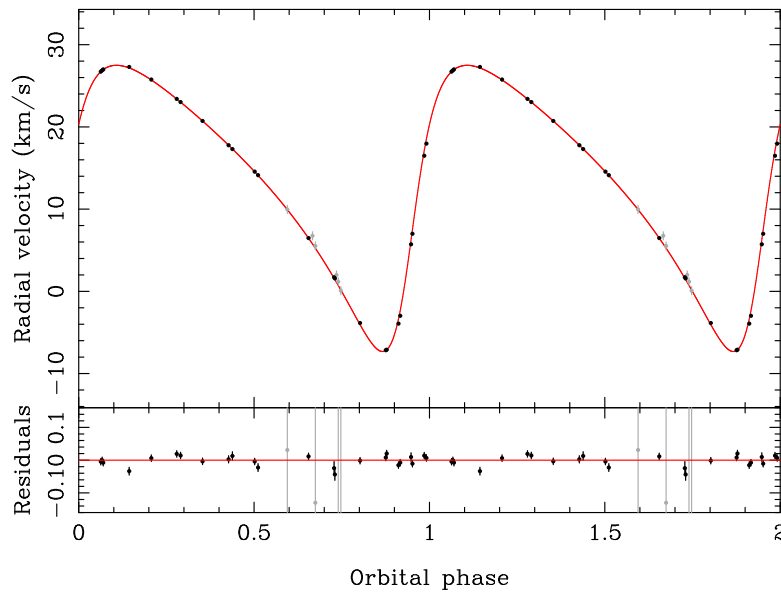


Figure 5.2: Phase-folded radial velocity plot for the main-sequence star in TYC 7218-934-1. The lower panel shows the residuals to the best fit. Data from the Du Pont echelle are shown in grey and from FEROS in black. The G-star clearly moves in an eccentric orbit around a low mass object.

5.3 SPHERE observations confirm the white dwarf to be the third object

To distinguish whether the white dwarf is orbiting the G star or being the distant companion, we observed TYC 7218-934-1 with SPHERE to search for the third object. We used the combined IRDIS/IFS mode as the IFS spectrum allows to distinguish between a WD (blue spectrum) and a low mass main sequence

5.3. SPHERE OBSERVATIONS CONFIRM THE WHITE DWARF TO BE THE THIRD OBJECT

(red spectrum) companion.

The IRDIS data were first preprocessed (sky background subtraction, flat-fielding, bad-pixels correction). The frames were recentered using the initial star center exposure with the four satellite spots. The IFS preprocessing consists of background subtraction and flat-field calibration. Then, each frame is calibrated with the integral field unit (IFU) flat. For wavelength calibration, the IFU is illuminated with four monochromatic lasers of known wavelength. We ended with a 39 monochromatic frames datacube. After pre-processing, IRDIS and IFS data have been reduced with *ad hoc* IDL routines to perform the Angular Differential Imaging

Figure 5.3 shows the SPHERE detection of the third star in the system. We find magnitude differences to the central star of 8.22 ± 0.03 in H2 and 8.30 ± 0.03 in H3. The position of the third object is given by a separation of $0.32''$ (about 54.7 AU from the G star) and a position angle of 179.75 ± 0.07 degrees.

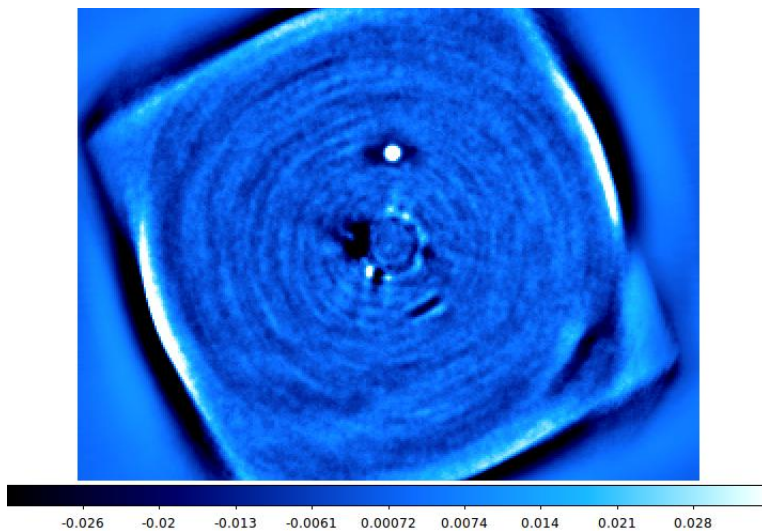


Figure 5.3: SPHERE image of TYC 7218-934-1 clearly confirming the existence of a wide companion in the system

The detection of the third object with IRDIS clearly shows that our interpretation of the eccentric orbit has been correct. However, to test if the third object is the WD or a low mass main sequence star, we need to check the IFS spectrum of TYC 7218-934-1. As shown in Fig. 5.4, the distant companion is the white dwarf as the IFS spectrum is clearly blue. This means that the third object has been the most massive star in the initial triple system and that this star might have

brought the inner binary consisting of the G star plus an unseen M dwarf companion closer together through the Kozai mechanism. We discuss this scenario in more detail in the next sections.

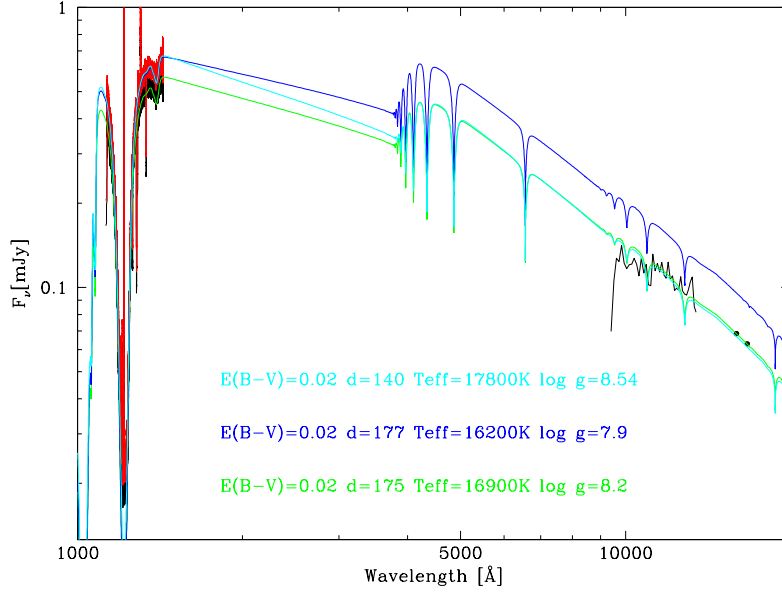


Figure 5.4: Spectral fit for the HST and SHPERE data (black line at $\sim 1000\text{\AA}$) of TYC 7218-934-1. The analysis was made assuming an extinction of $E(B-V)=0.02$ for the HST spectrum. The green line is the best fit for both HST and SPHERE data, giving a distance of 175 pc, which differs $\approx 10\%$ with the distance estimated by the GAIA mission (172.14 pc).

5.4 Kozai mechanisms at current stage

First, we study whether the system is currently under the effect of the SKM. Since we do not have information about the mutual inclination between the inner and outer orbits we use the GR precession and SKM timescales (equations (3.17) and 1.17 respectively) as references to measure its effect. Figure 5.5 shows that at $e_{out} \approx 0.92$ the SKM is able to affect the evolution of the system. However at such eccentricities the system is close to the stability limit (see Fig. 5.7). Therefore, it is very unlikely that there is currently SKM occurring in the system.

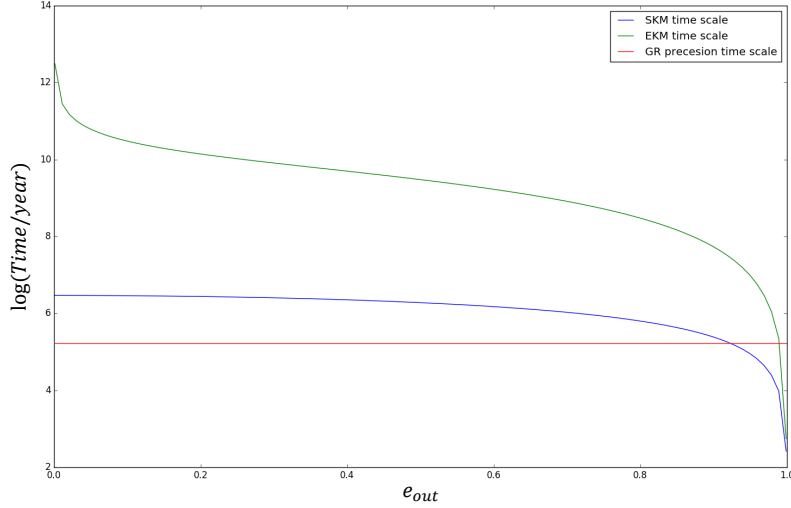


Figure 5.5: Comparison between the standard (blue line) and eccentric (green line) Kozai mechanisms against the GR precession timescale (red line). Both Kozai mechanisms depend on the outer eccentricity e_{out} , while the GR precession timescale does not (it only depends on the masses and orbital properties of the inner binary). Below the red line the Kozai mechanisms are not suppressed by GR precession.

Secondly, we will look for some indication of EKM using the criterion 2 of section 3.3, which states that the eccentric Kozai-Livod mechanism is important when $\epsilon_{oct} \geq 0.01$. In terms of the periods, ϵ_{oct} (Eq. 1.19) can be written as

$$\epsilon_{oct} = \left| \frac{m_1 - m_0}{m_1 + m_0} \right| \left(\frac{m_1 + m_0}{M_{tot}} \right)^{1/3} \left(\frac{P_{in}}{P_{out}} \right)^{2/3} \left(\frac{e_{out}}{1 - e_{out}^2} \right). \quad (5.1)$$

The fixed parameters will be the masses of the three components ($M_0 = 1.04M_\odot$ and $M_1 = 0.2, M_\odot, M_{WD} = 0.95$) and both the inner and outer periods ($P_{in} = 13.6$ and $P_{out} = 10^{4.7}$ days respectively), while we kept as a free parameter the outer eccentricity. For the (unseen) companion of the primary G-type we use the lower limit while we use the upper limit for the WD mass. Both choices do not affect the general conclusions that will be drawn in this section as the uncertainty related to the possible mass ranges are small compared to other uncertainties.

The estimated outer period of $10^{4.7}$ days was obtained supposing that the pro-

jected separation between the WD and the G-type star is the true separation (i.e. assuming that we see the outer orbital plane perpendicular to the line of sight) at apastron, giving us a lower limit of the real value of $P_{out,f}$ as

$$P = \left[\frac{4\pi^2}{G(M_1 + M_2 + M_{WD})} \left(\frac{(1 + e \cos(f))r}{(1 - e^2)} \right)^3 \right]^{1/2}, \quad (5.2)$$

where we have used Eq. (3.11) and the third Kepler's law. Here r is the projected separation and f the eccentric anomaly. For $f = 180^\circ$ Eq. (5.2) can be rewritten as

$$P = \left[\frac{4\pi^2}{G(M_1 + M_2 + M_{WD})} \left(\frac{r}{(1 + e)} \right)^3 \right]^{1/2}. \quad (5.3)$$

As shown in Fig. 5.6, the system is affected by the EKM only at eccentricities higher than ≈ 0.92 (using the ϵ_{oct} criterion). However, by comparing the GR precession and EKM timescales (Fig. 5.5) we found that the minimum eccentricity required to overcome the GR precession is $e_{out} \approx 0.98$. Finally, according to the Mardling-Aarseth's stability criterion, the system is unstable at eccentricities higher than ≈ 0.96 (Fig. 5.7). Therefore we can conclude that, at present, the system is unaffected by the EKM.

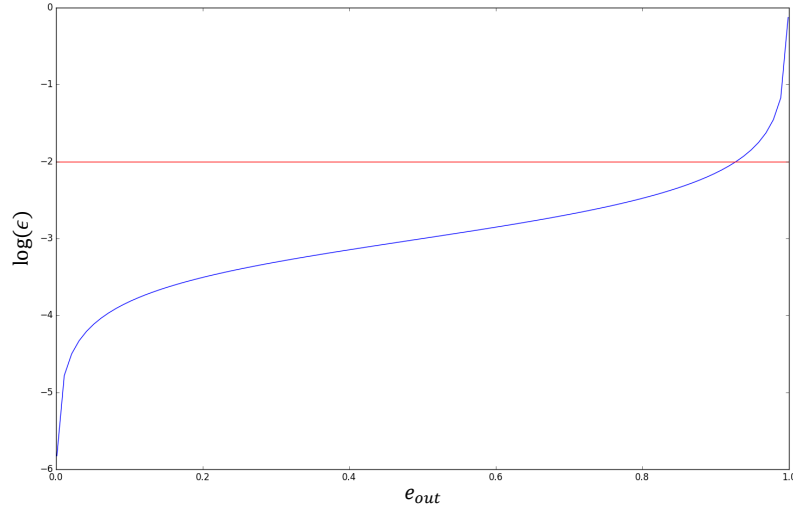


Figure 5.6: $\log \epsilon_{oct}$ as function of the outer eccentricity (blue line). Here we can see that only for extremely high eccentricity values ($e_{out} \gtrsim 0.95$) the eccentric Kozai mechanism is important ($\log \epsilon_{oct} \geq -2$, red line). The fixed values for the calculation of $\log \epsilon_{oct}$ are $m_0 = 1.04M_\odot$, $m_1 = 0.2, M_\odot$, $M_{WD} = 0.95$, $P_{in} = 13.6$ days, $P_{out} = 10^{4.7}$ days)

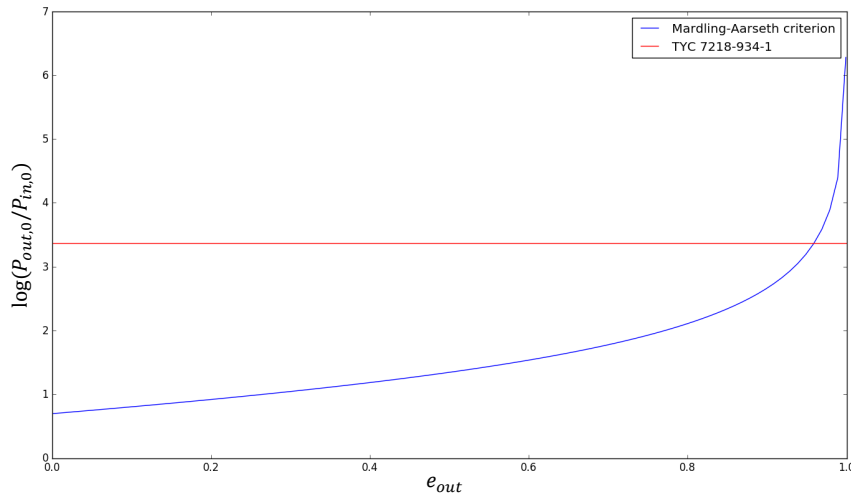


Figure 5.7: $\log(P_{out}/P_{in})$ vs outer eccentricity. Comparison between the Mardling-Aarseth's stability criterion (Eq. 2.2, blue line) and the ratio between the outer and inner period of TYC 7218-934-1 (red line), which marks the transition between dynamically stable (area below the red line) and unstable (area above the red line) configurations. the interception between the red and blue lines at $e_{out} \approx 0.96$ shows that for higher eccentricity values the system becomes unstable.

5.5 Kozai-Lidov mechanisms in the early stages of TYC 7218-934-1

To determine whether the system experienced the Kozai-Lidov mechanisms before the WD was formed, we compare the timescales of the standard (T_{SKM}) and eccentric (T_{EKM}) Kozai mechanisms (Eqs. 1.17 and 1.20) with the evolutionary (T_{MS}) and GR precession (T_{GRP}) timescales. If the Kozai-Lidov mechanisms timescales are less than T_{MS} and T_{GRP} , then the system is able to experience eccentricity oscillations. To estimate if this was potentially the case, we need to estimate the initial outer orbital period $P_{out,0}$ using the *adiabatic mass loss model* (appropriate for this type of systems, as discussed in Section 3.1). Thus:

$$P_{out,0} = P_{out,f} \left(\frac{M_{tot,f}}{M_{tot,0}} \right)^2. \quad (5.4)$$

This resulting outer period represents a lower limit of the true values if we assume the observed projected separation to be the real separation. For the mass of the WD progenitor (M_{prog}) we use the initial to final mass ratio (IFMR) derived in Catalán et al. [2008]

$$M_{WD} = (0.177 \pm 0.004)M_{prog} + (0.384 \pm 0.011), \quad (5.5)$$

that gives a mass range for the progenitor between $3.04M_{\odot}$ and $4.83M_{\odot}$. The initial masses of the G type star and its companion will be set at their current values ($m_0 = 1.04M_{\odot}$ and $m_1 = 0.2$, that is, we assume that their masses did not change significantly during the evolution of the system). Under this assumptions, the initial outer period ranges from $10^{3.66}$ to $10^{4.35}$ days. For the evolutionary timescale we assume that the main sequence lifetime of a star depends on mass following a power law as

$$T_{MS} = 10^{10} \left(\frac{M_{\odot}}{M} \right)^{\eta}, \quad (5.6)$$

where $\eta = -2.5$, and T_{MS} is in years. Thus, the time before the massive primary becomes a WD is $\approx 3.1 \times 10^8$ yr.

In order to compare the aforementioned timescales, it is crucial for the case of the Kozai-Lidov mechanisms to know the ratio between the outer and inner periods, since they depend strongly on it. Thus, in what follows, we combined our previously obtained lower limit for $P_{out,0}$ with the multiple star population synthesis of T14b to get the probability that the Kozai-Lidov mechanisms were present in the early stages of the system, taking into account all possible combinations of $P_{in,0}$, $e_{in,0}$ and $e_{out,0}$ for each $P_{out,0}$.

5.5.1 Modelling the probability to experience Kozai-Lidov oscillations by Montecarlo simulations

Supposing that TYC 7218-934-1 follows the statistical model proposed by T14b (i.e. masses and periods are independent variables) and our eccentricity distributions used in Chapter 2, we will try to quantify, assuming an initial outer period equal or greater than 10^4 days (this is our lower limit for $P_{out,0}$), whether the system experience Kozai-Lidov mechanisms as follows:

- We first determine the probability that the initial inner period was greater than 13.6 days (i.e., assuming that $P_{in,0}$ was reduced during the evolution of the system, mainly by tidal interactions).
- We then estimate how many of the systems with $P_{out,0} \geq 10^4$ days and $P_{in,0} \geq 13.6$ days are susceptible to suffer Kozai-Lidov oscillations (taking into account the GR precession and evolutionary time of the WD progenitor).

Figure 5.8 shows how we determine which configurations are susceptible to suffer Kozai-Lidov oscillations for the particular case where $P_{out,0} = 10^4$ days, $e_{out,0} = 0.5$ and $e_{in,0} = 0$, leaving $P_{in,0}$ as free parameter. The minimum inner period required to overcome the GR precession by the eccentric Kozai-Lidov mechanism is $x_{in,0}^{EKM} = 1.61$ (≈ 41 days, given by the intersection of the green line and the dashed blue line), while for the standard Kozai mechanism there are no restrictions on period either by GR precession or the WD progenitor's lifetime.

We found that, on average, 83% of the configurations with $P_{out,0} \geq 10^4$ have inner periods greater than 13.6 days, and of those about 68% are susceptible to suffer Kozai-Lidov oscillations, which give us a probability of $\approx 56\%$ (0.83×0.68) that the observed eccentric orbit in TYC 7218-934-1 was due to Kozai-Lidov mechanism. This shows that a reasonable scenario for the evolution of the system is that close orbit of the inner binary has been generated by eccentricity variations that caused orbital energy to be lost through tidal effects. While the system is currently not affected by Kozai-Lidov effects, tidal effects are most likely still acting in the system and are supposed to further reduce the orbital period.

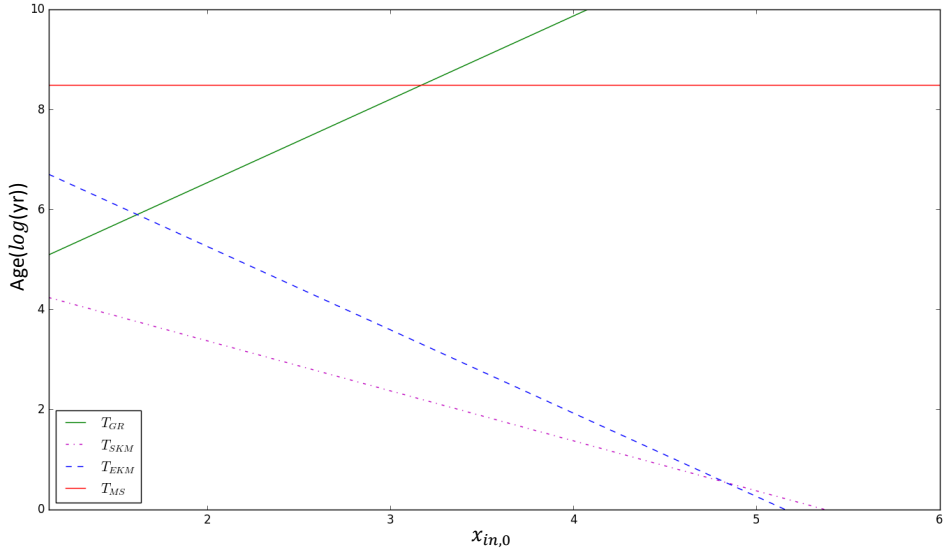


Figure 5.8: SKM and EKM timescales (dashed-dotted magenta line and dashed blue line respectively) at different initial inner periods compared with the estimate main sequence lifetime of the WD progenitor (solid red line) and the GR precession timescale (solid green line). The fixed orbital parameters used are $P_{out,0} = 10^4$ days, $e_{out,0} = 0.5$ and $e_{in,0} = 0$.

5.6 Conclusions

In order to explain the inner eccentric orbit observed in the hierarchical triple system TYC 7218-934-1, we propose that its distant component (i.e. the white dwarf) perturbs the inner binary producing the so called Kozai-Lidov oscillations. By using its observed orbital characteristics and the estimated masses of its components we conclude that currently the system is unaffected by the eccentric Kozai oscillations, and only for outer eccentricity values close to 0.92 the systems is able to experience standard Kozai-oscillations. However, since at such eccentricities the system is also close to the stability limit, it is unlikely that the standard Kozai mechanism currently exists.

Once we conclude that currently the system is unaffected by the Kozai-Lidov mechanisms, we explore its likely presence on the initial stages of the system (that is, before the white dwarf formed). By assuming that TYC 7218-934-1 follows the statistical model of Tokovinin [2014b] and the eccentricity distributions used in Chapter 2, we estimate that is highly likely that the initial inner period was greater than the observed one, favoring in turn the Kozai-Lidov oscillations in the early stages of the system.

CHAPTER 6

Summary

The study of close binaries composed by a main sequence star of spectral type F,G or K (FGK type) plus a white dwarf (WD) as potential Supernovae Ia progenitors is extremely important to constrain and refine the several pathways that have been proposed to describe this type of events. With this goal in mind, the *The White Dwarf Binary Pathways Survey I* (Parsons et al. [2016]) developed an effective method to identify unresolved Post Common Envelope Binaries (PCEBs) composed by a FGK stars with WD companions (FGK+WD systems), which is based on two main criteria :

- Confirmation of the binary system: Radial velocities measurements of the FGK star show the presence of a companion.
- Confirmation of a WD companion: The FGK spectrum shows excess flux at ultraviolet (UV) wavelengths, which is interpreted as a potential WD companion.

It is well established that the main formation channel of close FGK+WD binaries involves the Common Envelope (CE) phase. However, from the total of systems identified as FGK+WD with orbital properties measured, about $33\% \pm 12$ have eccentric orbits that can not be explained by CE evolution. Since the orbital solutions of such systems are based on radial velocities measured from the absorp-

tion lines of the FGK-type component, there are two possible general configurations. Either these objects are indeed close FGK+WD binaries formed through the Kozai-Lidov mechanisms by means of a unseen M-type star (FGK/WD+M configuration), providing the first observational evidence for a new channel towards SN Ia, or the WD is the third distant object that triggered the Kozai-Lidov mechanisms, which led to the formation of the eccentric inner binary star consisting of the FGK-type star plus an unseen late M dwarf (FGK/M+WD configuration).

To test the hypothesis that the identified eccentric systems are triples, we generate and evolve a population of binaries and triples to compare the final amount of triple systems with FGK/WD+M and FGK/M+WD configurations with the number of binaries FGK+WD that passed through the common envelope phase. The steps involved in our work can be summarized as follow:

- *Population synthesis of binary and triple systems:* We reproduce the multiple star population synthesis algorithm developed by Tokovinin [2014b] to obtain initial mass ratios and orbital periods. Initial masses, eccentricities, time of evolution, and inclination between orbits (for the case of triple systems) were included based on observational distributions found in the literature.
- *Evolution of binary and triple systems:* The initial population of binary and triple systems were evolved with the Binary Stellar Evolution (BSE) code, which is able to reproduce the evolution of single and binary stars in a fast way. Since BSE is not capable to evolve triple systems, as a first approximation we evolve the inner binary and its distant companion independently, and by using the *adiabatic mass loss model* we obtain the final period of the latter.
- *Selection of PCEBs binaries and FGK/WD+M - FGK/M+WD triples:* From the BSE output we select the PCEBs (the main target in the survey) and the triple systems with both FGK/WD+M and FGK/M+WD configurations.
- *Identify FGK/WD+M and FGK/M+WD systems with Kozai mechanisms:* Based on a list of criteria obtained from numerical simulations made in previous works, we select the FGK/WD+M and FGK/M+WD systems that would potentially be affected by the Kozai-Lidov mechanisms and compare the total numbers of these triples and PCEBs.

-
- *Apply the ejection and time-scale filters:* Due to mass loss either in the inner binary or the distant component in a triple, the system may be fragmented into a binary and single stars by ejecting one of them. To determine which systems suffer ejections we use as a first approximation the *Impulse regime evolution*, i.e assuming instant mass loss. This prescription most likely overestimates the number of fragmented systems. In addition, we compare the Kozai mechanisms time-scales with the general relativity (GR) precession time-scale and evolutionary time of the triple in order to select only those systems where the Kozai mechanisms can act freely.

We found that, without filters $\approx 23\%$ of the observationally identified FGK+WD systems would indeed be triple systems, where the ratio between FGK/WD+M and FGK/M+WD systems is ≈ 0.25 . When the the ejection filters are applied, the fraction of triples is reduced to a 18 per cent. Thus, although we have used many (reasonable) approximations, and taking into account the estimated uncertainty of 12% in the observed fraction of systems with eccentric orbits, our fraction of triple systems with Kozai-Lidov oscillations agrees well with the observed fraction of systems with eccentric orbits, showing that the majority, if not all of the observed WD/FGK candidates with eccentric orbits would be triples.

In the last part of this work we studied the system TYC 7218-934-1, which corresponds to one of the observed FGK+WD systems with eccentric orbits. It is the first object confirmed as a FGK/M+WD triple, supporting our hypothesis of the presence of triple dynamics. Furthermore, this system supports the result obtained in our simulations that about 79% of the intrinsic population of triples that might be confused as close FGK+WD binaries in the survey, have the WD as the third companion. Of course further characterizations of a larger number of eccentric systems is required before firm conclusions can be drawn. Finally, assuming that TYC 7218-934-1 follows the statistical model proposed by Tokovinin [2014b], we calculated that, given an initial outer period equal or greater than 10^4 days, there is a probability of $\approx 56\%$ that the observed eccentric orbit in TYC 7218-934-1 was caused by the Kozai-Lidov mechanisms in the early stages of the system. This rough estimate shows that the scenario outlined for TYC 7218-934-1, i.e. Kozai-Lidov triggering large eccentricities when all stars

were on the main sequence, is a reasonable one.

6.1 Statement

The acquisition, reduction and models fitted to SPHERE's data of TYC 7218-934-1 was not part of this work, and I only used its calculated stellar and orbital parameter in the analysis of Chapter five. In the same way, the radial velocities measurements, and observed fraction of FGK+WD systems were taken from Parsons et al. [2016].

APPENDIX A

Appendix

A.1 Tables

(a) without filters

PCEBs	WD/FGK : 221487	Total PCEBs: 233147				Total: 289648
	WD/FGK+M: 11669	SKM ₀ : 5610	Total C1: 12429		Total Cont.: 56501	
contaminants	WD/FGK+M	EKM ₀ : 5957				
		MIEK: 862				
	FGK/M+WD	SKM ₀ : 30065	Total C2: 44072			
		EKM ₀ : 10680				
		$P_{in} \leq 100d$: 3327				

(b) with filters

PCEBs	WD/FGK: 221487	Total PCEBs: 231101 ± 43				Total: 262487 ± 207
	WD/FGK+M*: 9614 ± 43	SKM ₀ : 2921 ± 19	Total C1: 7693 ± 52		Total Cont.: 31386 ± 164	
contaminants	WD/FGK+M	EKM ₀ : 4237 ± 27				
		MIEK: 535 ± 6				
	FGK/M+WD	SKM ₀ : 13430 ± 51	Total C2: 23693 ± 112			
		EKM ₀ : 7732 ± 39				
		$P_{in} \leq 100d^*$: 2531 ± 22				

Table A.1: SL03

(a) without filters

PCEBs	WD/FGK : 197348	Total PCEBs: 207440				Total: 274068
	WD/FGK+M: 10092					
contaminants	WD/FGK+M	SKM ₀ : 5869	Total C1: 12727	Total Cont.: 66628		
		EKM ₀ : 5979				
		MIEK: 879				
	FGK/M+WD	SKM ₀ : 35505	Total C2: 53901			
		EKM ₀ : 15157				
$P_{in} \leq 100d$: 3239						

(b) with filters

PCEBs	WD/FGK: 197348	Total PCEBs: 205649 ± 38				Total: 244724 ± 214
	WD/FGK+M*: 8301 ± 38					
contaminants	WD/FGK+M	SKM ₀ : 3882 ± 19	Total C1: 8669 ± 53	Total Cont.: 39075 ± 176		
		EKM ₀ : 4235 ± 28				
		MIEK: 552 ± 6				
	FGK/M+WD	SKM ₀ : 16928 ± 55	Total C2: 30406 ± 123			
		EKM ₀ : 11012 ± 47				
$P_{in} \leq 100d^*$: 2466 ± 21						

Table A.2: SL05

(a) without filters

PCEBs	WD/FGK : 201373	Total PCEBs: 212292				Total: 274757
	WD/FGK+M: 10919					
contaminants	WD/FGK+M	SKM ₀ : 8868	Total C1: 14188	Total Cont.: 62465		
		EKM ₀ : 4616				
		MIEK: 704				
	FGK/M+WD	SKM ₀ : 36797	Total C2: 48277			
		EKM ₀ : 8043				
$P_{in} \leq 100d$: 3437						

(b) with filters

PCEBs	WD/FGK: 201373	Total PCEBs: 210586 ± 34				Total: 246449 ± 185
	WD/FGK+M*: 9213 ± 34					
contaminants	WD/FGK+M	SKM ₀ : 6289 ± 21	Total C1: 10030 ± 51	Total Cont.: 35863 ± 151		
		EKM ₀ : 3282 ± 25				
		MIEK: 459 ± 5				
	FGK/M+WD	SKM ₀ : 17370 ± 49	Total C2: 25833 ± 100			
		EKM ₀ : 5926 ± 31				
$P_{in} \leq 100d^*$: 2537 ± 20						

Table A.3: SU03

(a) without filters

PCEBs	WD/FGK : 176384	Total PCEBs: 185604				Total: 250417
	WD/FGK+M: 9220					
contaminants	WD/FGK+M	SKM ₀ : 8994	Total C1: 14133			Total Cont.: 64813
		EKM ₀ : 4568				
		MIEK: 671				
	FGK/M+WD	SKM ₀ : 38434	Total C2: 50680			
		EKM ₀ : 8800				
$P_{in} \leq 100\mu\text{t}$: 3446						

(b) with filters

PCEBs	WD/FGK: 176384	Total PCEBs: 184136 ± 30				Total: 221184 ± 192
	WD/FGK+M*: 7752 ± 30					
contaminants	WD/FGK+M	SKM ₀ : 6111 ± 20	Total C1: 9791 ± 50			Total Cont.: 37048 ± 162
		EKM ₀ : 3230 ± 25				
		MIEK: 450 ± 5				
	FGK/M+WD	SKM ₀ : 18290 ± 54	Total C2: 27257 ± 112			
		EKM ₀ : 6418 ± 35				
$P_{in} \leq 100\mu\text{t}$: 2549 ± 23						

Table A.4: SU05

Bibliography

- Abt H. A., 1983, *ARA&A*, 21, 343
- Abt H. A., Gomez A. E., Levy S. G., 1990, *ApJS*, 74, 551
- Abt H. A., Levy S. G., 1976, *ApJS*, 30, 273
- Allard F., Homeier D., Freytag B., 2012, *Philosophical Transactions of the Royal Society of London A: Mathematical, Physical and Engineering Sciences*, 370, 2765
- Bayo, A. , Rodrigo, C. , Barrado y Navascués, D. , Solano, E. , Gutiérrez, R. , Morales-Calderón, M. , Allard, F. , 2008, *AA*, 492, 277
- Carquillat J.-M., Prieur J.-L., 2007, *MNRAS*, 380, 1064
- Catalán S., Isern J., García-Berro E., Ribas I., 2008, *MNRAS*, 387, 1693
- Coelho P., Barbuy B., Meléndez J., Schiavon R. P., Castilho B. V., 2005, *A&A*, 443, 735
- Cui X.-Q. et al., 2012, *Research in Astronomy and Astrophysics*, 12, 1197
- Dilday B. et al., 2012, *Science*, 337, 942
- D’Odorico S. et al., 2006, in *Proc. SPIE*, Vol. 6269, p. 98
- Duchêne G., Kraus A., 2013, *ARA&A*, 51, 269
- Duquennoy A., Mayor M., 1991, *A&A*, 248, 485
- Eastman J., Gaudi B. S., Agol E., 2013, *PASP*, 125, 83
- Eggleton P. P., 1983, *ApJ*, 268, 368
- Eggleton P. P., Kisseleva-Eggleton L., 2006, *Ap&SS*, 304, 75

- Fabrycky D., Tremaine S., 2007, *ApJ*, 669, 1298
- Garmany C. D., Conti P. S., Massey P., 1980, *ApJ*, 242, 1063
- Hadjidemetriou J. D., 1963, *Icarus*, 2, 440
- Harrington R. S., 1968, *AJ*, 73, 190
- Hubeny I., Lanz T., 1995, *ApJ*, 439, 875
- Husser, T.-O. , Wende-von Berg, S. , Dreizler, S. , Homeier, D. , Reiners, A. ,
Barman, T. , Hauschildt, P. H. , 2013, *AA*, 553, A6
- Kiminki D. C., Kobulnicky H. A., 2012, *ApJ*, 751, 4
- Kordopatis G. et al., 2013, *AJ*, 146, 134
- Kouwenhoven M. B. N., Brown A. G. A., Portegies Zwart S. F., Kaper L., 2007,
A&A, 474, 77
- Kouwenhoven M. B. N., Brown A. G. A., Zinnecker H., Kaper L., Portegies Zwart
S. F., 2005, *A&A*, 430, 137
- Kozai Y., 1962, *AJ*, 67, 591
- Kroupa P., 2001, *MNRAS*, 322, 231
- Li G., Naoz S., Kocsis B., Loeb A., 2015, *MNRAS*, 451, 1341
- Lidov M. L., 1962, *Planet. Space Sci.*, 9, 719
- Lithwick Y., Naoz S., 2011, *ApJ*, 742, 94
- Luo A.-L. et al., 2012, *Research in Astronomy and Astrophysics*, 12, 1243
- Maoz D., Mannucci F., 2012, , 29, 447
- Mardling R. A., Aarseth S. J., 2001, *MNRAS*, 321, 398
- Martin D. C. et al., 2005, *The Astrophysical Journal Letters*, 619, L1
- Naoz S., 2016, *ARA&A*, 54, 441
- Naoz S., Fabrycky D. C., 2014, *ApJ*, 793, 137

- Naoz S., Farr W. M., Lithwick Y., Rasio F. A., Teyssandier J., 2011, *Nature*, 473, 187
- Nomoto K., Kondo Y., 1991, *ApJ*, 367, L19
- Parsons S. G., Rebassa-Mansergas A., Schreiber M. R., Gänsicke B. T., Zorotovic M., Ren J. J., 2016, *MNRAS*, 463, 2125
- Patat F. et al., 2007, *Science*, 317, 924
- Peter D., Feldt M., Henning T., Hormuth F., 2012, *VizieR Online Data Catalog*, 353
- Raghavan D. et al., 2010, *ApJS*, 190, 1
- Saffer R. A., Livio M., Yungelson L. R., 1998, *ApJ*, 502, 394
- Sana H. et al., 2012, *Science*, 337, 444
- Shappee B. J., Thompson T. A., 2013, *ApJ*, 766, 64
- Shatsky N., 2001, *A&A*, 380, 238
- Simon J. D. et al., 2009, *ApJ*, 702, 1157
- Sternberg A. et al., 2011, *Science*, 333, 856
- Sterzik M. F., Tokovinin A. A., Shatsky N. I., 2003, in *Astronomical Society of the Pacific Conference Series*, Vol. 287, De Buizer J. M., van der Bliek N. S., eds, *Galactic Star Formation Across the Stellar Mass Spectrum*, p. 403
- Tokovinin A., 2004, in *Revista Mexicana de Astronomia y Astrofisica Conference Series*, Vol. 21, Allen C., Scarfe C., eds, *Revista Mexicana de Astronomia y Astrofisica Conference Series*, p. 7
- Tokovinin A., 2008, *MNRAS*, 389, 925
- Tokovinin A., 2014a, *AJ*, 147, 86
- Tokovinin A., 2014b, *AJ*, 147, 87
- Tokovinin A., Kiyaeva O., 2016, *MNRAS*, 456, 2070
- Tokovinin A. A., 1997, *A&AS*, 124, 75

- Toonen S., Hamers A., Portegies Zwart S., 2016, *Computational Astrophysics and Cosmology*, 3, 6
- Torres G., Andersen J., Giménez A., 2010, *A&A Rev.*, 18, 67
- Turner N. H., ten Brummelaar T. A., Roberts L. C., Mason B. D., Hartkopf W. I., Gies D. R., 2008, *AJ*, 136, 554
- Tutukov A., Yungelson L., 1979, in *IAU Symposium, Vol. 83*, Conti P. S., De Loore C. W. H., eds, *Mass Loss and Evolution of O-Type Stars*, p. 401
- Veras D., Wyatt M. C., Mustill A. J., Bonsor A., Eldridge J. J., 2011, *MNRAS*, 417, 2104
- Yuan H.-B. et al., 2015, *MNRAS*, 448, 855
- Zorotovic M., Schreiber M. R., Gänsicke B. T., Nebot Gómez-Morán A., 2010, *A&A*, 520, A86